Tests of supersymmetric couplings at high energy colliders

Dissertation
zur Erlangung des Doktorgrades
des Fachbereichs Physik
der Universität Hamburg

vorgelegt von
Marcus Weber
aus Köln

Hamburg
2001

Gutachter der Dissertation:	Prof. Dr. J. Bartels Prof. Dr. P. M. Zerwas
Gutachter der Disputation:	Prof. Dr. B. A. Kniehl Prof. Dr. P. M. Zerwas
Datum der Disputation:	27.11.2001
Dekan des Fachbereichs Physik Vorsitzender des Promotionsausschusses:	Prof. Dr. F.-W. Büßer

Abstract

The next-to-leading order corrections in α_s to the process $e^+e^- \to q\bar{\tilde{q}}\tilde{g}$ are presented in the framework of the Minimal Supersymmetric Standard Model (MSSM). In addition to being the leading order process for gluino production at e^+e^- colliders, this process can be used to measure the supersymmetric $q\bar{\tilde{q}}\tilde{g}$ Yukawa coupling. A comparison of this coupling with the strong gauge coupling tests the supersymmetric $SU(3)$ coupling relation. In the parameter range interesting for such a comparison, the NLO corrections have been found to enhance the leading order cross section. Since the dependence on the renormalization scale is reduced at the same time, the accuracy and reliability of the theoretical prediction for this process is therefore improved.

Zusammenfassung

In dieser Arbeit wird die Berechnung der Korrekturen zum Prozeß $e^+e^- \to q\bar{\tilde{q}}\tilde{g}$ in nächstführender Ordnung in der starken Kopplungskonstante α_s im Rahmen des Minimalen Supersymmetrischen Standardmodells (MSSM) präsentiert. Dieser Prozeß ist einerseits der führende Prozeß zur Produktion von Gluinos an e^+e^- Beschleunigern, andererseits kann er zur Messung der supersymmetrischen $q\bar{\tilde{q}}\tilde{g}$ Yukawa Kopplung benutzt werden. Durch Vergleich dieser Kopplung mit der starken Eichkopplung ist ein Test der supersymmetrischen $SU(3)$ Kopplungsrelation möglich. In dem dafür interessanten Parameterbereich wird der Wirkungsquerschnitt in führender Ordnung durch die Strahlungskorrekturen vergrößert. Da sich gleichzeitig die Abhängigkeit von der Renormierungsskala verkleinert, wird die Genauigkeit und Verlässlichkeit der theoretischen Vorhersage für diesen Prozeß durch die Einbeziehung der nächstführenden Korrekturen verbessert.

Für meinen Vater

Contents

1 Introduction **1**

2 Supersymmetry **5**
2.1 Motivation for supersymmetry 5
2.1.1 Hierarchy and naturalness problems 5
2.1.2 Coupling unification 7
2.1.3 Haag-Lopuszanski-Sohnius theorem 8
2.1.4 Incorporation of gravity 9
2.2 The supersymmetry algebra 9
2.3 Construction of supersymmetric Lagrangians 11
2.3.1 Gauge kinetic terms 12
2.3.2 Matter kinetic terms 12
2.3.3 Matter self interactions 13
2.3.4 D-terms and F-terms 14

3 Minimal Supersymmetric Standard Model **15**
3.1 Particle content 15
3.2 R parity 16
3.3 Soft supersymmetry breaking 17
3.4 Supersymmetric QCD 18
3.5 Gauge and Yukawa couplings 20
3.6 Experimental searches 22

4 Squark and gluino production at LO **25**
4.1 Processes 25
4.1.1 $e^+e^- \to \tilde{q}\bar{\tilde{q}}$ 25
4.1.2 $e^+e^- \to \tilde{q}\bar{\tilde{q}}g$ 26
4.1.3 $e^+e^- \to q\bar{\tilde{q}}\tilde{g}$ 28
4.1.4 $e^+e^- \to q\bar{q}\tilde{g}\tilde{g}$ 30
4.1.5 Squark and gluino decays 31
4.2 Testing supersymmetric coupling relations 31
4.3 Leading order numerical results 33

5 Gluino production in NLO **37**
5.1 Outline of the calculation 37
5.2 Virtual corrections 40
5.2.1 Feynman diagrams 40
5.2.2 Loop integrals 43
5.2.3 Regularization and supersymmetry 45
5.2.4 Renormalization 46
5.2.5 Infrared divergences 49
5.3 Real corrections 49
5.3.1 Soft and collinear limits 51
5.3.2 Definition of phase space splitting 53
5.3.3 Contributions from soft phase space 55
5.3.4 Contributions from collinear phase space 56
5.3.5 Contributions from hard phase space 58
5.4 Checks of the calculation 59
5.5 Numerical results 61

6 Conclusions **67**

A Feynman rules **69**

B Leading order cross section for $e^+e^- \to q\bar{\tilde{q}}\tilde{g}$ **75**

C Scalar and soft integrals **77**
C.1 Scalar integrals 77
C.2 Soft integrals 83

D Renormalization constants **85**

Bibliography **87**

Chapter 1

Introduction

The Standard Model of elementary particle physics [1] provides a remarkably successful description of high energy physics phenomena. It is a renormalizable quantum field theory based on Lorentz and gauge symmetries with the gauge group $SU(3)_C \times SU(2)_L \times U(1)_Y$. The masses of gauge bosons and fermions are generated via the Higgs mechanism [2] in a way that preserves gauge invariance and renormalizability.

The force sector of the Standard Model has been experimentally established by the discovery of the gluon [3] and the massive electroweak gauge bosons $W^{\pm}$ and Z^0 [4]. Following these discoveries, high precision measurements have allowed first steps towards the verification of the non-abelian coupling structure and, in some cases, have tested the Standard Model even to the level of radiative corrections. The recent discoveries of the top quark [5] and the τ neutrino [6] leave the Higgs particle as the only missing ingredient of the Standard Model. Though collider experiments have not shown any deviations from the Standard Model up to now, neutrino oscillations have been recently found [7], implying neutrinos to be massive. Neutrino masses can however be incorporated into the Standard Model, without changing the general structure.

Despite its success, there exist several conceptual problems in the Standard Model, which indicate the existence of new physics. First of all, gravity, the fourth fundamental force of nature, is not included in the Standard Model, though it will become relevant at the Planck scale $M_P \approx 10^{19}\,\mathrm{GeV}$. Furthermore, the specific gauge group of the Standard Model, the quantum numbers of particles, and the parameters, i.e. the couplings and masses, are all chosen ad hoc to fit observations, with no underlying principle guiding this choice. The latter point makes Grand Unified Theories (GUT's) attractive, which simplify the symmetry structure and can partly explain the quantum numbers of particles. The extrapolation of the three Standard Model couplings to high energies using the renormalization group equations suggests a unification scale $M_{\mathrm{GUT}} \approx 10^{14} - 10^{16}\,\mathrm{GeV}$. It seems therefore inevitable that new physics at energy scales much larger than the electroweak scale has to be introduced.

However, such large scale hierarchies are destabilized by radiative corrections in the Standard Model. This problem is called the naturalness problem [8], and it arises in the Higgs sector from quadratically divergent radiative corrections to the Higgs mass.

By introducing supersymmetry [9], which relates fermionic and bosonic states, the naturalness problem can be solved. In a supersymmetric extension of the Standard Model all fermions are accompanied by bosonic superpartners with the same quantum numbers but different spin, and vice versa. The particle content is therefore effectively doubled. Since fermions and bosons contribute with opposite signs in loops, the quadratic divergences are cancelled in a supersymmetric theory. This is however only valid if the gauge couplings are equal to the corresponding supersymmetric Yukawa couplings, as guaranteed by supersymmetry. Furthermore, assuming a grand unified scenario the weak mixing angle can be predicted from the measured values of α_{em} and α_s at the electroweak scale. This prediction agrees with the measured value within supersymmetry, but not within the Standard Model alone. Finally, supersymmetry naturally includes gravity if it is implemented as a local symmetry.

If supersymmetry is realized in nature it has to be broken, in order to remove the mass degeneracy between the Standard Model particles and their supersymmetric partners. Since different supersymmetry breaking mechanisms with different predictions for electroweak scale supersymmetry have been proposed, the breaking is parameterised by the introduction of the most general explicit breaking terms compatible with renormalizability and gauge symmetry. These would however reintroduce quadratic divergences into the theory, leading to a reappearance of the naturalness problem. If supersymmetry is required to solve the naturalness problem, only soft breaking terms which do not lead to new quadratic divergences are allowed. The cancellation of the quadratic divergences is invariably tied to the validity of the supersymmetric coupling relations between the gauge and the Yukawa couplings. Only if these supersymmetric coupling relations hold is the cancellation of quadratic divergences ensured.

The minimal supersymmetric extension of the Standard Model with soft breaking terms included is called the Minimal Supersymmetric Standard Model (MSSM) [10, 11, 12], and is used for this analysis. In the MSSM with soft supersymmetry breaking, the supersymmetric coupling relations still hold.

To establish softly broken supersymmetry experimentally, several steps are necessary. First of all, the superpartner particles have to be discovered. In a next step, the quantum numbers of these particles, including their spin, have to be measured, making sure that these particles are indeed the superpartners of the Standard Model particles. However, even if all superpartners have been found, supersymmetry is not yet firmly established, and a last step is necessary: the verification of the supersymmetric coupling relations, which ensure the cancellation of quadratic divergences. Only then it can be said that supersymmetry is realized in nature.

The motivation for this investigation is the experimental verification of the supersymmetric coupling relation in the $SU(3)$ sector of the MSSM. This sector contains the spin-0 squarks ($\tilde{q}$) and the spin-$\frac{1}{2}$ gluinos ($\tilde{g}$) as superpartners of the quarks and gluons. The supersymmetric $SU(3)$ coupling relation requires equality of the gauge coupling appearing in the $q\bar{q}g$- and $\tilde{q}\bar{\tilde{q}}g$-vertices, and the Yukawa coupling appearing in the $q\bar{\tilde{q}}\tilde{g}$-vertex.

Due to the clean initial state and high luminosity, future e^+e^- linear colliders will be an ideal tool for a comparison of these couplings with high precision. The gauge coupling can be measured in the processes $e^+e^- \to q\bar{q}g$ or $e^+e^- \to \tilde{q}\bar{\tilde{q}}g$ in the 3-jet region. The Yukawa coupling can be obtained from studying the process $e^+e^- \to q\bar{\tilde{q}}\tilde{g}$, which contains the $q\bar{\tilde{q}}\tilde{g}$-vertex at tree level. Since an accurate and reliable theoretical prediction for these processes is needed for a precise verification of the supersymmetric coupling relations, and QCD radiative corrections are generally large, a complete calculation at next-to-leading order in α_s for these processes is necessary. The aim of this investigation is therefore the calculation of the total cross section for the process $e^+e^- \to q\bar{\tilde{q}}\tilde{g}$ in next-to-leading order in the strong coupling constant α_s.

Outline of the Thesis

The next two chapters are devoted to the presentation of the theory used as a framework for this calculation. In the next chapter, a short introduction and motivation to supersymmetry in general is given. In Chapter 3, we introduce the Minimal Supersymmetric Standard Model, which provides the framework for our calculation. The role of the gauge and Yukawa couplings in the QCD sector of the MSSM is discussed in detail.

Squark and gluino production at tree level in e^+e^- collisions will be reviewed in Chapter 4. Here, we will also discuss which processes are relevant for testing the supersymmetric coupling relations for different regions of parameter space. Furthermore, the notation for the NLO calculation is partially set up in this chapter.

The calculation of the NLO corrections to the process $e^+e^- \to q\bar{\tilde{q}}\tilde{g}$ is presented in detail in Chapter 5, where the numerical results are also shown, and finally, conclusions are drawn in Chapter 6.

The complete set of Feynman rules used is given in Appendix A. Appendix B contains the total cross section for $e^+e^- \to q\bar{\tilde{q}}\tilde{g}$ in leading order. The scalar integrals that appear in the calculation of the virtual corrections are given in Appendix C, along with the soft integrals from the real corrections. Finally, Appendix D lists the mass and wave function renormalization constants explicitly.

Chapter 2

Supersymmetry

2.1 Motivation for supersymmetry

2.1.1 Hierarchy and naturalness problems

Though the Standard Model is very successful at energies up to the electroweak scale, it can only be an effective theory, that is not valid up to arbitrarily high energies. For example, it does not incorporate gravity, which however will become strong at the Planck scale $M_P \approx 10^{19}\,\mathrm{GeV}$, making it necessary to extend the Standard Model at this scale. Furthermore, grand unification may be realized in nature with GUT scales in the range $10^{14} - 10^{16}\,\mathrm{GeV}$, as suggested by the renormalization group evolution of the Standard Model gauge couplings. However, if there is no new physics between such a high scale and the electroweak scale (grand desert scenario), several problems arise. First, the large hierarchy between the electroweak scale $M_{\mathrm{ew}} \approx 100\,\mathrm{GeV}$ and the Planck or the GUT scale cannot be explained by the Standard Model, a fact that is known as the hierarchy problem [13].

However, even once such a large hierarchy is introduced, it is not stable against radiative corrections within the Standard Model. This problem is known as the naturalness problem [8], and it arises if one calculates radiative corrections to the Higgs boson mass. Contributions originating from fermion loops are quadratically divergent. Cutting off the loop momentum integrations at the scale Λ, where new physics beyond the Standard Model enters, the leading divergences of these contributions are given by

$$\delta m_H^2 = -2\frac{\lambda_f^2}{16\pi^2}\Lambda^2 + \ldots, \tag{2.1}$$

where λ_f is the Higgs-fermion coupling. If one inserts the Planck mass M_P for Λ, the mass correction is of order M_P^2. The natural value for the Higgs mass is therefore of the order of the Planck scale. Of course the quadratic divergence

can be absorbed during the renormalization procedure by introducing a counterterm to cancel the Λ^2 term. But if this counterterm is to cancel the quadratic divergence nearly perfectly yielding a total mass correction that is several orders of magnitude smaller, an extreme amount of fine-tuning is necessary. This is generally considered as very unnatural. Note that for logarithmic divergences no fine-tuning is necessary, since $\log(m_P^2/m_{\text{ew}}^2) \approx \log(10^{34}) = \mathcal{O}(10)$, so that there is no problem for corrections to fermion or gauge boson masses. Thus, within the context of the Standard Model, the natural value of the electroweak scale is equal to the scale of new physics Λ, if fine-tuning is to be avoided.

The naturalness problem can be solved by introducing a pair of complex scalars associated with the fermion, that have the same quantum numbers as the fermion, and couple to the Higgs-boson with a coupling λ_S. They give another quadratically divergent contribution to the Higgs mass correction

$$\delta m_H^2 = 2\frac{\lambda_S}{16\pi^2}\Lambda^2 + \ldots, \tag{2.2}$$

that is equal to the fermion contribution, but with different sign due to the different statistics of the particles. If $\lambda_f^2 = \lambda_S$ the quadratic divergences from (2.1) and (2.2) cancel, and there only remain logarithmic divergences. Adjusting the couplings in this way to ensure the cancellation of the quadratic divergences is possible by imposing supersymmetry. This symmetry relates fermions and bosons, and as a consequence a supersymmetric theory contains associated bosons for all fermions in the theory and vice versa. These superpartners belong to the same representation of the gauge group and have the same quantum numbers and masses, apart from their spin, which differs by 1/2. Supersymmetry also relates the couplings of the fermions and the associated bosons in a way that ensures the cancellation of all quadratic divergences. This can be shown to be valid to all orders of perturbation theory. Supersymmetry is therefore able to stabilize large mass hierarchies against radiative corrections and thus solves the naturalness problem, though it can not explain the origin of such large hierarchies.

Though the quadratic divergences cancel in a supersymmetric theory, the mass correction still contains a finite term

$$\delta m_H^2 \propto \lambda_f^2(m_f^2 - m_{\tilde{f}}^2), \tag{2.3}$$

where m_f and $m_{\tilde{f}}$ are the masses of the fermion and the associated scalar in the loop. These masses would have to be equal, if supersymmetry was an exact symmetry of nature. But as will be explained below, supersymmetry has to be broken, allowing the masses to be different. However, if the mass difference appearing here is much larger than the electroweak scale the naturalness problem reappears. This is the reason why one generally expects supersymmetric particles to be not much heavier than about 1 TeV. Supersymmetry can therefore only solve the naturalness problem, if it is relevant in the vicinity of the electroweak scale.

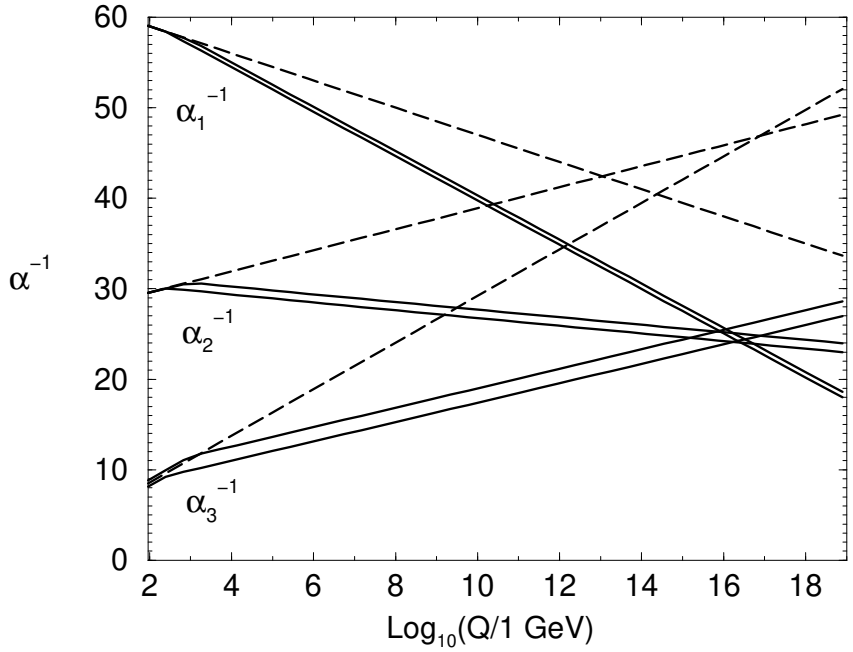

Figure 2.1: Renormalization group evolution of the inverse gauge couplings $\alpha_s^{-1}(Q)$ in the Standard Model (dashed lines) and the MSSM (solid lines) including two loop effects. In the MSSM case, $\alpha_3(m_Z)$ is varied between 0.113 and 0.123, and the sparticle mass thresholds between 250 GeV and 1 TeV. Figure from Ref. [15].

2.1.2 Coupling unification

Another hint for supersymmetry comes from the unification of coupling constants within the MSSM, which opens up the possibility of grand unification. In grand unified theories (GUT's) [14] the Standard Model gauge group $G_{\rm SM} = SU(3)_C \times SU(2)_L \times U(1)_Y$ is embedded at high energies into a larger GUT gauge group, like $SU(5)$ or $SO(10)$. This GUT symmetry is broken down to the Standard Model symmetry at the very high GUT scale $M_{\rm GUT}$. Since all gauge forces are unified at the GUT scale, there is only a single gauge coupling at this scale, and therefore the three Standard Model gauge couplings are equal at $M_{\rm GUT}$. The value of these couplings at the electroweak scale can therefore be calculated using the renormalization group equations. Alternatively, the measured values of the couplings at low energy can be evolved to higher scales, and these curves must meet in a single point if such a scenario is indeed realized in nature.

The three gauge couplings at different scales are related at one-loop by

$$\frac{1}{\alpha_i(Q)} = \frac{1}{\alpha_i(\mu)} + \frac{b_i}{2\pi} \log\left(\frac{\mu}{Q}\right). \tag{2.4}$$

The coefficients b_i depend on the particle content of the low-energy theory. In the Standard Model, they are given by

$$\begin{aligned} b_1 &= \frac{4}{3}N_g + \frac{N_H}{10} \\ b_2 &= -\frac{22}{3} + \frac{4}{3}N_g + \frac{N_H}{6} \\ b_3 &= -11 + \frac{4}{3}N_g, \end{aligned} \tag{2.5}$$

where $N_g = 3$ is the number of generations, and $N_H = 1$ the number of Higgs doublets. Using the measured values at $\mu = m_Z$ as input values, the evolution of the three inverse couplings is shown in Fig. 2.1. Obviously the running couplings do not meet in the Standard Model.

In the supersymmetric extension of the Standard Model, the additional particles modify the evolution equations. The coefficients b_i are given by [17]

$$\begin{aligned} b_1 &= 2N_g + \frac{3}{10}N_H \\ b_2 &= -6 + 2N_g + \frac{N_H}{2} \\ b_3 &= -9 + 2N_g. \end{aligned} \tag{2.6}$$

As will be explained below, a supersymmetric extension of the Standard Model needs two Higgs doublets, thus $N_H = 2$. The resulting evolution of the inverse couplings is also shown in Fig. 2.1. In this case the couplings do indeed meet at a scale $M \approx 10^{16}\,\mathrm{GeV}$ [18].

Equivalently, by postulating the three couplings to meet, the value of the weak mixing angle at the electroweak scale can be predicted from the measured values of α_{em} and α_s. While the Standard Model prediction is far from the measured value, the prediction of supersymmetry agrees with the experimental value with an accuracy of about 2%. Supersymmetry therefore allows the embedding of the weak scale theory into a grand unified theory at high energies, whereas this is not possible in the non-supersymmetric Standard Model.

2.1.3 Haag-Lopuszanski-Sohnius theorem

Since symmetries have played a great role in physics, it is natural to ask if the symmetries of the Standard Model can be extended in any way. This question has been answered by a series of so called No-Go theorems culminating in the Coleman-Mandula theorem [19]. It states that the most general symmetry an interacting quantum field theory can possess is the Poincaré symmetry of space-time plus an arbitrary number of additional internal symmetries, like e.g. gauge symmetries. But it is possible to circumvent this No-Go theorem allowing a real extension of the Poincaré symmetry by including also fermionic symmetry

generators in addition to the usual bosonic ones. These fermionic symmetry generators connect bosons and fermions with each other. The symmetry algebra will then be a Z_2-graded Lie algebra, which is given in terms of commutators as well as anticommutators. The most general symmetry of this type with a non-trivial S-matrix is N-extended supersymmetry [20]. It contains N sets of 2 component Weyl spinors Q^i_α, $\bar{Q}^i_{\dot{\alpha}}$ $(i = 1 \dots N)$ in addition to the generators of the Poincaré algebra. Though extended supersymmetry has some remarkable properties, e.g. $N = 4$ supersymmetric theories are completely finite [21], it cannot be relevant for physics at the electroweak scale since in 4 space-time dimensions it does not allow chiral fermions or parity violation which are both needed in Standard Model. Therefore only $N = 1$ supersymmetric models can be phenomenologically relevant, and only these will be considered below.

2.1.4 Incorporation of gravity

For studying low energy phenomenology, supersymmetry is realized as a global symmetry. But it can also be realized as a local symmetry. In analogy to usual gauge theories, promoting supersymmetry to a local symmetry makes it necessary to introduce additional gauge fields to maintain invariance of the theory [22]. In the case of local supersymmetry these additional fields are the spin 2 graviton and its superpartner, the spin 3/2 gravitino, which are both massless. The resulting theory therefore incorporates gravity. It can also be seen from the supersymmetry algebra that invariance under local supersymmetry transformations implies invariance under local coordinate changes. This is however the invariance principle General Relativity is based upon. Local supersymmetry therefore naturally incorporates gravity, and is also called supergravity [23]. However, supergravity is a non-renormalizable theory and can not be seen as a full quantum theory of gravity.

2.2 The supersymmetry algebra

As already mentioned, the supersymmetry algebra is an extension of the Poincaré algebra. The Poincaré algebra itself contains the generators of space-time translations P_μ and the generators of rotations and Lorentz boosts $M_{\mu\nu}$. In addition to these the supersymmetry algebra includes the fermionic generators of supersymmetry transformations Q_α and $\bar{Q}_{\dot{\alpha}}$, which are left-handed and right-handed

2-component Weyl-spinors. The supersymmetry algebra is given by

$$\begin{aligned}
\{Q_\alpha, \bar{Q}_{\dot{\beta}}\} &= 2\sigma^\mu_{\alpha\dot{\beta}} P_\mu \\
\{Q_\alpha, Q_\beta\} &= \{\bar{Q}_{\dot{\alpha}}, \bar{Q}_{\dot{\beta}}\} = 0 \\
[P^\mu, Q_\alpha] &= [P^\mu, \bar{Q}_{\dot{\alpha}}] = 0 \\
[M^{\mu\nu}, Q_\alpha] &= -i(\sigma^{\mu\nu} Q)_\alpha \\
[M^{\mu\nu}, \bar{Q}^{\dot{\alpha}}] &= -i(\bar{\sigma}^{\mu\nu} \bar{Q})^{\dot{\alpha}}
\end{aligned} \tag{2.7}$$

where $\sigma^\mu = (\mathbf{1}, \sigma^\mathbf{i})$, $\bar{\sigma}^\mu = (\mathbf{1}, -\sigma^\mathbf{i})$ with the Pauli matrices $\sigma^\mathbf{i}$, and $\sigma^{\mu\nu} = \frac{1}{4}(\sigma^\mu \bar{\sigma}^\nu - \sigma^\nu \bar{\sigma}^\mu)$. The last two relations of the algebra express the fact that the supersymmetry generators transform as spinors under Lorentz transformations and rotations. Since the generators of supersymmetry transformations are fermionic objects, supersymmetry connects bosons and fermions.

In a theory with unbroken supersymmetry, the one-particle states form a representation of the supersymmetry algebra. The one-particle states fall into irreducible representations, which are known as supermultiplets. The various particles in a supermultiplet are called superpartners and the corresponding quantum fields are called component fields.

Since the mass^2 operator P^2 obviously commutes with the supersymmetry generators, all particles in a supermultiplet have equal masses. The supersymmetry generators also commute with all generators of the internal gauge symmetries. Therefore all particles in a supermultiplet belong to the same representation of the gauge group, and have the same gauge quantum numbers. The supersymmetry generators do however not commute with the generalised spin operator $W^2 = W^\mu W_\mu$, where $W^\mu = \frac{1}{2}\epsilon_{\mu\nu\rho\sigma} P^\nu M^{\rho\sigma}$ is the Pauli-Lubanski vector. Though W^2 is a Casimir operator of the Poincaré algebra, it is no Casimir operator of the supersymmetry algebra, implying that supermultiplets contain particles of different spin. Explicit construction of the supermultiplets shows that they contain fermions and bosons with spins differing by $\frac{1}{2}$. It can furthermore be shown that supermultiplets contain an equal number of bosonic and fermionic degrees of freedom.

Supersymmetry therefore predicts that for each fermion in the theory there is a corresponding boson with the same mass and gauge quantum numbers and vice versa. The mass degeneracy of superpartners can however be removed if supersymmetry is broken. Since none of the superpartners of the Standard Model particles have been discovered so far, their masses must be significantly greater than the masses of their Standard Model counterparts. If supersymmetry is realized in nature it has to be broken.

2.3 Construction of supersymmetric Lagrangians

In this section we will give a brief introduction to the construction of supersymmetric Lagrangians. Since this construction is in general rather complicated only a general overview of the method will be given. A detailed account of the procedure and the necessary formalism can be found in the literature [24, 25].

In principle such a construction could be done in terms of the component fields of the theory once the particle content has been chosen. Writing down a Lagrangian invariant under the required gauge symmetries and under supersymmetry is however very complicated. Though it is simple to write down gauge invariant terms, these terms are not invariant under supersymmetry transformations, because it mixes bosonic and fermionic fields. Instead, only cancellation of the variations of several terms render the Lagrangian invariant under supersymmetry. It is therefore much more convenient to use the fact that the fields of a supersymmetric theory can be classified into supermultiplets, consisting of fields that transform into each other under supersymmetry transformations. Superfields can be assembled from these component fields of a supermultiplet, providing the building blocks for the further construction of the supersymmetric Lagrangian. Introducing anticommuting coordinates θ and $\bar{\theta}$, the 4-dimensional space-time can be extended to superspace, labelled by $z = (x, \theta, \bar{\theta})$. Superfields can be written as functions in superspace $\hat{F} = \hat{F}(z) = \hat{F}(x, \theta, \bar{\theta})$. By expanding a superfield in a power series in θ and $\bar{\theta}$, the component fields are recovered as the coefficients. Using this superfield approach, Lagrangians that are manifestly invariant under gauge symmetries and supersymmetry can be easily written down.

Two types of superfields are relevant for a low-energy supersymmetric theory. The first one is the complex chiral superfield $\hat{\phi} = (A, \psi_L, F)$, containing a complex left-handed Weyl-spinor ψ_L and two complex scalars A and F. The auxiliary field F does not have a kinetic term and can therefore be eliminated from the Lagrangian using the equations of motion. The other relevant superfield is the real vector superfield $\hat{V} = (\lambda_L, V^\mu, D)$, which in the Wess-Zumino gauge contains a complex left-handed Weyl-spinor λ_L, a real massless vector field V^μ and an auxiliary real scalar field D. The auxiliary D field can again be eliminated by its equations of motion. In accordance with supersymmetry the chiral and vector superfields both contain the same number of fermionic and bosonic degrees of freedom. The gauge fields of a low energy supersymmetric theory can be accommodated within vector superfields, whereas the matter fermions as well as the Higgs particles fall into chiral superfields.

The elementary superfields can be combined to form new composite superfields. The product of any number of chiral superfields is again a chiral superfield. Similarly, the product of a chiral superfield with its complex conjugate or the product of several vector superfields is again a vector superfield. Furthermore, by integrating a superfield over the anticommuting coordinates of superspace, an expression transforming into a total derivative under supersymmetry transforma-

tions is obtained. This yields an invariant action, if surface terms are neglected. Thus, by using the basic gauge and matter superfields to construct composite chiral and vector superfields and integrating out the anticommuting coordinates of superspace, supersymmetric Lagrangians can be easily constructed. For a chiral superfield the superspace integration extracts the F component field, while the D component field is extracted from a vector superfield.

We will now shortly present all possible renormalizable supersymmetric terms for a general non-abelian gauge theory in terms of superfields.

2.3.1 Gauge kinetic terms

In a non-supersymmetric gauge theory, the kinetic energy terms for the gauge fields are given by $\mathcal{L}_{\text{gauge}} = -\frac{1}{4}F^a_{\mu\nu}F^{a\mu\nu}$, with the field strength tensor $F^a_{\mu\nu}$ defined in terms of the gauge field V^a_μ. This term does not only contain the kinetic terms of gauge fields, but for a non-abelian gauge theory also the 3- and 4-gauge boson self interactions.

The supersymmetric generalisation of the field strength tensor is the chiral spinor superfield $\hat{W}^\alpha$, which can be defined in terms of the gauge vector superfield $\hat{V}^a$. The supersymmetric gauge kinetic term is given by

$$\mathcal{L}_{\text{gauge}} = \left[\hat{W}^\alpha \hat{W}_\alpha\right]_F + \text{h.c.}, \tag{2.8}$$

where $[\dots]_F$ denotes the F-component of the chiral superfield in brackets. This term includes the kinetic terms for the gauge boson, and the usual gauge boson self interactions known from the non-supersymmetric theory. It also includes the kinetic term for the Majorana gaugino. In addition to these, it contains a gaugino gauge-boson interaction, in component fields given by

$$\mathcal{L}_{V\tilde{V}\tilde{V}} = \frac{1}{2}igf_{abc}\bar{\tilde{V}}^a\gamma^\mu\tilde{V}^bV^c_\mu, \tag{2.9}$$

where $\tilde{V}^a$ denotes the 4-component Majorana spinor of the gaugino. This interaction does not appear for a $U(1)$ gauge group, because the structure constants f_{abc} vanish in this case.

2.3.2 Matter kinetic terms

In an ordinary gauge theory the interactions of the fermionic and scalar matter fields with the gauge fields are governed by gauge invariance. To ensure gauge invariance the ordinary space-time derivatives in the kinetic terms of matter fields have to be replaced by gauge covariant derivatives. This uniquely determines the gauge matter interactions.

The supersymmetric generalisation of such a gauge covariant kinetic term for a matter superfield $\hat{\phi}$ is given by

$$\mathcal{L}_{\text{matter, kin}} = \left[\hat{\phi}^+ e^{2g\hat{V}}\hat{\phi}\right]_D = \left[\hat{\phi}^+\hat{\phi} + 2g\hat{\phi}^+\hat{V}\hat{\phi} + 2g^2\hat{\phi}^+\hat{V}^2\hat{\phi}\right]_D, \tag{2.10}$$

where the subscript D stands for the extraction of the D-component. Furthermore, we have defined $\hat{V} = T^a\hat{V}^a$, with the generators of the gauge group in the representation of the matter superfield $\hat{\phi}$ denoted by T^a. The expansion of the exponential does only generate terms at most quadratic in the vector superfield, since $\hat{V}^3 = 0$ in the Wess-Zumino gauge. The first term on the r.h.s. yields the purely kinetic terms of the matter fields. The interactions of matter fields with the gauge supermultiplet are contained in the last two terms. These do of course include the interactions between gauge bosons and fermionic as well as scalar matter fields required by gauge invariance. Additionally, these also yield a gaugino-fermion-sfermion interaction of the form

$$\mathcal{L}_{\tilde{V}\psi A} = -\sqrt{2}gT^a_{ij}\left(\bar{\tilde{V}}^a P_L\psi_j A_i^* + \bar{\psi}_j P_R\tilde{V}^a A_i\right), \tag{2.11}$$

where ψ and A are the fermionic and bosonic component fields of the matter superfield $\hat{\phi}$, and $P_{R,L} = \frac{1}{2}(1 \pm \gamma_5)$ are the chiral projection operators. This interaction term is not required by gauge invariance, but is necessary to render the Lagrangian invariant under supersymmetry.

2.3.3 Matter self interactions

The kinetic terms of the Lagrangian shown so far are completely fixed by the requirements of gauge invariance and supersymmetry once the particle content and the gauge group have been chosen, and the matter supermultiplets have been assigned to representations of the gauge group. The only freedom in the construction of the Lagrangian remains in the choice of the so-called superpotential $W(\hat{\phi}_i)$, which is a chiral superfield. It is a polynomial in the chiral matter superfields of the theory and determines their self-interactions. If renormalizability is imposed the superpotential can be at most cubic in the matter superfields, and can be written as

$$W(\hat{\phi}_i) = m_{ij}\hat{\phi}_i\hat{\phi}_j + \lambda_{ijk}\hat{\phi}_i\hat{\phi}_j\hat{\phi}_k. \tag{2.12}$$

The linear term has been omitted here, since it can be absorbed by a redefinition of the superfields. The mass matrix m_{ij} and the dimensionless couplings λ_{ijk} can be chosen arbitrarily under the restriction that the superpotential has to be gauge invariant. The matter self interaction term in the Lagrangian is given by

$$\mathcal{L}_{\text{matter, int}} = \left[W(\hat{\phi}_i)\right]_F + \text{h.c.} \tag{2.13}$$

It contains mass terms for the matter fields as well as Yukawa-type interactions. In a supersymmetric extension of the Standard Model the Higgs Yukawa terms giving masses to the fermions via the Higgs mechanism are contained in this term.

2.3.4 D-terms and F-terms

The terms given above yield the most general Lagrangian of a renormalizable supersymmetric gauge theory. However, if the Lagrangian is written down in terms of the component fields, it still contains the auxiliary F and D fields of the chiral and vector superfields. The elimination of these auxiliary fields using the equations of motion leads to self interactions among the scalar fields, that we will now discuss.

The D-terms of the component field Lagrangian originate from the kinetic term of the gauge multiplet and the kinetic terms of the matter fields. It is given by

$$\mathcal{L}_D = \frac{1}{2} D^a D^a + g D^a A_i^* T_{ij}^a A_j, \tag{2.14}$$

where A_i is the scalar field component of the chiral superfield $\hat{\phi}$. A summation over all matter supermultiplets is performed implicitly in the last term. The equation of motions for D^a are very simple

$$D^a = -g A_i^* T_{ij}^a A_j, \tag{2.15}$$

and can be substituted back into $\mathcal{L}_D$. The resulting D^a term contribution to the Lagrangian reads

$$\mathcal{L}_D = -\frac{1}{2} D^a D^a, \tag{2.16}$$

where D^a is given by (2.15). It gives rise to interactions among 4 scalar particles.

The F-terms arise from the kinetic terms of the matter supermultiplets and the superpotential. They can be written as

$$\mathcal{L}_F = F_i^* F_i + \left(\frac{\partial W}{\partial A_i} F_i + \text{h.c.} \right), \tag{2.17}$$

with the auxiliary component of the matter superfield $\hat{\phi}$ denoted by F_i. The derivative of the superpotential appearing above is defined by first substituting the A_i fields for the $\hat{\phi}$ superfields in $W(\hat{\phi})$ and then calculating the derivative. The equations of motion for F_i are again trivial

$$F_i^* = -\frac{\partial W}{\partial A_i} \qquad\qquad F_i = -\left(\frac{\partial W}{\partial A_i} \right)^* . \tag{2.18}$$

After substituting them back into (2.17) the F-term contribution to the Lagrangian is given by

$$\mathcal{L}_F = -F_i^* F_i, \tag{2.19}$$

with F_i given by (2.18). This contribution contains the mass terms for the scalar fields as well as cubic and quartic scalar self interactions.

Chapter 3

Minimal Supersymmetric Standard Model

3.1 Particle content

The minimal supersymmetric extension of the Standard Model (MSSM) [10, 11, 12] is obtained by taking the Standard Model as a starting point and then adding the corresponding superpartners of all particles. In addition to these the model contains two Higgs doublets with opposite hypercharge. This is the minimal structure of the Higgs sector in a supersymmetric theory, because the superpotential must not contain complex conjugate superfields, making it impossible to generate masses for up-type and down-type fermions with only one Higgs doublet. Furthermore, the anomalies from the fermionic superpartners of the Higgs scalars only cancel with two Higgs doublets. The MSSM therefore contains 5 physical Higgs bosons after electroweak symmetry breaking. The resulting particle content of the MSSM is shown in Tabs. 3.1 and 3.2. Superpartners of Standard Model particles are denoted by a tilde. The names of the fermionic superpartners are obtained by appending -ino to the name of the boson, while the scalar superpartners of fermions receive a prefix s- before the fermion name. Thus the superpartners of the gauge bosons (gluon, W^a and B) are called gauginos (gluino, Wino and Bino), and the fermionic partners of the Higgs scalars are called Higgsinos. The scalar superpartners of the leptons and quarks are the sleptons and squarks[1]. The Tabs. 3.1 and 3.2 list the interaction eigenstates, and states with the same $SU(3) \times U(1)_{\mathrm{em}}$ quantum numbers can mix to form mass eigenstates. For example, the charged Winos and higgsinos mix to form the charginos $\tilde{\chi}_i^{\pm}$ $(i = 1, 2)$, while the neutral Wino, the Bino and the neutral higgsinos mix to form the neutralinos $\tilde{\chi}_i^0$ $(i = 1, \ldots, 4)$.

[1]Sfermions, i.e. sleptons and squarks, carry an index L or R, which denotes the chirality of their fermionic superpartner. As spin 0 particles they do not possess a chirality, but are nevertheless usually called left-handed or right-handed sfermions.

Superfield	Spin 1 Bosons	Spin $\frac{1}{2}$ Fermions	$SU(3)_C$	$SU(2)_L$	$U(1)_Y$
$\hat{G}$	g	$\tilde{g}$	8	1	0
$\hat{W}^a$	W^a	$\tilde{W}^a$	1	3	0
$\hat{B}$	B	$\tilde{B}$	1	1	0

Table 3.1: Particle content of the MSSM, vector supermultiplets.

Superfield	Spin 0 Bosons	Spin $\frac{1}{2}$ Fermions	$SU(3)_C$	$SU(2)_L$	$U(1)_Y$
$\hat{L}$	$\tilde{L} = (\tilde{\nu}_L, \tilde{e}_L)$	(ν_L, e_L)	1	2	$-\frac{1}{2}$
$\hat{E}$	$\tilde{E} = \tilde{e}_R^*$	e_L^c	1	1	1
$\hat{Q}$	$\tilde{Q} = (\tilde{u}_L, \tilde{d}_L)$	(u_L, d_L)	3	2	1/6
$\hat{U}$	$\tilde{U} = \tilde{u}_R^*$	u_L^c	$\bar{3}$	1	$-2/3$
$\hat{D}$	$\tilde{D} = \tilde{d}_R^*$	d_L^c	$\bar{3}$	1	1/3
$\hat{H}_1$	(H_1^0, H_1^-)	$(\tilde{H}_1^0, \tilde{H}_1^-)_L$	1	2	$-\frac{1}{2}$
$\hat{H}_1$	(H_2^+, H_2^0)	$(\tilde{H}_2^+, \tilde{H}_2^0)_L$	1	2	$\frac{1}{2}$

Table 3.2: Particle content of the MSSM, matter supermultiplets. Charge conjugate fermion fields are denoted by f^c.

Given the particle content, the Lagrangian of the MSSM can now be constructed as described in Section 2.3. The generalised gauge covariant kinetic terms for the gauge fields, the matter and the Higgs multiplets are completely fixed by requiring gauge and supersymmetry invariance. This leaves only the superpotential to be chosen.

3.2 R parity

The most general superpotential for the MSSM respecting gauge invariance is given by

$$W = W_R + W_{\not R}, \tag{3.1}$$

with

$$W_R = \epsilon_{ij}\left[h_\tau \hat{H}_1^i \hat{L}^j \hat{E} + h_b \hat{H}_1^i \hat{Q}^j \hat{D} - h_t \hat{H}_2^i \hat{Q}^j \hat{U} - \mu \hat{H}_1^i \hat{H}_2^j\right] \tag{3.2}$$

$$W_{\not R} = \epsilon_{ij}\left[\lambda_1 \hat{L}^i \hat{L}^j \hat{E} + \lambda_2 \hat{L}^i \hat{Q}^j \hat{D} - \mu' \hat{L}^i \hat{H}_2^j\right] + \lambda_3 \hat{U}\hat{D}\hat{D}. \tag{3.3}$$

Here $\epsilon_{ij} = -\epsilon_{ji}$ (with $\epsilon_{12} = +1$) contracts the $SU(2)$ indices i and j, the Yukawa couplings h_τ, h_b and h_t are 3×3 matrices in generation space and μ is the Higgs

superfield mass parameter. The first part, W_R, contains the Yukawa interactions that give masses to fermions via the Higgs mechanism. Since the superpotential must not contain complex conjugate superfields, the second Higgs doublet $\hat{H}_2$ is needed to give masses to up-type quarks.

However, the interactions of the second part, $W_{\not R}$, violate baryon number (B) or lepton number (L) at tree level

$$\begin{array}{cc} \hat{L}\hat{L}\hat{E}, \hat{L}\hat{Q}\hat{D}, \hat{L}\hat{H} & \Delta L \neq 0, \\ \hat{U}\hat{D}\hat{D} & \Delta B \neq 0. \end{array} \tag{3.4}$$

Whereas gauge symmetry alone has been enough to forbid B or L violating terms of mass dimension 4 or less in the Standard Model, this not the case anymore in the MSSM. These interactions can mediate fast proton decay at tree level, if λ_2 and λ_3 are both nonzero. Since proton decay has not been observed, the product $\lambda_2\lambda_3$ has to be extremely small. Less severe but nevertheless significant constraints on different combinations of the R-parity violating couplings come from other processes [26]. Settings these couplings to values small enough to evade the experimental bounds is in principle possible, but is considered unsatisfactory and a discrete symmetry is invoked instead to forbid the interactions in $W_{\not R}$.

This discrete Z_2 symmetry is called R-parity [27], and can be defined as

$$R = (-1)^{3(B-L)+2S} \tag{3.5}$$

for a particle of spin S, baryon number B and lepton number L. All Standard Model particle have $R = +1$, whereas their supersymmetric partners have $R = -1$. As a consequence supersymmetric particles can only be produced in pairs in a collider experiment and the lightest supersymmetric particle (LSP) is stable. For cosmological reasons the LSP must also be colour and charge neutral and thus interacts only weakly with ordinary particles. It will therefore escape undetected in experiments giving rise to the missing energy signature of supersymmetric particles. The LSP is also a good candidate for cold dark matter [28].

3.3 Soft supersymmetry breaking

In the model constructed so far supersymmetry is still an exact symmetry, though it has to be broken in nature as was argued above. Since spontaneous symmetry breaking is very attractive, one could try to construct a mechanism that breaks supersymmetry spontaneously inside the MSSM. This has been attempted in the past without success. The main problems in this scheme are mass sum rules which require at least some of the superpartners in a supermultiplet to be lighter than their Standard Model counterparts. Since this is phenomenologically unacceptable one now believes that there is an additional sector in which supersymmetry is broken spontaneously. This sector does not directly couple to the Standard

Model particles and is therefore hidden. The supersymmetry breaking is communicated to the MSSM by common interactions shared by both sectors, giving rise to effective supersymmetry breaking terms at the electroweak scale. Models have been successfully constructed in which supersymmetry breaking is communicated to the MSSM by gravitational interactions [11] or by new gauge forces [29].

For phenomenological purposes one can adopt the point of view that effective supersymmetry breaking terms at the electroweak scale are generated by some unknown breaking mechanism and simply include all supersymmetry breaking terms compatible with renormalizability, gauge symmetry and R-parity. But if broken supersymmetry is still to solve the hierarchy problem, only terms which do not reintroduce quadratic divergences can be allowed. These so-called soft breaking terms are [30]

- gaugino mass terms,
- mass terms for all scalar particles, including scalar superpartners of Standard Model fermions as well as the Higgs scalars,
- trilinear interactions among scalar particles.

These breaking terms supply masses for all superpartner particles, which can therefore become arbitrarily heavy, evading experimental mass bounds. It is important to note that the equality of gauge couplings and supersymmetric Yukawa couplings is still maintained in softly broken supersymmetry. This is of course necessary because it ensures the cancellation of quadratic divergences.

3.4 Supersymmetric QCD

For the calculation of squark and gluino production processes only the supersymmetric QCD sector of the MSSM is needed besides the Standard Model. Supersymmetric QCD contains gluinos ($\tilde{g}$) and squarks ($\tilde{q}_L$,$\tilde{q}_R$) in addition to the quarks (q) and gluons (g) of usual QCD. The superpartner of the gluon, the gluino, is a Majorana fermion transforming according to the the adjoint representation of $SU(3)$. The superpartners of the left- and right-handed quarks, the L- and R-squarks, are scalar particles forming a fundamental representation of $SU(3)$.

The soft supersymmetry breaking terms can in principle lead to mixing of L- and R-squarks as well as to mixing between squarks of different flavours. We will assume that there is no flavour mixing in the following. Since the non-diagonal terms in the L/R squark mass matrix are proportional to the corresponding quark mass, mixing can be ignored for the five light-flavour squarks, i.e. the superpartners of the five light quarks. Only for stops L/R-mixing is relevant. But since in this calculation stops do only occur inside loops we neglect L/R-mixing also for stops. Besides neglecting squark mixing, we also assume all

squarks including the stops to be mass degenerate. In the quark sector, we treat the five light flavours as massless, only the top quark mass is non-zero, with $m_t = 175\,\mathrm{GeV}$.

With these assumptions, the complete Lagrangian for SUSY QCD including the gauge fixing and ghost part is given by [12]

$$\begin{aligned}
\mathcal{L}_{\mathrm{SQCD}} &= \mathcal{L}_{\mathrm{gauge}} + \mathcal{L}_{\mathrm{matter}} + \mathcal{L}_{\mathrm{GF}} + \mathcal{L}_{\mathrm{FP}} \\
\mathcal{L}_{\mathrm{gauge}} &= -\frac{1}{4} G^a_{\mu\nu} G^{a\mu\nu} + \frac{1}{2} \bar{\tilde{g}}^a (i \not{D}^{ab} - m_{\tilde{g}} \delta^{ab}) \tilde{g}^b \\
\mathcal{L}_{\mathrm{matter}} &= \bar{q}(i \not{D} - m_q) q + (D_\mu \tilde{q})^* (D^\mu \tilde{q}) - m^2_{\tilde{q}} \tilde{q}^* \tilde{q} - \frac{1}{2} D^a D^a \\
&\quad - \sqrt{2} \hat{g}_3 T^a_{ij} \left(\bar{\tilde{g}}_a P_L q^j \tilde{q}^{i*}_L + \bar{q}^i P_R \tilde{g}_a \tilde{q}^j_L - \bar{\tilde{g}}_a P_R q^j \tilde{q}^{i*}_R - \bar{q}^i P_L \tilde{g}_a \tilde{q}^j_R \right) \\
\mathcal{L}_{\mathrm{GF}} &= -\frac{1}{2\xi} (\partial_\mu G^{a\mu})^2 \\
\mathcal{L}_{\mathrm{FP}} &= (\partial^\mu \bar{c}^a) D^{ab}_\mu c^b,
\end{aligned} \tag{3.6}$$

with the gluon field strength tensor defined by

$$G^a_{\mu\nu} = \partial_\mu G^a_\nu - \partial_\nu G^a_\nu - g_3 f^{abc} G^b_\mu G^c_\nu. \tag{3.7}$$

The gauge covariant derivatives in the fundamental and the adjoint representation are given by

$$\begin{aligned}
D_\mu &= \partial_\mu + i g_3 T^a G^a_\mu \\
D^{ab}_\mu &= \partial_\mu \delta^{ab} + i g_3 (T^c)^{ab} G^c_\mu \\
&= \partial_\mu \delta^{ab} + g_3 f^{abc} G^c_\mu,
\end{aligned} \tag{3.8}$$

with the generators of $SU(3)$ in the adjoint representation defined by $(T^a)^{bc} = -if^{abc}$. Finally, D^a is the auxiliary component of the gluon vector superfield. It gives rise to four-squark interactions, after eliminating it by its equation of motion

$$D^a = -\hat{g}'_3 \sum_g \left(\tilde{Q}^*_g T^a \tilde{Q}_g - \tilde{U}_g T^{a*} \tilde{U}_g - \tilde{D}_g T^{a*} \tilde{D}_g \right), \tag{3.9}$$

where a sum over all three generations is included using the index g, and the quark fields are written in the notation of Tab. 3.2.

In the Lagrangian given above we have denoted the strong coupling constant with g_3, the supersymmetric Yukawa coupling with $\hat{g}_3$, and the four-squark coupling with $\hat{g}'_3$. These three couplings are numerically equal, and the reason to distinguish between them will be explained in the next section.

We will use the Feynman gauge, i.e. $\xi = 1$, in our calculation. The effects of soft supersymmetry breaking are accounted for in the Lagrangian by the explicit gluino mass term, and different quark and squark masses. Trilinear scalar interactions of coloured particles do not appear, because they are forbidden by gauge invariance.

The interactions of the SUSY QCD particles with photons and Z^0's can be determined by including the electroweak gauge fields in the covariant derivatives. The corresponding terms in the Lagrangian are given by

$$\begin{aligned}
\mathcal{L}_{\text{SQCD-EW}} &= \mathcal{L}_{q\bar{q}\gamma} + \mathcal{L}_{q\bar{q}Z} + \mathcal{L}_{\tilde{q}\tilde{q}V} + \mathcal{L}_{\tilde{q}\tilde{q}gV} \\
\mathcal{L}_{q\bar{q}\gamma} &= -eQ_q A^\mu \bar{q}\gamma_\mu q \\
\mathcal{L}_{q\bar{q}Z} &= -e\frac{e}{c_w s_w} Z_\mu \bar{q}\gamma^\mu \left[\left(\frac{T_3^L}{2} - Q_q s_w^2\right) + \frac{T_3^L}{2}\gamma_5\right] q \\
\mathcal{L}_{\tilde{q}\tilde{q}V} &= -\frac{ie}{c_w s_w} Z_\mu \left(T_3^{\tilde{q}} - Q_{\tilde{q}} s_w^2\right) \tilde{q}_i^* \overset{\leftrightarrow}{\partial^\mu} \tilde{q}_i - ieA_\mu Q_{\tilde{q}} \tilde{q}_i^* \overset{\leftrightarrow}{\partial^\mu} \tilde{q}_i \\
\mathcal{L}_{\tilde{q}\tilde{q}gV} &= 2eg_3 A_\mu G_a^\mu Q_{\tilde{q}} \tilde{q}_i^* T_{ij}^a \tilde{q}_j + 2\frac{eg_3}{c_w s_w} Z_\mu G_a^\mu \left(T_3^{\tilde{q}} - Q_{\tilde{q}} s_w^2\right) \tilde{q}_i^* T_{ij}^a \tilde{q}_j, \qquad (3.10)
\end{aligned}$$

where $s_w = \sin\theta_W$, $c_w = \cos\theta_W$, $T_3^{\tilde{q}} = \pm\frac{1}{2}$ for L-squarks, and $T_3^{\tilde{q}} = 0$ for R-squarks, and the charge Q is given in units of the positron charge e. The unusual $\tilde{q}\bar{\tilde{q}}gV$ interaction for $V = \gamma, Z^0$ appears as a consequence of gauge invariance, since squarks transform nontrivially under both $SU(3)$ and $SU(2) \times U(1)$. The full set of Feynman rules for supersymmetric QCD is given in Appendix A.

3.5 Gauge and Yukawa couplings

We will now discuss gauge and supersymmetry invariance of the SUSY-QCD Lagrangian and the related issue of gauge and Yukawa couplings. Apart from the ghost and gauge fixing parts, the Lagrangian presented in the previous section is invariant under infinitesimal $SU(3)$ gauge transformations, given by

$$\begin{aligned}
\delta G_\mu^a &= -f^{abc}\theta^b G_\mu^c - \frac{1}{g_3}\partial_\mu \theta^a \\
\delta q &= i\theta^a T^a q \\
\delta \tilde{q} &= i\theta^a T^a \tilde{q} \\
\delta \tilde{g}^a &= i\theta^b (T^b)_{ac} \tilde{g}^c = -f^{abc}\theta^b \tilde{g}^c, \qquad (3.11)
\end{aligned}$$

and parameterised by the space-time dependent functions $\theta^a(x)$. The kinetic terms of the coloured particles are written in a manifestly gauge invariant way by using the gluon field strength tensor $G_{\mu\nu}^a$ and the gauge covariant derivatives D_μ for the fundamental and D_μ^{ab} for the adjoint representation. Of course, gauge invariance can only be achieved if the coupling constants appearing in the covariant derivatives and the definition of the gluon field strength tensor are the same. Gauge invariance thus fixes the $q\bar{q}g$-, $\tilde{q}\bar{\tilde{q}}g$-, and the $\tilde{g}\tilde{g}g$-couplings to be identical to the 3-gluon coupling. Gauge invariance also fixes the strong coupling appearing in the $\tilde{q}\tilde{q}gV$-interaction to the 3-gluon coupling, though this is not apparent, because $\mathcal{L}_{\text{SQCD-EW}}$ is not written in a manifestly gauge invariant way.

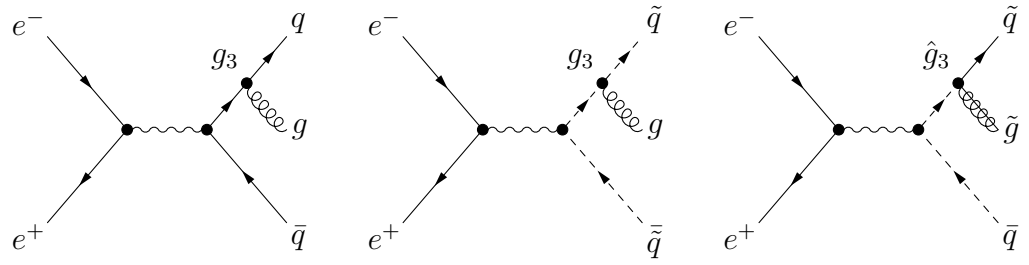

Figure 3.1: Selected Feynman diagrams for processes involving the strong gauge coupling g_3 or the Yukawa coupling $\hat{g}_3$. $SU(3)$ couplings are explicitly shown at vertices.

However, the couplings $\hat{g}_3$ and $\hat{g}'_3$ are not fixed by gauge invariance. The four $q\tilde{q}\tilde{g}$ interaction terms are each separately gauge invariant, regardless of the value of $\hat{g}_3$. All four of these terms contain the same coupling $\hat{g}_3$, because they are mixed by C- and P-transformations, both conserved symmetries of the strong interactions. The four-squark interaction term is also separately invariant under gauge transformations. Thus, if the theory were non-supersymmetric, $\hat{g}_3$ and $\hat{g}'_3$ could be chosen arbitrarily without spoiling gauge invariance.

It is only the requirement of invariance under supersymmetry transformations that ensures the relation

$$g_3 = \hat{g}_3 = \hat{g}'_3, \tag{3.12}$$

and therefore fixes the SUSY-Yukawa and the four-squark couplings. This can easily be understood in the light of the discussion of Section 2.3. The gaugino-fermion-sfermion interaction is obtained from the generalised kinetic terms of the matter supermultiplets. Since the coupling g appearing in this term has to be the gauge coupling to ensure gauge invariance, the gaugino-fermion-sfermion interaction is also fixed. Essentially the same argument applies to the four-squark interactions. The coupling relation (3.12) is also valid in the softly broken theory, since it is vital for the cancellation of the quadratic divergences.

Of course, the supersymmetric coupling relations (3.12) hold not only for the $SU(3)$ coupling g_3, but also for the $SU(2)$ and $U(1)$ couplings g_2 and g_1. Since these coupling relations are genuine predictions of softly broken supersymmetry, they have to be verified in order to establish supersymmetry experimentally.

For this verification e^+e^- colliders are an ideal tool, since they provide a clean initial state allowing to perform high precision measurements. The testing of the $SU(2)$ and the $U(1)$ SUSY coupling relations has been studied in [31] and [32]. For testing the $SU(3)$ coupling relation, the three processes involving the gauge coupling g_3 and the Yukawa coupling $\hat{g}_3$ shown in Fig. 3.1 are relevant. The $SU(3)$ SUSY Yukawa coupling can be measured in the process $e^+e^- \to q\bar{\tilde{q}}\tilde{g}$, whose cross section is proportional to $\hat{\alpha}_s$ at tree level. Comparing this with the gauge coupling measured in $e^+e^- \to q\bar{q}g$ or $e^+e^- \to \tilde{q}\bar{\tilde{q}}g$, the supersymmetric coupling relation (3.12) can be verified.

Future e^+e^- colliders may be able to operate in the e^-e^- mode, allowing selectron pairs to be produced through t-channel neutralino exchange in the process $e^-e^- \to \tilde{e}_R^-\tilde{e}_R^-$. This process contains the supersymmetric $U(1)$ Yukawa coupling at tree level, and may therefore be used to verify the corresponding supersymmetric $U(1)$ coupling relation [33].

Finally, e^+e^- colliders can operate as $\gamma\gamma$ colliders, with the photons produced by backscattering of laser light. Production of squark-antisquark pairs is possible at tree level with sizeable cross sections at such a machine. Gluinos can also be produced, either in the loop induced process $\gamma\gamma \to \tilde{g}\tilde{g}$ or from quarks and gluons at tree level if the photons resolve into a hadronic structure [34]. Since these gluino production processes also contain the supersymmetric $SU(3)$ Yukawa coupling, a further possibility for the verification of the supersymmetric $SU(3)$ coupling relation arises here.

3.6 Experimental searches

Experimental searches of supersymmetric particles have been performed in a variety of different channels at lepton and hadron colliders, without finding any of these particles so far. It has therefore been possible to set lower limits on the masses of the supersymmetric particles [35]. The lower mass bounds for neutralinos and charginos lie in the region 30 GeV to 100 GeV, depending on the particle considered and the specific model assumptions used in the analysis. Limits for the slepton masses range between 70 GeV and 90 GeV.

In the QCD sector, the most stringent limits for squark and gluino masses currently come from the Tevatron experiments D0 [36] and CDF [37, 38]. The produced squarks and gluinos decay to charginos and neutralinos, which in turn decay via a cascade to the lightest neutralino, assumed to be the LSP. Therefore these analyses use the signatures of jets plus missing transverse energy (E_T) from the undetected LSP, or jets plus multileptons plus missing E_T. Furthermore, the searches are performed within a supergravity inspired scenario, where all scalar (squark and slepton) masses unify to the universal scalar mass m_0 at the GUT scale, while all gaugino masses unify to $m_{1/2}$. Since the gluino mass in such a scenario cannot be much larger than the squark mass, there are no limits in this region of parameter space. The results are given in Fig. 3.2 as exclusion contours in the $m_{\tilde{q}}$-$m_{\tilde{g}}$ plane.

It is also possible to obtain limits on the squark masses from the upper limit on the invisible Z^0 decay width [39]. Although these limits are significantly weaker than the Tevatron limits, they are largely independent of model assumptions, and specifically do not depend on the squark decay pattern. The resulting mass bounds are about 35 GeV – 40 GeV [35].

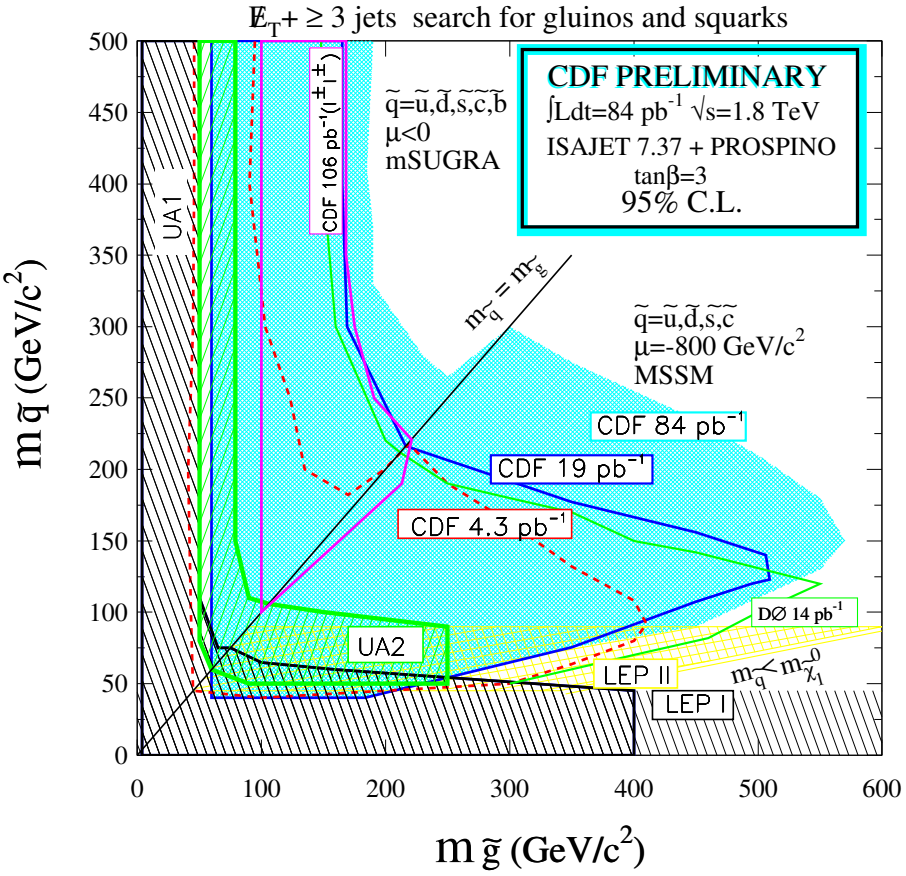

Figure 3.2: CDF limits for squark and gluino masses from direct searches [38].

Chapter 4

Squark and gluino production at leading order

In this chapter we will review the production of squarks and gluinos in e^+e^- collisions at tree level, and discuss how these processes can be used to test the supersymmetric coupling relation for the strong coupling constant g_3. Furthermore, we present leading order numerical results. Several different processes are relevant for this, depending on the parameters and the available centre-of-mass energy. In all of these, we only consider squarks of the 5 light flavours $f = u, d, s, c, b$. Since we take the corresponding quarks as massless, L/R-mixing of squarks can be neglected.

4.1 Processes

4.1.1 $e^+e^- \to \tilde{q}\bar{\tilde{q}}$

Squarks can be produced in pairs at e^+e^- colliders through the exchange of virtual photons and Z^0-bosons in the s-channel. The total cross section for this process is given by

$$\sigma(e^+e^- \to \tilde{q}_h\bar{\tilde{q}}_h) = \frac{\pi\alpha^2}{s} C_1^h \beta^3, \tag{4.1}$$

where $h = L/R$ for the production of L-squarks or R-squarks, $\beta = (1 - 4\frac{m_{\tilde{q}}^2}{s})^{1/2}$ is the velocity of the squarks, and

$$C_1^{L/R} = Q_q^2 + ({c_V^e}^2 + {c_A^e}^2)(c_V^q \pm c_A^q)^2\chi_Z^2 - 2Q_q c_V^e (c_V^q \pm c_A^q)\chi_Z, \tag{4.2}$$

with $\chi_Z = s/(s - m_Z^2)$. The quark charge Q_q is given in units of the positron charge e, and c_V^f, c_A^f are the vector- and axial-vector couplings of a fermion f to the Z^0, given explicitly by

$$c_V^f = \frac{T_3^f - 2Q_f \sin^2\theta_W}{2\sin\theta_W\cos\theta_W} \qquad\qquad c_A^f = \frac{T_3^f}{2\sin\theta_W\cos\theta_W}. \tag{4.3}$$

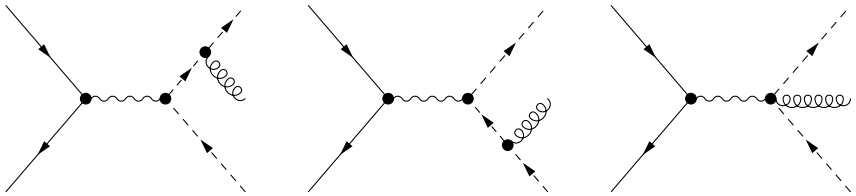

Figure 4.1: Feynman diagrams for $e^+e^- \to \tilde{q}\bar{\tilde{q}}g$.

Note that the vector- and axial-vector couplings of the quark corresponding to the produced squarks appear in (4.2). Furthermore, the decay width of the Z^0 has been neglected in the propagator, so that this formula is only valid sufficiently far away from the Z^0 resonance. Given the experimental mass bounds for squarks and gluinos, this approximation is clearly justified, and will be made for all processes discussed here. This process is the main production mechanism for squarks at e^+e^- colliders with cross sections up to several 100 fb in the energy range of next generation linear colliders.

The SUSY-QCD radiative corrections to this process have been calculated in [40], including the effects of L/R squark mixing. These corrections typically enhance the leading order cross section by about $15 - 20\%$, with the main part coming from the standard gluonic corrections.

4.1.2 $e^+e^- \to \tilde{q}\bar{\tilde{q}}g$

This process differs from the squark pair production of the preceding section only by an additional gluon in the final state. Therefore, the differential cross section diverges in the 2-jet region due to infrared singularities, and has to be included in the NLO corrections to squark pair production in this region.

If restricted to the 3-jet region, this process can be viewed as an independent one, and has been studied in [41]. The contributing Feynman diagrams are shown in Fig. 4.1. They contain the gauge coupling g_3, which can therefore be measured using this process.

The particle momenta are given by

$$e^+(p_+)\, e^-(p_-) \to (\gamma^*, Z^*) \to \tilde{q}_h(p_1)\, \bar{\tilde{q}}_h(p_2)\, g(p_3). \tag{4.4}$$

In the overall CMS, where $q^\mu = (p_+ + p_-)^\mu = (\sqrt{s}, \vec{0})$, we define the corresponding

scaled energies, 3-momenta and masses by

$$\begin{aligned} x_i &= \frac{2}{\sqrt{s}} E_i, \\ \tilde{x}_i &= \frac{2}{\sqrt{s}} |\vec{p}_i| = \sqrt{x_i^2 - 4\mu_i}, \\ \mu_i &= \frac{m_i^2}{s}. \end{aligned} \tag{4.5}$$

Since $m_1 = m_2 = m_{\tilde{q}}$ and $m_3 = 0$, we have $\tilde{x}_3 = x_3$, $\mu_3 = 0$ and $\mu \equiv \mu_1 = \mu_2 = 0$. The Dalitz plot density, i.e. the differential cross section with respect to the scaled energies of the squark and the antisquark, is given by [41]

$$\begin{aligned} \frac{d\sigma(e^+e^- \to \tilde{q}_h \bar{\tilde{q}}_h g)}{dx_1\, dx_2} = \frac{\alpha^2 \alpha_s}{4s} C_1^h \Bigg[16 - \frac{16}{3} \frac{\mu_1 \tilde{x}_1^2}{(1-x_1)^2} - \frac{16}{3} \frac{\mu_2 \tilde{x}_2^2}{(1-x_2)^2} \\ - \frac{8}{3} \frac{(2\mu_1 - 1)(\tilde{x}_1^2 - \tilde{x}_3^2 + \tilde{x}_2^2)}{(1-x_1)(1-x_2)} \Bigg], \end{aligned} \tag{4.6}$$

with C_1^h from (4.2). The phase space integration of this density can be performed analytically. Of course, the part of the 2-jet region of phase space containing the infrared divergences has to be excluded, since this region contributes to the NLO corrections to squark pair production. This can be done by imposing the cut

$$E_g \geq E_{g,\mathrm{cut}} \tag{4.7}$$

on the gluon energy in the centre-of-mass system (CMS). This cut excludes the infrared, but not the collinear 2-jet region, where the gluon is collinear to one of the final state squarks. This is not a problem, because in this process there are no associated collinear divergences. These can only occur if a gluon becomes collinear to a massless particle. The total cross section using the cut (4.7) is given by

$$\begin{aligned} \sigma(e^+e^- \to \tilde{q}_h \bar{\tilde{q}}_h g) = \sigma(e^+e^- \to \tilde{q}_h \bar{\tilde{q}}_h) \cdot \frac{\alpha_s}{4\pi} \frac{1}{\beta^3} \\ \cdot \Bigg\{ \frac{32}{3}(1-4\mu)(1-2\mu) \Bigg[-\frac{\omega^2 \ln(\omega) - \omega^2 + \ln(\omega) + 1}{1+\omega^2} \log\left(\frac{1-\rho\omega}{\rho-\omega}\right) \\ - \mathrm{Li}_2(1-\rho\omega) - \mathrm{Li}_2\left(1 - \frac{\rho}{\omega}\right) - \frac{1}{2}\ln^2(\omega) - \frac{1}{2}\ln^2(\rho) \Bigg] \\ + \frac{32}{3}\big(2\mu(1-\mu) - (1-4\mu)x_{\mathrm{cut}}\big)\ln(\rho) \\ + \frac{16}{3}(1-x_{\mathrm{cut}})(5 + x_{\mathrm{cut}} - 14\mu)\frac{1-\rho}{1+\rho} \Bigg\}, \end{aligned} \tag{4.8}$$

with $\beta = \sqrt{1-4\mu}$, the scaled cut parameter $x_{\text{cut}} = \frac{2E_{g,\text{cut}}}{\sqrt{s}}$, and

$$\begin{aligned}\omega &= \frac{1-\beta}{1+\beta} \\ \rho &= \frac{1-\sqrt{1-4\frac{\mu}{1-x_{\text{cut}}}}}{1+\sqrt{1-4\frac{\mu}{1-x_{\text{cut}}}}}.\end{aligned} \tag{4.9}$$

This process is suppressed with respect to the squark pair production by an additional factor α_s, but still yields cross sections of several 10 fb.

4.1.3 $e^+e^- \to q\bar{\tilde{q}}\tilde{g}$

This is the leading order process for the production of gluinos at e^+e^- colliders and includes the four subprocesses

$$e^+(p_+)\,e^-(p_-) \to (\gamma^*, Z^*) \to q(p_1)\,\tilde{g}(p_2)\,\bar{\tilde{q}}_L(p_3) \tag{4.10a}$$
$$e^+(p_+)\,e^-(p_-) \to (\gamma^*, Z^*) \to q(p_1)\,\tilde{g}(p_2)\,\bar{\tilde{q}}_R(p_3) \tag{4.10b}$$
$$e^+(p_+)\,e^-(p_-) \to (\gamma^*, Z^*) \to \bar{q}(p_1)\,\tilde{g}(p_2)\,\tilde{q}_L(p_3) \tag{4.10c}$$
$$e^+(p_+)\,e^-(p_-) \to (\gamma^*, Z^*) \to \bar{q}(p_1)\,\tilde{g}(p_2)\,\tilde{q}_R(p_3), \tag{4.10d}$$

which have first been studied in [41]. These four reactions are however not independent, but are related by CP-invariance

$$\begin{aligned}M(e^+(p_+)\,e^-(p_-) \to q(p_1)\,\tilde{g}(p_2)\,\bar{\tilde{q}}_L(p_3)) \\ &= M(e^-(\tilde{p}_+)\,e^+(\tilde{p}_-) \to \bar{q}(\tilde{p}_1)\,\tilde{g}(\tilde{p}_2)\,\tilde{q}_L(\tilde{p}_3)) \\ &\overset{\text{CMS}}{=} M(e^+(p_+)\,e^-(p_-) \to \bar{q}(\tilde{p}_1)\,\tilde{g}(\tilde{p}_2)\,\tilde{q}_L(\tilde{p}_3)) \\ M(e^+(p_+)\,e^-(p_-) \to q(p_1)\,\tilde{g}(p_2)\,\bar{\tilde{q}}_R(p_3)) \\ &= M(e^-(\tilde{p}_+)\,e^+(\tilde{p}_-) \to \bar{q}(\tilde{p}_1)\,\tilde{g}(\tilde{p}_2)\,\tilde{q}_R(\tilde{p}_3)) \\ &\overset{\text{CMS}}{=} M(e^+(p_+)\,e^-(p_-) \to \bar{q}(\tilde{p}_1)\,\tilde{g}(\tilde{p}_2)\,\tilde{q}_R(\tilde{p}_3)),\end{aligned} \tag{4.11}$$

with $\tilde{p} = (p^0, -\vec{p})$, and therefore $\tilde{p}_\pm = p_\mp$ in the CMS. This implies

$$d\sigma(e^+e^- \to q\tilde{g}\bar{\tilde{q}}_h) = d\sigma(e^+e^- \to \bar{q}\tilde{g}\tilde{q}_h) \tag{4.12}$$

for the angle-integrated differential cross sections $d\sigma$. We will therefore consider only the reactions (4.10a) and (4.10b) in the following.

At tree level two Feynman diagrams contribute to these processes, which are shown in Fig. 4.2, where particle momenta and colour indices are given for the external particles. Since the Feynman diagrams contain the $q\tilde{q}\tilde{g}$ interaction vertex, they are proportional to the supersymmetric Yukawa coupling $\hat{g}_3$, which can therefore be measured using this process.

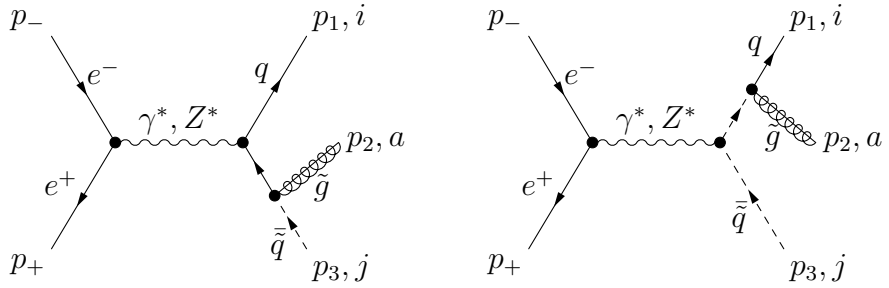

Figure 4.2: Feynman diagrams for gluino production at tree level.

In order to fix the notation for the next-to-leading order calculation, we will not only show the result, but also write down some intermediate steps. Since the calculation of the total cross section in next-to-leading order is our goal, we will not give the angular dependence of the differential cross section, which however can be found in [41].

The matrix element for the production of L- or R-squarks can be written in factorized form as

$$M_0^{L/R} = \left[L_\mu^\gamma Q_q + L_\mu^Z (c_V^q \pm c_A^q)\right] H_0^{L/R,\mu} = L_\mu^{L/R} H_0^{L/R,\mu}, \tag{4.13}$$

with the leptonic part

$$\begin{aligned} L_\mu^\gamma &= e\frac{1}{s}\bar{v}(p^+)\gamma_\mu u(p^-), \\ L_\mu^Z &= -e\frac{1}{s-m_Z^2}\bar{v}(p^+)(c_V^e + c_A^e\gamma_5)\gamma_\mu u(p^-), \end{aligned} \tag{4.14}$$

and the hadronic part

$$H_0^{L/R,\mu} = \pm i\sqrt{2}e\hat{g}_3 T_{ij}^a \bar{u}(p_1)\left[\gamma^\mu \frac{\not{p}_2 + \not{p}_3}{(p_2+p_3)^2} + \frac{2p_3^\mu}{(p_1+p_2)^2 - m_{\tilde{q}}^2}\right] P_{R/L} v(p_2). \tag{4.15}$$

Here, T_{ij}^a denote the $SU(3)$ generators in the fundamental representation, and $P_{L/R} = \frac{1}{2}(1\mp\gamma_5)$ are the chiral projection operators. We define the scaled energies, 3-momenta, and masses in the overall CMS as in (4.5), and have $m_2 = m_{\tilde{g}}$, $m_3 = m_{\tilde{q}}$, and since we use massless quarks $\mu_1 = 0$ and $\tilde{x}_1 = x_1$. Energy conservation is expressed by the relation $x_1 + x_2 + x_3 = 2$. The 3-particle phase space can be written as

$$\begin{aligned} d\Phi_3(q \to p_1 + p_2 + p_3) &= \left[\prod_{i=1}^{3} \frac{d^3p_i}{(2\pi)^3\, 2p_i^0}\right] (2\pi)^4 \delta^{(4)}(q - p_1 - p_2 - p_3) \\ &= \frac{s}{32(2\pi)^5} d\Omega\, d\phi\, dx_1\, dx_3, \end{aligned} \tag{4.16}$$

where the solid angle Ω and the azimuthal angle ϕ describe the orientation of the final state. Due to the factorized form (4.13) of the matrix element, these angle integrations can be carried out implicitly, resulting in

$$\int d\Omega\, d\psi \sum_{\substack{\text{spins,}\\ \text{colours}}} \left|M_0^h\right|^2 = \frac{128\pi^3\alpha}{3s} C_1^h P_{\mu\nu} H_0^{h,\mu\nu}, \tag{4.17}$$

with the projector $P_{\mu\nu}$ and the hadronic tensor $H_0^{h,\mu\nu}$ given by

$$P_{\mu\nu} = -g_{\mu\nu} + \frac{q_\mu q_\nu}{q^2} \qquad\qquad H_0^{h,\mu\nu} = H_0^{h,\mu} H_0^{h,\nu *}, \tag{4.18}$$

and C_1^h from (4.2). Though the hadronic tensor $H_0^{h,\mu\nu}$ differs for L- and R-squarks, the product $P_{\mu\nu} H_0^{h,\mu\nu}$ does not. The reason is that the hadronic tensors for the production of L- and R-squarks differ only by angular asymmetries, which however vanish after integration over the final state orientation. The only dependence on the "chirality" of the squark is therefore contained in the prefactor C_1^h.

From the angle-integrated squared matrix element we finally obtain the Dalitz plot density

$$\begin{aligned}
\frac{d^2\sigma^h}{dx_1\, dx_3} &= \frac{1}{2s} \int\limits_{\Omega,\phi} d\Phi_3(q \to p_1 + p_2 + p_3) \frac{1}{4} \sum_{\substack{\text{spins,}\\ \text{colours}}} \left|M_0^h\right|^2 \\
&= \frac{2\alpha^2 \hat{\alpha}_s}{3s} C_1^h \Bigg\{ \frac{1}{(1-x_3)^2} \tilde{x}_3^2 (1 - x_3 - \mu) + \frac{1}{(1-x_1)^2} \\
&\quad \cdot \left[3(1-x_1)(1-x_2) + 3\mu - x_1^2 \mu - \frac{1}{2}(1-x_1)(\tilde{x}_1^2 - \tilde{x}_2^2 + \tilde{x}_3^2) \right] \\
&\quad + \frac{1}{(1-x_1)(1-x_3)} \left[x_1 \tilde{x}_3^2 - \frac{1}{2}(x_3 + 2\mu)(\tilde{x}_1^2 - \tilde{x}_2^2 + \tilde{x}_3^2) \right] \Bigg\},
\end{aligned} \tag{4.19}$$

where we have introduced $\mu \equiv \mu_2 - \mu_3$. The integration boundaries for x_1, x_3 are explicitly given by

$$\begin{aligned}
2\sqrt{\mu_3} \leq x_3 &\leq 1 + \mu_3 - \mu_2 \\
x_1 &\lessgtr \frac{1 - x_3 + \mu_3 - \mu_2}{2(1 - x_3 + \mu_3)} \left[(2 - x_3) \pm \sqrt{x_3^2 - 4\mu_3} \right].
\end{aligned} \tag{4.20}$$

In the case $m_{\tilde{q}} < m_{\tilde{g}}$, it is possible to perform the phase space integration analytically, leading to an expression involving dilogarithms. Since the result is rather lengthy, we present it in Appendix B.

4.1.4 $e^+e^- \to q\bar{q}\tilde{g}\tilde{g}$

At tree level, gluinos can be produced in pairs only in conjunction with a $q\bar{q}$-pair in the process [42]

$$e^+e^- \to (\gamma^*, Z^*) \to q\bar{q}\tilde{g}\tilde{g}. \tag{4.21}$$

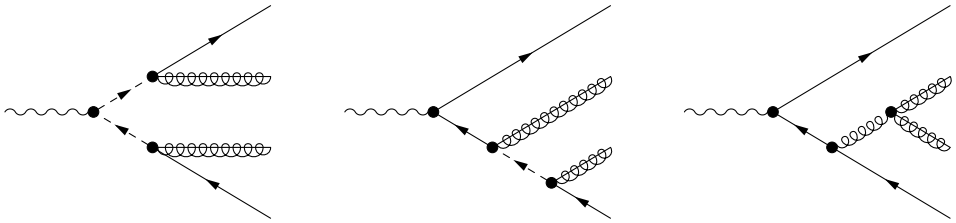

Figure 4.3: Some Feynman diagrams for $e^+e^- \to q\bar{q}\tilde{g}\tilde{g}$. Initial state particles are not shown.

Some of the contributing Feynman diagrams are shown in Fig. 4.3. This process contains the gauge coupling g_3 as well as the Yukawa coupling $\hat{g}_3$. However, the cross section is of $\mathcal{O}(\alpha^2\alpha_s^2)$, and therefore suppressed by an additional factor α_s compared to the 3-jet processes of the preceding sections. It will therefore be extremely difficult to observe this channel.

4.1.5 Squark and gluino decays

As we will see below, squark and gluino decays can also be relevant for verifying the SUSY coupling relations. The partial decay widths for squarks decaying into gluinos and vice versa are given by

$$\begin{aligned}\Gamma(\tilde{q} \to q\tilde{g}) &= \frac{\hat{\alpha}_s C_F}{2} m_{\tilde{q}} \left(1 - \frac{m_{\tilde{g}}^2}{m_{\tilde{q}}^2}\right)^2 \\ \Gamma(\tilde{g} \to q\bar{\tilde{q}} + \bar{q}\tilde{q}) &= 4N_f \frac{\hat{\alpha}_s}{8} m_{\tilde{g}} \left(1 - \frac{m_{\tilde{q}}^2}{m_{\tilde{g}}^2}\right)^2 \end{aligned} \tag{4.22}$$

at tree level. Both decay widths contain the SUSY Yukawa coupling, or rather the corresponding $\hat{\alpha}_s$, making them relevant for the verification of the coupling relations. The SUSY QCD radiative corrections to this decay widths have been calculated in [43]. The inclusion of the NLO corrections enhances the squark decay width by 10% to 30%, the gluino decay width changes by -10% to $+10\%$.

There are several other decay channels, like e.g. $\tilde{q} \to q\tilde{\gamma}$ or $\tilde{g} \to g\tilde{\gamma}$, which depend on parameters outside the QCD sector of the MSSM. These channels are not directly relevant to our discussion below, but contribute of course to the total decay widths.

4.2 Testing supersymmetric coupling relations

The processes discussed above can be used to test the supersymmetric coupling relation for the strong coupling constant. Since different processes are relevant

	region	centre-of-mass energy	relevant final states			
	Ia	$2m_{\tilde{q}} \leq \sqrt{s} \leq m_{\tilde{q}} + m_{\tilde{g}}$	$\tilde{q}\bar{\tilde{q}}$	$\tilde{q}\bar{\tilde{q}}g$		
$m_{\tilde{q}} < m_{\tilde{g}}$	Ib	$m_{\tilde{q}} + m_{\tilde{g}} \leq \sqrt{s} \leq 2m_{\tilde{g}}$	$\tilde{q}\bar{\tilde{q}}$	$\tilde{q}\bar{\tilde{q}}g$	$\mathbf{q\bar{\tilde{q}}\tilde{g}}$	
	Ic	$2m_{\tilde{g}} \leq \sqrt{s}$	$\tilde{q}\bar{\tilde{q}}$	$\tilde{q}\bar{\tilde{q}}g$	$\mathbf{q\bar{\tilde{q}}\tilde{g}}$	$q\bar{q}\tilde{g}\tilde{g}$
	IIa	$2m_{\tilde{g}} \leq \sqrt{s} \leq m_{\tilde{q}} + m_{\tilde{g}}$				$q\bar{q}\tilde{g}\tilde{g}$
$m_{\tilde{q}} > m_{\tilde{g}}$	IIb	$m_{\tilde{q}} + m_{\tilde{g}} \leq \sqrt{s} \leq 2m_{\tilde{q}}$			$\mathbf{q\bar{\tilde{q}}\tilde{g}}$	$q\bar{q}\tilde{g}\tilde{g}$
	IIc	$2m_{\tilde{q}} \leq \sqrt{s}$	$\mathbf{\tilde{q}\bar{\tilde{q}}}$	$\tilde{q}\bar{\tilde{q}}g$	$q\bar{\tilde{q}}\tilde{g}$	$q\bar{q}\tilde{g}\tilde{g}$

Table 4.1: Kinematically accessible processes at different c.m. energies for $m_{\tilde{q}} < m_{\tilde{g}}$ (case I) and $m_{\tilde{q}} > m_{\tilde{g}}$ (case II). Processes are identified by final state particles. Processes relevant for the measurement of the Yukawa coupling $\hat{g}_3$ are shown in boldface.

for different masses, we distinguish the two cases

$$\begin{aligned} \text{I} \quad & m_{\tilde{q}} < m_{\tilde{g}} \\ \text{II} \quad & m_{\tilde{q}} > m_{\tilde{g}}. \end{aligned} \tag{4.23}$$

The thresholds for squark and gluino pair production and associated squark-gluino production subdivide each case in 3 regions, as shown in Tab. 4.1, where the kinematically accessible processes for each region are given. The processes that are most promising for a measurement of the supersymmetric Yukawa coupling are shown in boldface.

If $m_{\tilde{q}} < m_{\tilde{g}}$, the lowest threshold is the squark pair production threshold. Above this threshold squark pair production and $\tilde{q}\bar{\tilde{q}}g$-production are relevant throughout all 3 regions. At $\sqrt{s} = m_{\tilde{q}} + m_{\tilde{g}}$ the squark-gluino threshold is crossed, and $q\bar{\tilde{q}}\tilde{g}$-production becomes possible. In the regions Ib and I*c* it is therefore possible to measure the SUSY-Yukawa coupling $\hat{g}_3$ directly in $q\bar{\tilde{q}}\tilde{g}$-production, and compare this to the gauge coupling measured in $\tilde{q}\bar{\tilde{q}}g$-production, or alternatively in the usual QCD 3-jet production with a $q\bar{q}g$ final state. In the region Ia below the squark-gluino threshold the Yukawa coupling cannot be measured directly. But since it enters the NLO corrections for $\tilde{q}\bar{\tilde{q}}$- and $\tilde{q}\bar{\tilde{q}}g$-production, it can be constrained indirectly. Of course, this will not be as accurate as the direct measurement possible in regions Ib and Ic. Region Ia can however be avoided in principle by increasing the centre-of-mass energy, alleviating this problem. For $\sqrt{s} > 2m_{\tilde{g}}$ (region Ic) $q\bar{q}\tilde{g}\tilde{g}$-production is also possible. The cross section is however so small that this process is not relevant in practice.

If $m_{\tilde{q}} > m_{\tilde{g}}$, the gluino pair production threshold is the lowest one. In the region IIa directly above this threshold only $q\bar{q}\tilde{g}\tilde{g}$-production is kinematically accessible. The corresponding cross sections are however extremely small, making

it very likely impossible to measure the SUSY Yukawa coupling in this region. In region IIb, above the squark-gluino threshold, $q\bar{\tilde{q}}\tilde{g}$-production is possible, allowing a direct measurement of $\hat{g}_3$. Since the $\tilde{q}\bar{\tilde{q}}g$-channel is not open in this case, the gauge coupling g_3 can only be measured in $q\bar{q}g$-production. Above the squark pair production threshold, the phase space for the $q\bar{\tilde{q}}\tilde{g}$-process contains a region where two on-shell squarks may be produced, with one of them decaying via $\tilde{q} \to q\tilde{g}$ afterwards. This corresponds to the right Feynman diagram in Fig. 4.2. The $q\bar{\tilde{q}}\tilde{g}$-production is therefore replaced by squark pair production in region IIc, though $q\bar{\tilde{q}}\tilde{g}$-production in the region of phase space where the virtual squark is off-shell can still be investigated by imposing suitable kinematical cuts. In addition, $\tilde{q}\bar{\tilde{q}}g$ 3-jet production is also relevant in this region. By investigating decays of the final state squarks into gluinos, the Yukawa coupling can still be measured, since $\Gamma(\tilde{q} \to q\tilde{g})$ is proportional to $\hat{\alpha}_s$. This partial decay width can be obtained from the measured values of the total decay width $\Gamma_{\text{tot}}(\tilde{q})$ and the branching fraction $\text{BR}(\tilde{q} \to q\tilde{g})$. Since the threshold behaviour of the cross section for squark pair production depends on the total squark decay width, a scan of this region can be used not only to determine the squark mass, but also its total decay width. The branching fractions can be determined from the investigation of different squark decay channels. This allows the determination of the Yukawa coupling $\hat{g}_3$, the gauge coupling can be measured using either $\tilde{q}\bar{\tilde{q}}g$- or $q\bar{q}g$-production in the 3-jet regime.

In order to allow a high precision comparison of the gauge and Yukawa couplings, accurate theoretical predictions for the corresponding processes are necessary. Since next-to-leading order QCD corrections are usually large, a NLO calculation for these processes is needed. For the determination of the Yukawa coupling from squark decays, the NLO corrections for the process $e^+e^- \to \tilde{q}\bar{\tilde{q}}$ and the partial squark decay widths are needed. These have already been calculated in the past in [40, 43]. Therefore NLO calculations for the processes $e^+e^- \to q\bar{\tilde{q}}\tilde{g}$ and $e^+e^- \to \tilde{q}\bar{\tilde{q}}g$ remain to be done. The calculation of the NLO corrections to the $q\bar{\tilde{q}}\tilde{g}$-production process is the aim of this thesis, while the $\tilde{q}\bar{\tilde{q}}g$-process is treated in a parallel work [44].

4.3 Leading order numerical results

Numerical results in leading order for the production processes discussed above are shown in Fig. 4.4 for case I and in Fig. 4.5 for case II. In these results, we have summed up the cross sections for the 5 light flavours, and for L- and R-squarks. For associated squark-gluino production, the summation extends over the 4 final states (4.10a)-(4.10d). Furthermore, we have used the scale dependent coupling $\alpha_s(\mu)$ with one-loop running included, evaluated at the scale $\mu = m_{\tilde{q}} + m_{\tilde{g}}$. For the process $e^+e^- \to \tilde{q}\bar{\tilde{q}}g$, we have used the cut $E_g > 50\,\text{GeV}$ for the gluon energy in the CMS to exclude the part of the 2-jet region containing the infrared

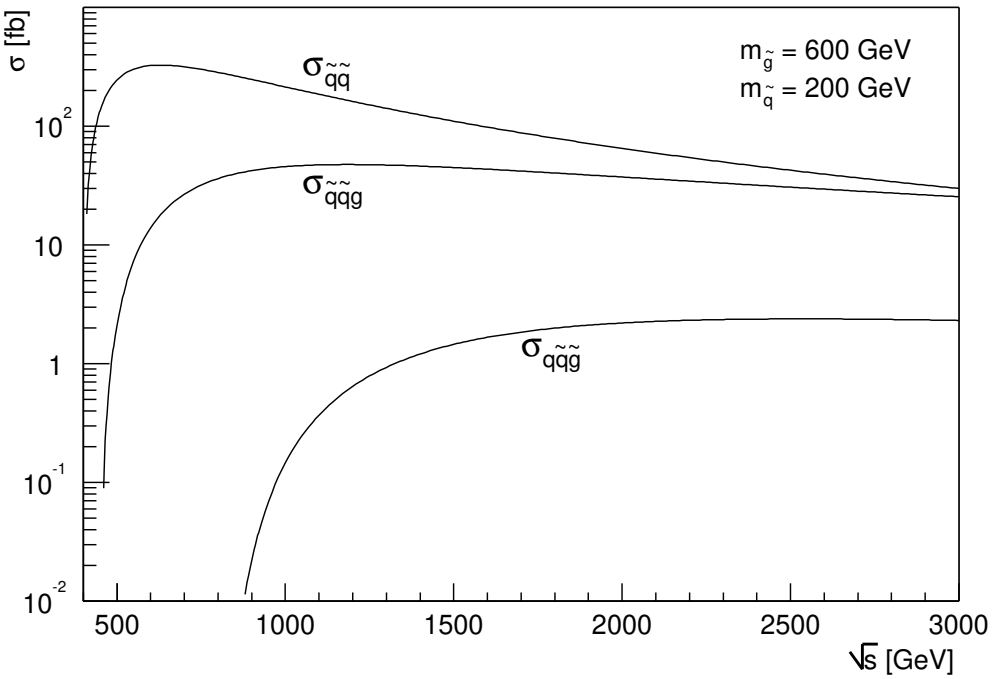

Figure 4.4: Leading order cross sections of squark and gluino production in e^+e^--collisions for case I ($m_{\tilde{g}} > m_{\tilde{q}}$).

divergences.

For case I we have used the masses $m_{\tilde{g}} = 600\,\text{GeV}$ and $m_{\tilde{q}} = 200\,\text{GeV}$, which lie well outside the current CDF boundaries of Fig. 3.2. The dominant process is squark pair production, with cross sections exceeding 100 fb in a wide range of $\sqrt{s}$. The cross section for $\tilde{q}\bar{\tilde{q}}g$ 3-jet production is only moderately smaller, with values of several 10 fb away from the kinematical threshold, which is increased compared to the $\tilde{q}\bar{\tilde{q}}$-production by the requirement of a minimal gluon energy of 50 GeV. Production of gluinos in the $q\bar{\tilde{q}}\tilde{g}$-channel becomes possible above $\sqrt{s} = 750\,\text{GeV}$, but the cross section stays below 1 fb up to $\sqrt{s} \approx 1300\,\text{GeV}$. Above this point, this process will probably be observable at future e^+e^- linear colliders with sufficient energy, since these machines should reach luminosities in the range of $1000\,\text{fb}^{-1}\text{y}^{-1}$. For example, the design luminosity of the planned TESLA linear collider is $L = 10^{34}\text{cm}^{-2}\text{s}^{-1}$ at 800 GeV, which translates to $L \approx 1000\,\text{fb}^{-1}\text{y}^{-1}$ for an annual operation time of 5000 hours [45]. In this case, the best possibility for the verification of the supersymmetric coupling relation therefore lies in the measurement of $\hat{g}_3$ in the $q\bar{\tilde{q}}\tilde{g}$-production process for sufficiently high c.m. energies in region IIb/c.

The parameters we have chosen for case II are $m_{\tilde{g}} = 200\,\text{GeV}$ and $m_{\tilde{q}} = 500\,\text{GeV}$. These lie just outside the CDF boundaries. The $q\bar{q}\tilde{g}\tilde{g}$-production pro-

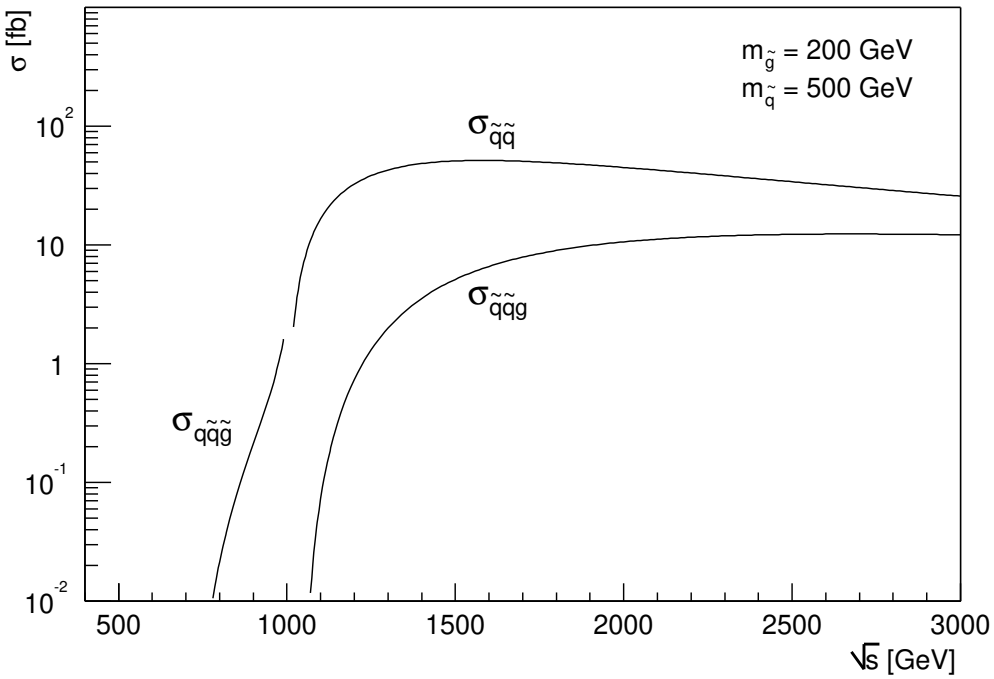

Figure 4.5: Leading order cross sections of squark and gluino production in e^+e^--collisions for case II ($m_{\tilde{g}} < m_{\tilde{q}}$).

cess is not shown, because the cross sections are only of the order 10^{-4} fb. This process is therefore clearly not relevant. In region IIb only $q\bar{\tilde{q}}\tilde{g}$ production is possible, however the cross section exceeds 1 fb only near the squark pair production threshold. It could therefore be difficult to observe the process in this case, even with the high luminosities of future e^+e^- linear colliders. Above the squark pair production threshold $\tilde{q}\bar{\tilde{q}}$- and $\tilde{q}\bar{\tilde{q}}g$-production are possible, albeit the cross sections are somewhat smaller than in case I. Therefore, the measurement of $\hat{g}_3$ in squark decays in region IIc is the most promising possibility for the verification of the supersymmetric coupling relation in this case.

Chapter 5

Gluino production in next-to-leading order

5.1 Outline of the calculation

In this chapter the complete calculation of the total cross section for the process $e^+e^- \to q\bar{\tilde{q}}\tilde{g}$ at next-to-leading order in the strong coupling constant α_s is presented. To obtain the NLO cross section, the effects of virtual particles in loops as well as the emission of real gluons have to be taken into account.

The loop diagrams of the virtual corrections contain momentum integrals, which may diverge due to contributions from large loop momenta (ultraviolet- or UV-divergence) or from loop momenta that are small or collinear to another momentum (infrared- or IR-divergence). Though these divergences cancel in the final result as explained below, it is necessary to introduce a regularization prescription in order to manipulate the divergent integrals during intermediate steps of the calculation. Within such a regularization scheme the divergent integrals are written as diverging limits. Only after the cancellation of all divergences in the final result the limit can be taken, thereby removing the regularization. For our calculation dimensional regularization [46] is used, where all momentum integrals, i.e. loop momentum and phase space integrals, are performed in D space-time dimensions, where D is being treated as a complex parameter. The UV and IR divergences do then appear as poles at $D = 4$ in the complex D plane. As will be explained in detail later, special care has to be taken if dimensional regularization is used within a supersymmetric theory.

The appearance of UV divergences in the virtual corrections is related to the fact that the masses and couplings in the Lagrangian are not directly measurable quantities. Of course, any observable can be calculated in terms of the parameters, but these relations receive UV divergent radiative corrections. The relations between different observables are however finite to all orders of perturbation theory in a renormalizable theory, thus allowing meaningful predictions.

This implies that the parameters can be viewed as UV divergent, but unobservable, quantities, such that the divergences in the parameters cancel the ones arising in the loop corrections, leading to finite results. One could now calculate observables in terms of a set of others used as input parameters, by first calculating all observables as functions of the parameters, use some of this relations to determine the parameters from the set of chosen observables, and finally insert these expressions for the parameters in the remaining relations. However this is rather cumbersome in a practical calculation, and so we will use the counterterm approach instead. Here the parameters are split into a renormalized part and a renormalization constant, such that predictions for observables in terms of renormalized quantities are UV finite. The renormalized parameters are finite, while the renormalization constants are UV divergent. There is a remaining freedom of finite redefinitions of the renormalized parameters, which is fixed by imposing a set of renormalization conditions, called a renormalization scheme. The splitting of parameters also implies a division of the Lagrangian into a renormalized part, having the same form as the original Lagrangian, but expressed by renormalized quantities, and a counterterm part. The counterterm part contains the UV divergent renormalization constants and can be treated as an interaction in perturbation theory, giving rise to additional Feynman diagrams, which cancel the UV divergences of the loop diagrams. Though renormalizing the parameters of the theory is sufficient to obtain finite S-matrix elements, the Green functions are still UV divergent. In order to get finite Green functions, it is necessary to renormalize also the fields themselves. After the renormalization procedure there still remain IR divergences in the virtual corrections.

However, the IR divergences cancel in the incoherent sum over all indistinguishable final states, as was shown in the Bloch-Nordsieck [47] and Kinoshita-Lee-Nauenberg [48] theorems. A final state which contains additional soft gluons with arbitrarily small energies cannot be distinguished from the final state without these gluons, due to the finite energy resolution of any real detector. Similarly, if two final state particles become collinear, they cannot be resolved due to the limited angle resolution, thus appearing as only one particle with the combined momentum. This means that any observable has to be insensitive to the number of soft and collinear particles in the final state, and therefore has to include the effects of the emission of additional soft and collinear particles. The total cross section that we calculate is such an infrared- and collinear-safe observable. The matrix elements for the additional processes have singularities in the soft and collinear limits, which result in IR divergences after integration over the soft and collinear regions of phase space. These divergences exactly cancel the IR divergences from the virtual corrections, leading to a completely finite result, as required by the Bloch-Nordsieck and Kinoshita-Lee-Nauenberg theorems.

In our calculation we have to include the effects of real gluon emission from the process

$$e^+e^- \to q\bar{\tilde{q}}\tilde{g}g. \tag{5.1}$$

The matrix element for this process has singularities if the gluon is soft or is collinear to the quark. Soft and collinear divergences will arise from the phase space integration over the corresponding regions, and cancel the divergences of the virtual corrections.

Of course, the cancellation of the IR divergences has to be implemented analytically. In practice, it is however impossible to perform the phase space integration for the process (5.1) over the full 4-particle phase space analytically. We therefore use the phase space slicing method [49] extended to incorporate massive particles to extract the divergences from the real corrections. In this method the phase space is separated into a soft, a collinear, and a remaining hard part using a dimensionless parameter $x_{\text{cut}} \ll 1$. Only in the soft and collinear parts the matrix element contains singularities, whereas it is completely regular in the hard phase space. The integration over the hard phase space can therefore be done numerically in $D = 4$ dimensions. In the soft and collinear regions the matrix element approximately factorizes into the tree level matrix element M_0 and a factor containing the singularities. This singular factor is universal, and has a very simple form. The phase space in these regions can also be factorized into the leading order 3-particle phase space and a soft/collinear phase space factor, making it possible to perform the phase space integration over the soft and collinear regions analytically within dimensional regularization. However, the soft and collinear approximations of the matrix element and the corresponding phase space introduce $\mathcal{O}(x_{\text{cut}})$ errors, so that the limit $x_{\text{cut}} \to 0$ has to be taken numerically. Since numerical cancellations between the contributions from the hard phase space and the soft and collinear phase space grow as $x_{\text{cut}} \to 0$, the value of x_{cut} has to be chosen carefully.

The structure of the calculation of the NLO corrections σ_2 to the total cross section can be schematically written as

$$\sigma_2 = \int d\Phi_3 \left[d\sigma_2^V + \int\limits_{\substack{\text{soft}\\ \text{coll.}}} d\Phi_1^{\text{sc}}\, d\sigma_2^R \right] + \int\limits_{\text{hard}} d\Phi_4\, d\sigma_2^R, \tag{5.2}$$

where $d\sigma_2^V$ and $d\sigma_2^R$ are the differential cross sections for the virtual and the real corrections, $d\Phi_n$ is the n-particle phase space measure, and the factorized form of the 4-particle phase space in the soft and collinear regions has been written as $d\Phi_4 = d\Phi_3 d\Phi_1^{\text{sc}}$. In this equation all IR divergences are contained in the two terms in the brackets, and only the $d\Phi_1^{\text{sc}}$ integration has to be performed analytically in D dimensions. These divergences cancel each other, and the $d\Phi_3$ and $d\Phi_4$ integrations are performed numerically in 4 dimensions. For these numerical integrations we use the VEGAS algorithm for adaptive Monte Carlo integration [50].

5.2 Virtual corrections

5.2.1 Feynman diagrams

We will first describe the calculation of the virtual corrections. The loop diagrams contribute to the total cross section through their interference with the Born matrix element. The differential cross section for this contribution can be written as

$$\begin{aligned} d\sigma_2^V(e^+e^- \to q\bar{\tilde{q}}\tilde{g}) &= \frac{1}{8s} d\Phi_3(q \to p_1 + p_2 + p_3) \sum_{\substack{\text{spins,}\\ \text{colours}}} (M_0 M_1^* + M_0^* M_1) \\ &= \frac{1}{8s} d\Phi_3(q \to p_1 + p_2 + p_3) \sum_{\substack{\text{spins,}\\ \text{colours}}} 2\,\mathrm{Re}\, M_0^* M_1, \end{aligned} \tag{5.3}$$

where M_1 is the NLO matrix element for $q\bar{\tilde{q}}\tilde{g}$-production.

The diagrams contributing to M_1 are shown in Fig. 5.1. They are given in terms of one-particle irreducible (1PI) vertex functions, represented by circles. Apart from the self energy corrections, vertex corrections to 3- and 4-particle interactions have to be calculated, leading to 3- and 4-point loop integrals. Some diagrams contributing to the squark self energy, the $q\tilde{q}\tilde{g}$-vertex, and the $Z^0 q\tilde{q}\tilde{g}$-vertex are shown in Fig. 5.2. The first diagram of Fig. 5.1 contains the effective $Z^0\tilde{g}\tilde{g}$ interaction, which does not exist at tree level. The $Z^0\tilde{g}\tilde{g}$ vertex corrections are therefore completely UV and IR finite. The other diagrams include UV divergent contributions, and some of them are also IR divergent.

Unlike at tree level, the NLO matrix element M_1 does not factorize completely into a leptonic and a hadronic part, but can only be written as a sum of factorizing terms

$$M_1^{L/R} = \left[Q_q L_\mu^\gamma + (c_V^q \pm c_A^q) L_\mu^Z\right] H_1^{L/R,\mu} \pm \sum_{q'} c_A^{q'} L_\mu^Z \tilde{H}_1^{L/R,\mu}(m_{q'}), \tag{5.4}$$

where the index L/R corresponds to the production of L/R-squarks. In this expression contributions from diagram 1 are solely contained in the $\tilde{H}_1$ term, while all other diagrams contribute only to the H_1 term. Since the flavour of the quarks/squarks in the loop diagrams of the $Z^0\tilde{g}\tilde{g}$ vertex corrections is not related to the flavour of the external quark/squark, this vertex correction includes a sum over all quark flavours q'. However, the flavour sum has to be extended only over $q' = t, b$, because we treat the first two generations of quarks as massless, and the $\tilde{H}_1$ contributions from an up-type quark and a mass degenerate down-type quark cancel each other.

The integration of the differential cross section (5.3) over the final state orientation can be done in analogy to the tree level case, resulting in the Dalitz plot

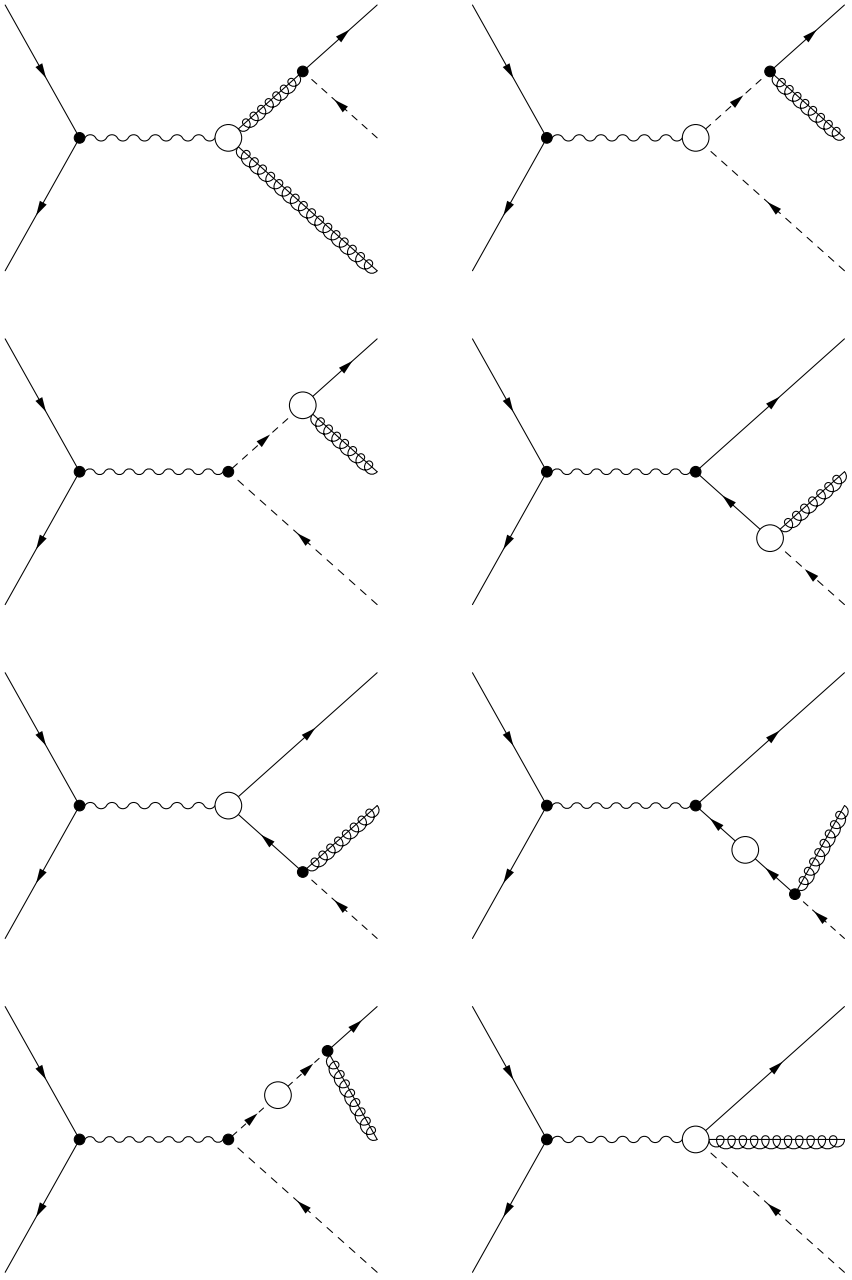

Figure 5.1: Virtual Feynman diagrams contributing to gluino production at NLO. White circles denote renormalized 1PI vertex functions.

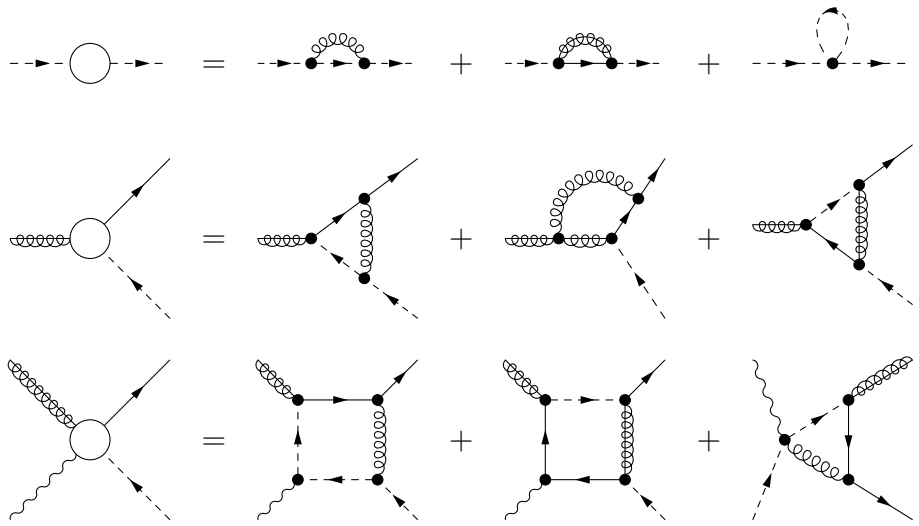

Figure 5.2: Example diagrams contribution to some 1PI vertex functions. Not all contributing diagrams are shown.

density for the virtual corrections

$$\begin{aligned}\frac{d^2\sigma_2^{V,h}}{dx_1\,dx_2} &= \frac{1}{8s}\int\limits_{\Omega,\phi} d\Phi_3(q\to p_1+p_2+p_3)\sum_{\substack{\text{spins,}\\ \text{colours}}} 2\,\mathrm{Re}\,M_0^{h*}M_1^h \\ &= \frac{\alpha}{192\pi^2 s}dx_1\,dx_2\Big[C_1^h P_{\mu\nu}2\,\mathrm{Re}\,H_0^{h,\mu*}H_1^{h,\nu} \\ &\qquad + \sum_{q'} C_2^{q',h}P_{\mu\nu}2\,\mathrm{Re}\,H_0^{h,\mu*}\tilde{H}_1^{h,\nu}(m_{q'})\Big], \end{aligned} \tag{5.5}$$

with

$$C_2^{q',L/R} = \pm c_A^{q'}\left[-Q_q c_V^e \chi_Z + ({c_V^e}^2 + {c_A^e}^2)(c_V^q \pm c_A^q)\chi_Z^2\right], \tag{5.6}$$

where the index q refers to the flavour of the external quark/squark, and C_1^h and $P_{\mu\nu}$ are given by Eqs. (4.18) and (4.2). As in the tree level case, the hadronic tensors $\mathrm{Re}\,H_0^{h,\mu*}H_1^{h,\nu}$ and $\mathrm{Re}\,H_0^{h,\mu*}\tilde{H}_1^{h,\nu}(m_{q'})$ for the production of L/R-squarks only differ by terms asymmetric in the angles, which of course vanish in the Dalitz plot density, so that the products $P_{\mu\nu}\,\mathrm{Re}\,H_0^{h,\mu*}H_1^{h,\nu}$ and $P_{\mu\nu}\,\mathrm{Re}\,H_0^{h,\mu*}\tilde{H}_1^{h,\nu}(m_{q'})$ are independent of h. All dependence on the squark "chirality" in (5.5) is therefore given by the factors C_1^h and C_2^h.

If $m_{\tilde{q}} < m_{\tilde{g}}$ and $\sqrt{s} \geq 2m_{\tilde{g}}$ (region Ic in Tab. 4.1), gluino pair production is kinematically allowed, and gluinos may decay into squarks. In this case, the phase space contains a region where the virtual gluino in the first diagram of Fig. 5.1 is on-shell. The relevant phase space region for gluino pair production could in principle be excluded by imposing suitable cuts. Since the contribution from this diagram turns out to be at least 3 orders of magnitude smaller than

the rest of the NLO contributions taken together, we have not followed this approach. Instead, we explicitly introduce a gluino decay width given by (4.22) in the relevant propagator, thus regularizing the phase space integrations.

5.2.2 Loop integrals

Evaluating the matrix element M_1 using the Feynman rules leads to expressions involving loop momentum integrals. These expressions contain the loop momentum in propagator factors in the denominator, and contracted with Dirac matrices or external momenta or as Lorentz vector in the numerator. These loop integrals can be written in terms of a set of standard scalar and tensor integrals. Apart from propagator denominators they may also include loop momenta in the numerator. Since the loop integrals can contain divergences, it is necessary to specify a regularization scheme at this point. As already mentioned above, we use dimensional regularization [46]. The integrals are performed in $D = 4 - 2\epsilon$ space-time dimensions, and the UV and IR divergences manifest themselves as poles at $\epsilon = 0$. A fully anticommuting γ_5 is used for this calculation, which is possible at one-loop level in anomaly free theories. Within this regularization scheme the four-point integrals are defined by

$$D_0; D_\mu; D_{\mu\nu} = \frac{16\pi^2}{i}\mu^{4-D}\int \frac{d^D k}{(2\pi)^D}\frac{1; k_\mu; k_\mu k_\nu}{D_0 D_1 D_2 D_3}, \tag{5.7}$$

with the propagator factors given by

$$\begin{aligned} D_0 &= k^2 - m_1^2 + i\epsilon \\ D_i &= (k + p_i)^2 - m_{i+1}^2 + i\epsilon \qquad\qquad i = 1 \ldots 3. \end{aligned} \tag{5.8}$$

The mass scale μ is an arbitrary scale appearing in dimensional regularization. It is introduced by the substitution $g_3 \to \mu^{2-D/2} g_3$ in order to keep the coupling constant dimensionless in D space-time dimensions. D_0 is the scalar 4-point integral, the other integrals are called tensor integrals. The one-, two-, and three-point integrals are defined analogously and are denoted by A, B, and C.

The tensor integrals can be further decomposed according to their tensor structure into symmetric basis tensors constructed from the external momenta p_i, and the metric $g_{\mu\nu}$. For the 4-point tensor integrals of rank 1 and 2 this decomposition reads

$$\begin{aligned} D_\mu &= p_{1\mu} D_2 + p_{2\mu} D_2 + p_{3\mu} D_3 \\ D_{\mu\nu} &= g_{\mu\nu} D_{00} + \sum_{i,j=1}^{3} p_{i\mu} p_{j\nu} D_{ij}, \end{aligned} \tag{5.9}$$

and tensor integrals of higher rank or different number of external particles are defined in a similar manner. The coefficient functions are Lorentz scalars and

depend only on the invariants constructed from the external momenta. They are totally symmetric in their indices, due to the symmetry of the tensor integrals themselves. These tensor coefficients can be algebraically reduced to linear combinations of scalar integrals, using the Passarino-Veltman reduction procedure [51]. We have implemented this tensor reduction procedure in the FORM [52] computer algebra language. Though the tensor reduction can result in large expressions especially in the case of the 4-point integrals, its advantage is that only scalar integrals have to be evaluated.

Among these scalar integrals, the one- and two-point integrals are the only ones possessing UV divergences, as can be seen using power counting arguments. IR divergences can only be contained in the derivatives of the two-point integrals, and in the three- and higher n-point integrals.

For the process considered here, we have to calculate IR divergent 3- and 4-point integrals. We have however not calculated the IR divergent 4-point integrals in $D = 4-2\epsilon$ dimensions directly, but have rewritten them in terms of the 4-point integrals in $D = 6$ dimensions, defined by

$$D_0^6 = \frac{1}{i\pi^2} \int d^6k \, \frac{1}{D_0 D_1 D_2 D_3}. \tag{5.10}$$

This is possible, because D_0^6 is directly related to the tensor coefficient D_{00} [53]

$$D_{00} = -\frac{1}{2\pi} D_0^6. \tag{5.11}$$

The equations from the tensor reduction can be used to express any D_0 as a linear combination of the corresponding D_{00} and several C_0's. The tensor coefficient D_{00} can be replaced by D_0^6 using (5.11). This substitution is useful because D_0^6 is IR finite, and all IR divergences contained in the 4-point integrals have therefore been moved to the simpler 3-point integrals. The IR divergences of the complete virtual corrections are all contained in scalar three-point integrals and derivatives of two-point integrals. This leads to a considerable simplification of the coefficients of the scalar integrals in the result. It also makes the extraction of the IR divergent part of the virtual corrections easy.

We have calculated the necessary six-dimensional box integrals using Feynman parameterisations with similar methods as for the four-dimensional box integrals. However, in one case it was easier to subtract the divergent three-point integrals from the D_0 in D dimensions, and calculate the remaining finite integral in $D = 4$ dimensions. Thus we have moved all IR divergences from the four-point integrals to the scalar three-point integrals. The results for this integrals are shown explicitly in Appendix C. There we also give the results for the other UV and IR divergent integrals.

5.2.3 Regularization and supersymmetry

Dimensional regularization (DREG) [46] is a very convenient regularization scheme for gauge theories like the Standard Model, because it respects all gauge symmetries and therefore all gauge Ward identities. Furthermore it regulates ultraviolet as well as infrared singularities. The Ward identities of supersymmetry however depend on the fact that there is an equal number of fermionic and bosonic degrees of freedom in every supermultiplet. In dimensional regularization all 4-vectors including the vector fields are continued to D space-time dimensions, so that the massless gauge fields now have $D-2$ physical degrees of freedom. On the other hand, Majorana spinor fields and therefore the gauginos still have 2 physical degrees of freedom. This mismatch of the degrees of freedom is the reason that dimensional regularization breaks supersymmetry and the supersymmetric Ward identities are violated in this scheme.

As a remedy, a modified scheme called dimensional reduction (DRED) has been proposed [54]. As in dimensional regularization, the momenta are continued to D dimensions, but the vector fields remain 4-dimensional. Since the gauge bosons and the associated gauginos now both have 2 physical degrees of freedom, dimensional reduction respects supersymmetry, and fulfils the supersymmetric Ward identities. However DRED is mathematically inconsistent [55], though it can be argued that these inconsistencies do not show up in a one-loop calculation [56]. In addition, there are problems with mass factorization [57], though these are also not relevant for our calculation.

For practical reasons we use another possible solution. Within this approach DREG is still used, but the Ward identities are restored by introducing additional counterterms. These counterterms can be uniquely determined by requiring the renormalized Green functions to obey all Ward identities. It is possible to extend this scheme to all orders, by introducing additional counterterms and fixing them by imposing the Ward identities order by order. The only violated Ward identity relevant for our calculation is the one expressing the equality of the $q\tilde{q}\tilde{g}$-Yukawa coupling and the gauge coupling. All other couplings appearing at tree level in our calculation are fixed by gauge symmetry, which is respected by DREG. Therefore an additional counterterm has to be introduced only for the $q\tilde{q}\tilde{g}$ Yukawa interaction. If the strong coupling appearing in the $q\tilde{q}\tilde{g}$ Yukawa interaction is denoted by $\hat{g}_3$, this counterterm can be incorporated into the Yukawa coupling

$$\hat{g}_3 = g_3 \left[1 + \frac{\alpha_s}{4\pi}\left(\frac{2}{3}C_A - \frac{1}{2}C_F\right)\right] = g_3\left[1 + \frac{\alpha_s}{3\pi}\right]. \tag{5.12}$$

Here $C_A = 3$ and $C_F = 4/3$ are the Casimir invariants of $SU(3)$. This relation has first been established in [58] by comparing the β-functions in DREG and DRED, and later in [43] by a direct comparison of the loop corrections to the $q\bar{q}g$- and the $q\tilde{\bar{q}}\tilde{g}$-vertices at small momentum transfer in the exact supersymmetric limit. Recently this result has also been formally proven, including the uniqueness of

the counterterm, using algebraic renormalization in the softly broken SUSY QCD [59]. Of course DRED and modified DREG are equivalent and yield the same results at 1-loop.

5.2.4 Renormalization

We now come to the renormalization of the SUSY QCD sector of the MSSM, and specify the renormalization scheme used. The renormalization of the ghosts and the massive top-quarks is not included, since we do not need it in this calculation. In higher orders in perturbation theory the parameters of the original Lagrangian (3.6) are interpreted as bare parameters, denoted with an index 0. They are split into renormalized parameters and renormalization constants according to

$$\begin{aligned} m_{\tilde{g},0} &= m_{\tilde{g}} + \delta m_{\tilde{q}} \\ m^2_{\tilde{q},0} &= m^2_{\tilde{q}} + \delta m^2_{\tilde{q}} \\ g_{3,0} &= g_3 + \delta g_3. \end{aligned} \tag{5.13}$$

An independent counterterm for the Yukawa coupling $\hat{g}_3$ has not to be introduced, since the supersymmetric Ward identities fix it in terms of the gauge coupling g_3. For the quarks of the five light flavours, which are considered massless for our analysis, there is no mass renormalization constant. Similarly, the bare fields are split into renormalized fields and wave function renormalization constants according to

$$\Phi_0 = (1 + \delta Z_\Phi)\Phi. \tag{5.14}$$

This induces a splitting of the bare Lagrangian into a renormalized and a counterterm Lagrangian

$$\mathcal{L}(m_0, g_{3,0}, \Phi_0) = \mathcal{L}(m, g_3, \Phi) + \mathcal{L}_{\text{c.t.}}(m, g_3, \Phi, \delta m, \delta g_3, \delta Z_\Phi), \tag{5.15}$$

where both the bare and the renormalized Lagrangian are given by (3.6) and (3.10) using the appropriate parameters and fields. The counterterm Lagrangian consists of all terms containing renormalization constants, and generates the counterterm Feynman rules. Since all renormalization constants are of $\mathcal{O}(g_3^2)$, the counterterm Lagrangian can be treated as an interaction in perturbation theory. The corresponding counterterm Feynman rules are given in Appendix A along with the usual Feynman rules generated by $\mathcal{L}(m, g_3, \Phi)$. Including the counterterm Feynman diagrams, one obtains the renormalized Green functions $G_R^{(n)}(p_1, \ldots, p_n)$, and the renormalized vertex functions $\Gamma_R^{(n)}(p_1, \ldots, p_n)$, which are the renormalized one-particle irreducible n-point functions. The renormalized two-point function $\Gamma_R^{(2)}$ is the inverse of the propagator up to a factor

$$\Gamma_R^{(2)}(p, -p) G_R^{(2)}(p, -p) = -1. \tag{5.16}$$

The divergent parts of the renormalization constants are fixed by the requirement of finite Green functions. The finite parts can however be arbitrary, and have to be fixed by imposing a set of renormalization conditions. For the mass and wave function renormalization we use the on-shell scheme [60, 61]. The renormalization conditions in this scheme are given by

$$\begin{aligned}
\lim_{p^2\to 0} \frac{-ig^{\mu\nu}}{p^2} \operatorname{Re}\Gamma^{GG}_{R,\nu\rho}(p)\epsilon^\rho(p) &= -\epsilon^\mu(p) \\
\operatorname{Re}\Gamma^{\tilde{g}\tilde{g}}_R(p)u(p)\Big|_{p^2=m^2_{\tilde{g}}} &= 0 \\
\lim_{p^2\to m^2_{\tilde{g}}} \frac{i(\not{p}+m_{\tilde{g}})}{p^2-m^2_{\tilde{g}}} \operatorname{Re}\Gamma^{\tilde{g}\tilde{g}}_R(p)u(p) &= -u(p) \\
\lim_{p^2\to 0} \frac{i\not{p}}{p^2} \operatorname{Re}\Gamma^{q\bar{q}}_R(p)u(p) &= -u(p) \\
\operatorname{Re}\Gamma^{\tilde{q}\bar{\tilde{q}}}_R(m^2_{\tilde{q}}) &= 0 \\
\lim_{p^2\to m^2_{\tilde{q}}} \frac{i}{p^2-m^2_{\tilde{q}}} \operatorname{Re}\Gamma^{\tilde{q}\bar{\tilde{q}}}_R(p) &= -1.
\end{aligned} \tag{5.17}$$

These conditions ensure that the real parts of the poles of the propagators are given by the mass parameters of the Lagrangian, which are therefore the physical particle masses. Furthermore, the propagators are required to have residue one. The propagator residues appear as Z-factors in the LSZ reduction formula, which describes the transition from Green functions to S-matrix elements. Requiring the residues to be one implies that no radiative corrections for external lines have to be taken into account explicitly. The renormalization conditions given above also demand that the renormalized two-point functions and therefore the propagators are UV finite.

To calculate the renormalization constants from the above conditions, the renormalized two-point functions $\Gamma^{(2)}_R$ can be split into the inverse tree-level propagators and the renormalized self-energies Σ_R, which contain the loop and counterterm diagrams and can be decomposed according to

$$\begin{aligned}
&= -i\Sigma^{GG}_{R,\mu\nu}(p) \\
&= -i\Big(g_{\mu\nu} - \frac{p_\mu p_\nu}{p^2}\Big)\Sigma^{GG}_{R,T}(p^2) - i\frac{p_\mu p_\nu}{p^2}\Sigma^{GG}_{R,L}(p^2)
\end{aligned}$$

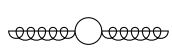

$$= i\Sigma^{\tilde{g}\tilde{g}}_R(p) = i\left[\not{p}\Sigma^{\tilde{g}\tilde{g}}_{R,V}(p^2) + m_{\tilde{g}}\Sigma^{\tilde{g}\tilde{g}}_{R,S}(p^2)\right]$$

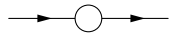

$$= i\Sigma^{q\bar{q}}_R(p) = i\not{p}\Sigma^{q\bar{q}}_{R,V}(p^2)$$

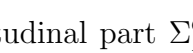

$$= -i\Sigma^{\tilde{q}\bar{\tilde{q}}}_R(p^2). \tag{5.18}$$

The longitudinal part $\Sigma^{GG}_{R,L}(p^2)$ of the gluon self energy vanishes due to a ward identity. Inserting these decompositions into the renormalization conditions, it is

possible to calculate the renormalization constants from the unrenormalized self energies Σ, resulting in

$$\begin{aligned}
\delta Z_g &= -\operatorname{Re}\Sigma_T^{GG\prime}(0) \\
\delta m_{\tilde{g}} &= m_{\tilde{g}} \operatorname{Re}\left[\Sigma_V^{\tilde{g}\tilde{g}}(m_{\tilde{g}}^2) + \Sigma_S^{\tilde{g}\tilde{g}}(m_{\tilde{g}}^2)\right] \\
\delta Z_{\tilde{g}} &= -\operatorname{Re}\Sigma_V^{\tilde{g}\tilde{g}}(m_{\tilde{g}}^2) - 2m_{\tilde{g}}^2 \operatorname{Re}\left[\Sigma_V^{\tilde{g}\tilde{g}\prime}(m_{\tilde{g}}^2) + \Sigma_S^{\tilde{g}\tilde{g}\prime}(m_{\tilde{g}}^2)\right] \\
\delta Z_q &= -\operatorname{Re}\Sigma_V^{q\bar{q}}(0) \\
\delta m_{\tilde{q}}^2 &= -\operatorname{Re}\Sigma^{\tilde{q}\bar{\tilde{q}}}(m_{\tilde{q}}^2) \\
\delta Z_{\tilde{q}} &= \operatorname{Re}\Sigma^{\tilde{q}\bar{\tilde{q}}\prime}(m_{\tilde{q}}^2),
\end{aligned} \tag{5.19}$$

where $\Sigma'(p^2) = \frac{\partial\Sigma(k^2)}{\partial k^2}\Big|_{k^2=p^2}$ denotes the derivative of the self energy. Explicit results in terms of scalar integrals are given in Appendix D. The renormalization constants given above do not only contain the UV divergences necessary to render the two-point functions UV finite, but also IR divergences.

For the remaining coupling constant renormalization we use the $\overline{MS}$-scheme [62], where only the $\frac{1}{\epsilon}$-poles along with some accompanying terms are included in the renormalization constants. The counterterm for the strong coupling g_3 is given by

$$\delta g_3 = -\frac{\alpha_s}{8\pi}\beta_0\left(\frac{1}{\epsilon} - \gamma + \ln 4\pi\right), \tag{5.20}$$

with

$$\beta_0 = 3N_c - N_f. \tag{5.21}$$

Using the renormalization constants (5.19) and (5.20) all Green functions are UV finite. We have explicitly checked the finiteness of the off-shell Green functions. Finally, the finite counterterm for the $q\bar{\tilde{q}}\tilde{g}$ Yukawa vertex given by (5.12) has to be included.

The strong coupling defined by (5.20) depends on the renormalization scale μ, and the corresponding one-loop beta function describing this scale dependence is given by

$$\beta(g_3) = \mu\frac{\partial g_3(\mu)}{\partial\mu} = -\beta_0\frac{g_3^3}{16\pi^2}. \tag{5.22}$$

In our scheme all coloured particles contribute to the scale dependence of α_s. Experimental values for $\alpha_s(m_Z)$ are however given within non-supersymmetric QCD with five active flavours. In SUSY QCD this corresponds to a renormalization scheme where all heavy particles (i.e. gluinos, squarks and the top quark) are decoupled from the scale dependence of α_s. The relation between $\alpha_s^{\mathrm{QCD}}(m_Z)$ in this scheme and $\alpha_s(m_Z)$ in our scheme is given by

$$\begin{aligned}
\alpha_s(m_Z) &= \alpha_s^{\mathrm{QCD}}(m_Z)\left[1 + \Delta(m_Z)\right]^2 \\
\Delta(m_Z) &= \frac{\alpha_s^{\mathrm{QCD}}(m_Z)}{4\pi}\left[\frac{N_c}{3}\ln\left(\frac{m_Z^2}{m_{\tilde{g}}^2}\right) + \frac{1}{3}\ln\left(\frac{m_Z^2}{m_t^2}\right) + \frac{N_f}{6}\ln\left(\frac{m_Z^2}{m_{\tilde{q}}^2}\right)\right],
\end{aligned} \tag{5.23}$$

where $N_c = 3$ is the number of colours and $N_f = 6$ is the number of active flavours in our scheme.

5.2.5 Infrared divergences

After renormalization there still remain IR divergences in the virtual corrections. Since we have moved all IR divergences from the 4-point to the 3-point integrals as described above, all IR divergences reside in scalar three-point integrals and derivatives of two-point integrals. The coefficients of the IR divergent scalar integrals become very simple, and the IR divergent contribution of the virtual corrections can be written as

$$\begin{aligned} d\sigma_2^V\big|_{\text{IR}} = d\sigma_1 \frac{\alpha_s}{\pi}\Bigg[&-\frac{19}{6}\frac{1}{\epsilon} - \frac{3}{2}(1-\mu_2-\mu_3-x_1)sC_0(s_{23}, m_{\tilde{q}}^2, m_{\tilde{g}}^2, m_{\tilde{g}}, m_{\tilde{q}}, 0) \\ &- \frac{3}{2}(1+\mu_3-\mu_2-x_3)sC_0(0, s_{12}, m_{\tilde{g}}^2, 0, 0, m_{\tilde{g}}) \\ &- \frac{1}{6}(1+\mu_3-\mu_2-x_1-x_3)sC_0(0, s_{12}, m_{\tilde{q}}^2, 0, 0, m_{\tilde{q}})\Bigg], \end{aligned} \tag{5.24}$$

where $d\sigma_1$ is the leading-order differential cross section, evaluated in D dimensions. Inserting the IR divergent parts of the scalar integrals, one obtains

$$\begin{aligned} d\sigma_2^V\big|_{\text{IR}} = d\sigma_1 \frac{\alpha_s}{\pi} C_\epsilon \Bigg[&-\frac{2}{3}\frac{1}{\epsilon^2} - \frac{19}{6}\frac{1}{\epsilon} + \frac{1}{6}\frac{1}{\epsilon}\ln\left(\frac{\mu m_{\tilde{q}}}{t_{13}}\right) - \frac{3}{2}\frac{1}{\epsilon}\ln\left(\frac{\mu m_{\tilde{g}}}{t_{12}}\right) \\ &- \frac{3}{4}\frac{1}{\epsilon}\frac{t_{23}}{\lambda^{\frac{1}{2}}(s_{23}, m_{\tilde{g}}^2, m_{\tilde{q}}^2)}\left[\ln\left(1-\frac{1}{x_+}\right) - \ln\left(1-\frac{1}{x_-}\right)\right]\Bigg], \end{aligned} \tag{5.25}$$

where $t_{ij} = 2p_ip_j$, $\lambda(a,b,c) = (a+b-c)^2 - 4ab$ is the usual 2-particle phase space function, and $x^\pm = (s_{23} + m_{\tilde{q}}^2 - m_{\tilde{g}}^2 \pm \lambda^{\frac{1}{2}}(s_{23}, m_{\tilde{q}}^2, m_{\tilde{g}}^2))/(2s_{23})$. The factorization of the IR divergent part of the virtual corrections with respect to the leading-order cross section is a necessary prerequisite for the cancellation of the IR divergences with the divergences from the real corrections.

5.3 Real corrections

In this section we will describe in detail the calculation of the real corrections, especially the implementation of the phase space slicing method. The inclusion of the effects of additional real gluon emission is necessary to cancel the IR divergences appearing in the virtual corrections. Therefore, we have to calculate the process

$$e^+(p_+)\, e^-(p_-) \to (\gamma^*, Z^*) \to q_i(p_1)\, \tilde{g}_a(p_2)\, \bar{\tilde{q}}_j(p_3) g_b(k), \tag{5.26}$$

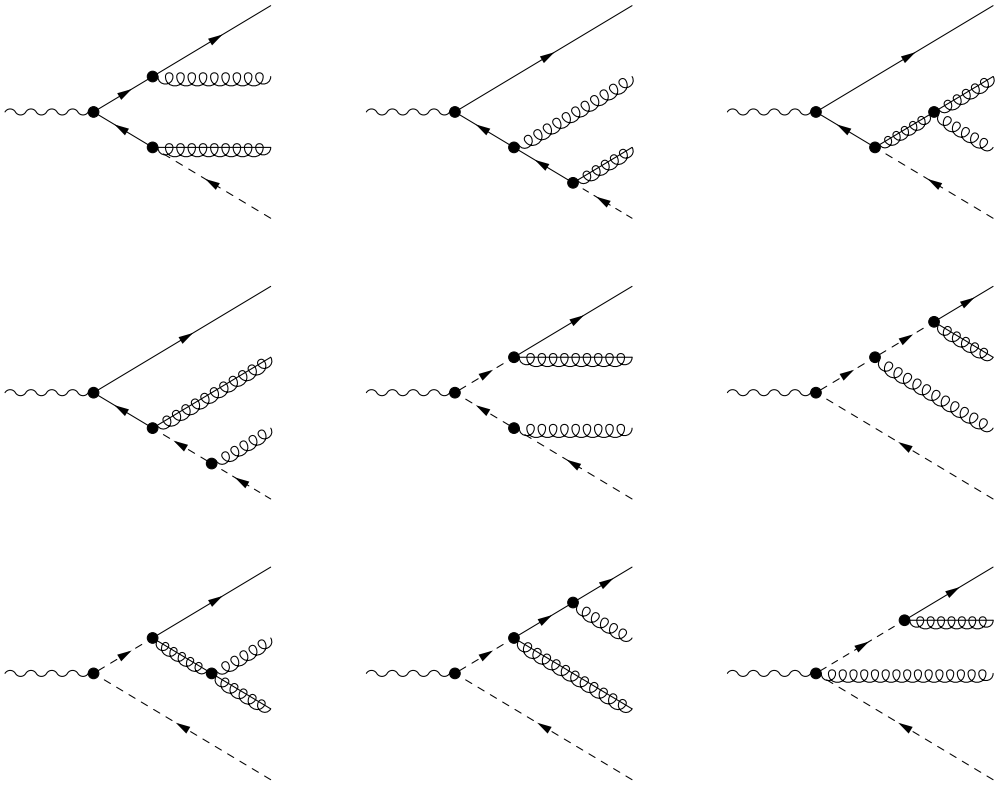

Figure 5.3: Feynman diagrams for the real corrections. Initial state particles have been omitted.

where the colour indices are shown explicitly. This process is obtained from the tree level process $e^+e^- \to q\bar{\tilde{q}}\tilde{g}$ by adding a gluon of momentum k in the final state.

The 9 diagrams that contribute to this process are shown in Fig. 5.3. The matrix element can be written in factorized form as

$$M_R^{L/R} = \left[L_\mu^\gamma Q_q + L_\mu^Z (c_V^q \pm c_A^q)\right] H_R^{L/R,\mu} = L_\mu^{L/R} H_R^{L/R,\mu}, \tag{5.27}$$

where the upper/lower sign corresponds to the production of L/R-squarks, and the leptonic currents L_μ^γ and L_μ^Z are defined in Eq. (4.14). The calculation of the hadronic part $H_R^{h,\mu}$ from the Feynman rules is straightforward, but since the resulting expression is rather long, we do not give it explicitly.

The matrix elements for the tree level process Eq. (4.10a) and for the real gluon emission process Eq. (5.26) can be decomposed according to the colour structure as follows

$$\begin{aligned} M_0 &= T_{ij}^a S_a \\ M_R &= (T^a T^b)_{ij} S_{ab} + (T^b T^a)_{ij} S_{ba}, \end{aligned} \tag{5.28}$$

with no implied summations over colour indices. The coefficients S_a, S_{ab}, and S_{ba} of the colour structures are called colour ordered subamplitudes. The squared matrix elements can be written in terms of the colour ordered subamplitudes as

$$\sum_{\text{colours}} |M_0|^2 = C_F N_c |S_a|^2$$
$$\sum_{\text{colours}} |M_R|^2 = \frac{N_c^2}{2} C_F \Big[|S_{ab}|^2 + |S_{ba}|^2 - \frac{1}{N_c^2} |S_{ab} + S_{ba}|^2 \Big]. \tag{5.29}$$

This decomposition of $|M_R|^2$ is chosen, because all three contributions on the r.h.s. have simple soft limits, making the integrals over the soft phase space sufficiently simple to calculate them analytically in D dimensions. Furthermore, we will use a different phase space splitting for each of these 3 contributions, so that these contributions have to be treated separately.

As the full matrix elements M_0 and M_R, all colour ordered subamplitudes can be factorized in the form $S = L_\mu S^\mu$. The integration over the final state orientation can therefore be done in the same way as for the tree level kinematics

$$\int d\Omega \, d\psi \sum_{\text{spins}} |S|^2 = \frac{128\pi^3\alpha}{3s} C_1^{L/R} P_{\mu\nu} S^{\mu\nu}, \tag{5.30}$$

with $S^{\mu\nu} = S^\mu S^{\nu *}$. We can therefore construct the differential cross sections for the $|S_{ab}|^2$ contribution

$$\begin{aligned} d\sigma_R^{(ab)} &= \frac{1}{8s} \int\limits_{\Omega,\phi} d\Phi_4(q \to p_1 + p_2 + p_3 + k) \frac{N_c^2}{2} C_F |S_{ab}|^2 \\ &= \frac{16\pi^3\alpha}{3s^2} C_1^{L/R} \frac{N_c^2}{2} C_F d\Phi_4' P_{\mu\nu} S_{ab}^{\mu\nu}, \end{aligned} \tag{5.31}$$

where $d\Phi_4'$ is the 4 particle phase space measure with $d\Omega \, d\phi$ omitted. The contributions $d\sigma_R^{(ba)}$ and $d\sigma_R^{(ab+ba)}$ can be obtained in the same way, and the complete angle integrated differential cross section for the real corrections can be written

$$d\sigma_R = d\sigma_R^{(ab)} + d\sigma_R^{(ba)} + d\sigma_R^{(ab+ba)}. \tag{5.32}$$

5.3.1 Soft and collinear limits

We will now discuss the soft and collinear limits and introduce the corresponding approximations of the matrix element. These approximations only contain the singular behaviour and have a form simple enough to allow their analytical integration over the soft and collinear parts of phase space. The remaining regular parts can be neglected for a sufficiently small slicing parameter x_{cut}, since in the limit $x_{\text{cut}} \to 0$ the volume of the soft and collinear phase space regions approaches zero.

The soft and collinear approximations are universal, i.e. they can be written down once the process and therefore the external particles are specified, without actually having to calculate the matrix elements M_0 or M_R. They are furthermore valid in D dimensions, so that the appearing tree level matrix elements or squared matrix elements have to be evaluated in D dimensions. We have of course checked that our expression of the full squared matrix element, or rather the 3 colour contributions in Eq. (5.29), do reduce to the soft and collinear approximations given below.

In the soft limit, i.e. if the gluon momentum becomes small, the full matrix element M_R cannot be written in a simple, factorized form due to its nontrivial colour structure. However, the colour ordered subamplitudes factorize according to

$$\begin{aligned} S_{ab} &\xrightarrow{k \text{ soft}} g_3 e(p_2, p_3) S_a \\ S_{ba} &\xrightarrow{k \text{ soft}} g_3 e(p_1, p_2) S_a, \end{aligned} \tag{5.33}$$

with the eikonal factor $e(p_i, p_j)$ given by

$$e(p_i, p_j) = \epsilon_\mu^*(k, \lambda) \left(\frac{p_i^\mu}{p_i k} - \frac{p_j^\mu}{p_j k} \right), \tag{5.34}$$

where $\epsilon_\mu^*(k, \lambda)$ is the polarization vector of the gluon with polarization λ. In Eq. (5.33), terms of $\mathcal{O}(k_0)$ have been neglected, so that the factorization in the soft limit only holds exactly for vanishing gluon momentum k. Using these equations, the soft limits of the contributions appearing in Eq. (5.29) can be obtained

$$\begin{aligned} |S_{ab}|^2 &\xrightarrow{k \text{ soft}} g_3^2 f(p_2, p_3) |S_a|^2 \\ |S_{ba}|^2 &\xrightarrow{k \text{ soft}} g_3^2 f(p_1, p_2) |S_a|^2 \\ |S_{ab} + S_{ba}|^2 &\xrightarrow{k \text{ soft}} g_3^2 f(p_1, p_3) |S_a|^2, \end{aligned} \tag{5.35}$$

with

$$f(p_i, p_j) = |e(p_i, p_j)|^2 = \frac{2 p_i p_j}{(p_i k)(p_j k)} - \frac{m_i^2}{(p_i k)^2} - \frac{m_j^2}{(p_j k)^2}. \tag{5.36}$$

In the square of the eikonal factor we have used the gluon polarization sum $\sum_\lambda \epsilon_\mu(k, \lambda) \epsilon_\nu^*(k, \lambda) = -g_{\mu\nu}$, which is possible if only one external gluon is present. The simple structure of these soft limits is the reason for using colour ordered subamplitudes, and especially for writing $|M_R|^2$ in terms of $|S_{ab} + S_{ba}|^2$ and not in terms of $\mathrm{Re}(S_{ab} S_{ba}^*)$.

The other relevant limit is the collinear limit, which is defined by the gluon momentum being parallel to another external particle momentum. A singularity is only associated with this configuration if the other particle is massless, and the gluon couples to it. In the process (5.26) a collinear singularity therefore

only occurs if the gluon and the quark become collinear. In this case the squared matrix element factorizes according to

$$|M_R|^2 \overset{p_1||k}{\to} 4\pi\alpha_s \frac{1}{p_1 k} P_{q\to qg}(z)\, |M_0|^2, \tag{5.37}$$

where the Altarelli-Parisi splitting function is given within dimensional regularization by

$$P_{q\to qg}(z) = C_F \left[\frac{1+z^2}{1-z} - \epsilon(1-z)\right], \tag{5.38}$$

with the momentum fraction of the quark denoted by z, so that in the exact collinear limit we have

$$\begin{aligned} p_1 &= z(p_1+k) \\ k &= (1-z)(p_1+k). \end{aligned} \tag{5.39}$$

The collinear singularity in Eq. (5.37) is contained in the scalar product $p_1 k$, that can be written as $p_1 k = p_1^0 k^0 (1-\cos\theta_{1g})$, and vanishes for $\cos\theta_{1g} = 1$. For our implementation of the phase space slicing method we also need the collinear limits of the colour contributions in Eq. (5.29), which can be deduced from the limit of the full squared matrix element, and are given by

$$\left.\begin{matrix} |S_{ba}|^2 \\ |S_{ab}+S_{ba}|^2 \end{matrix}\right\} \overset{p_1||k}{\to} 4\pi\alpha_s \frac{1}{p_1 k} \frac{2}{N_c^2-1} \frac{P_{q\to qg}(z)}{C_F}\, |M_0|^2$$
$$|S_{ab}|^2 \overset{p_1||k}{\to} \text{regular}. \tag{5.40}$$

While $|S_{ba}|^2$ and $|S_{ab}+S_{ba}|^2$ have identical limits, the contribution $|S_{ab}|^2$ is not singular in the collinear region. The reason for this is that the diagrams where the gluon is emitted by the final state quark do not contribute to S_{ab}, but only to S_{ba}, and only these diagrams contain singularities.

5.3.2 Definition of phase space splitting

The approximations of the colour contributions to the squared matrix element given above have to be integrated analytically over the soft and collinear parts of phase space. In order to do this, we first have to define the splitting of phase space into a soft, a collinear, and a hard part. There is a certain freedom in the choice of this splitting, which we use to render the integrals as simple as possible. Since the gluon energy E_g and the angle θ_{1g} between the gluon and the quark directly appear in the soft and collinear limits (5.35) and (5.40), we define the separation of phase space into the different regions in terms of these variables. Motivated by the fact that the soft limits are given in terms of the function $f(p_i, p_j)$, containing a different set of only 3 of the 4 particle momenta

for each of the 3 contributions in (5.32), we choose a slightly different splitting for each of these 3 colour contributions. The integrals over soft phase space then take a very simple form.

Specifically, we use the gluon energy $E_g^{(ij)}$ and the polar angle $\theta_{ig}^{(ij)}$ between particle i and the gluon defined in the 3 particle CMS $p_i + p_j + k = Q_{ijg} = (\sqrt{s_{ijg}}, \vec{0})$, where p_i and p_j are two of the particles in the tree level process. The scaled energy $x_g^{(ij)}$ is defined by

$$x_g^{(ij)} = \frac{2E_g^{(ij)}}{\sqrt{s_{ijg}}} = \frac{2kQ_{ijg}}{s_{ijg}} = \frac{2k(p_i + p_j)}{s_{ijg}}. \tag{5.41}$$

Furthermore, if particle i is massless, $\cos\theta_{ig}^{(ij)}$ can be expressed in terms of invariants as

$$\cos\theta_{ig}^{(ij)} = 1 - \frac{p_i k \cdot s_{ijg}}{p_i Q_{ijg} \cdot k Q_{ijg}}. \tag{5.42}$$

In terms of these variables we will now define the splitting of phase space for the three colour contributions.

$|S_{ab}|^2$: This contribution has only soft, but no collinear singularities, so that it is sufficient to split the phase space into a soft and a hard part. We write this decomposition as an identity in terms of Heaviside functions Θ as

$$1 = \Theta(x_{\text{cut}} - x_g^{(23)}) + \Theta(x_g^{(23)} - x_{\text{cut}}), \tag{5.43}$$

where the first term corresponds to the soft part of phase space and the second term to the hard part.

$|S_{ba}|^2$: This contribution has soft and collinear singularities. We therefore split the phase space into three regions according to

$$\begin{aligned} 1 &= \left[\Theta(x_{\text{cut}} - x_g^{(12)}) + \Theta(x_g^{(12)} - x_{\text{cut}})\right] \\ &\quad \cdot \left[\Theta(1 - \cos\theta_{1g}^{(12)} - x_{\text{cut}}) + \Theta(x_{\text{cut}} - (1 - \cos\theta_{1g}^{(12)}))\right] \\ &= 1 \cdot \Theta(x_{\text{cut}} - x_g^{(12)}) \\ &\quad + \Theta(x_g^{(12)} - x_{\text{cut}})\Theta(x_{\text{cut}} - (1 - \cos\theta_{1g}^{(12)})) \\ &\quad + \Theta(x_g^{(12)} - x_{\text{cut}})\Theta(1 - \cos\theta_{1g}^{(12)} - x_{\text{cut}}). \end{aligned} \tag{5.44}$$

Here, the first term describes the soft region, which includes also the region where the gluon is both soft and collinear to the quark. The collinear but not soft part corresponds to the second term, and the remaining hard part is described by the last term.

$|S_{ab} + S_{ba}|^2$: The last contribution also has soft and collinear singularities, and the splitting is defined analogous to the previous case by

$$\begin{aligned}
1 &= \left[\Theta(x_{\text{cut}} - x_g^{(13)}) + \Theta(x_g^{(13)} - x_{\text{cut}})\right] \\
&\quad \cdot \left[\Theta(1 - \cos\theta_{1g}^{(13)} - x_{\text{cut}}) + \Theta(x_{\text{cut}} - (1 - \cos\theta_{1g}^{(13)}))\right] \\
&= 1 \cdot \Theta(x_{\text{cut}} - x_g^{(13)}) \\
&\quad + \Theta(x_g^{(13)} - x_{\text{cut}})\Theta(x_{\text{cut}} - (1 - \cos\theta_{1g}^{(13)})) \\
&\quad + \Theta(x_g^{(13)} - x_{\text{cut}})\Theta(1 - \cos\theta_{1g}^{(13)} - x_{\text{cut}}).
\end{aligned} \tag{5.45}$$

Again, the first term corresponds to the soft region, the second to the collinear and not soft region, and the third to the hard region of phase space.

5.3.3 Contributions from soft phase space

To perform the integration of the approximations (5.35) over the soft phase space, we have to factorize the full 4-particle phase space within the soft region. This factorization is very simple in the soft case, and can be written as

$$\begin{aligned}
d\Phi_4 \Theta(x_{\text{cut}} - x_g^{(ij)}) &= \prod_{l=1}^{3} \frac{d^{D-1}p_l}{(2\pi)^{D-1}\, 2p_l^0} \cdot \frac{d^{D-1}k}{(2\pi)^{D-1}\, 2k^0} (2\pi)^D \\
&\qquad \cdot \delta^{(D)}(q - \textstyle\sum_l p_l - k)\Theta(x_{\text{cut}} - x_g^{(ij)}) \\
&= d\Phi_3\, d\Phi_1^s,
\end{aligned} \tag{5.46}$$

with

$$d\Phi_1^s = \frac{d^{D-1}k}{(2\pi)^{D-1}\, 2k^0} \Theta(x_{\text{cut}} - x_g^{(ij)}). \tag{5.47}$$

In the soft limits (5.35) only the squared eikonal factors $f(p_i, p_j)$ depend on the gluon momentum. We therefore have to calculate the integrals

$$\begin{aligned}
S^{(ij)}(m_i, m_j) &= \mu^{4-D} \int d\Phi_1^s\, f(p_i, p_j) \\
&= \mu^{4-D} \int \frac{d^{D-1}k}{(2\pi)^{D-1}\, 2k^0} f(p_i, p_j) \Theta(x_{\text{cut}} - x_g^{(ij)}),
\end{aligned} \tag{5.48}$$

where the factor μ^{4-D}, necessary in dimensional regularization, is included. We need this integral for the case of one vanishing and one non-vanishing mass as well as for both masses nonzero. These integrals do only depend on the invariants of the leading order 3-body kinematics, and are given explicitly in Appendix C.

In terms of these integrals, the soft contribution to the angle integrated differential cross sections for the three colour parts are given by

$$\begin{aligned} d\sigma_R^{(ab),s} &= 4\pi\alpha_s \frac{N_c}{2} \cdot S^{(23)}(m_{\tilde{g}}, m_{\tilde{q}}) \cdot d\sigma_1 \\ d\sigma_R^{(ba),s} &= 4\pi\alpha_s \frac{N_c}{2} \cdot S^{(12)}(0, m_{\tilde{g}}) \cdot d\sigma_1 \\ d\sigma_R^{(ab+ba),s} &= -4\pi\alpha_s \frac{1}{2N_c} \cdot S^{(13)}(0, m_{\tilde{q}}) \cdot d\sigma_1. \end{aligned} \tag{5.49}$$

Adding these together, the total contribution from the soft phase space is obtained

$$d\sigma_2^s = d\sigma_1 \cdot 4\pi\alpha_s \frac{N_c}{2} \left[S^{(23)}(m_{\tilde{g}}, m_{\tilde{q}}) + S^{(12)}(0, m_{\tilde{g}}) - \frac{1}{N_c^2} S^{(13)}(0, m_{\tilde{q}}) \right]. \tag{5.50}$$

Using the explicit expressions for the integrals, the IR divergent part can be extracted. It is given by

$$\begin{aligned} d\sigma_2^s \Big|_{\text{IR div}} = d\sigma_1 \frac{\alpha_s N_c}{4\pi} C_\epsilon \Bigg[& \frac{N_c^2 - 1}{N_c^2} \frac{1}{\epsilon^2} + (3 - \frac{1}{N_c^2}) \frac{1}{\epsilon} + \ln\left(\frac{\mu^2 m_{\tilde{g}}^2}{s_{12}^2 x_{\text{cut}}^2} \right) \frac{1}{\epsilon} \\ & - \frac{1}{N_c^2} \ln\left(\frac{\mu^2 m_{\tilde{q}}^2}{s_{13}^2 x_{\text{cut}}^2} \right) \frac{1}{\epsilon} + \frac{t_{23}}{\lambda^{\frac{1}{2}}(s_{23}, m_{\tilde{g}}^2, m_{\tilde{q}}^2)} \ln\left(\sigma_2^{(23)} \sigma_3^{(23)} \right) \frac{1}{\epsilon} \Bigg], \end{aligned} \tag{5.51}$$

using the notations introduced in Appendix C.2. There are IR divergent terms containing $\ln(x_{\text{cut}})$, which originate from the split-up of the singular region into a collinear but not soft part, and a soft part. Therefore, these terms have to cancel against the corresponding terms from the collinear part.

5.3.4 Contributions from collinear phase space

In the collinear region, the phase space can be factorized according to

$$d\Phi_4 \frac{1}{p_1 k} \Theta(x_g^{(1i)} - x_{\text{cut}}) \Theta(x_{\text{cut}} - (1 - \cos\theta_{1g}^{(1i)})) = d\Phi_3 \, d\Phi_1^{c(i)}, \tag{5.52}$$

with

$$\begin{aligned} d\Phi_1^{c(i)} = \frac{1}{16\pi^3} \left(\frac{s_{1i}}{16\pi^2} \right)^{-2\epsilon} & (1 - \mu_i^{(1i)})^{-2\epsilon} dz \, dy \, d\Omega^{D-2} [z(1-z)]^{-2\epsilon} \\ & \cdot \frac{(1-y^2)^{-\epsilon}}{1-y} \Theta(x_{\text{cut}} - (1-y)) \Theta(1 - z_{\text{cut}} - z), \end{aligned} \tag{5.53}$$

where $y = \cos\theta_{1g}^{(1i)}$, $\mu_i^{(1i)} = \frac{m_i^2}{s_{1i}}$, and $z_{\text{cut}} = \frac{x_{\text{cut}}}{1 - \mu_i^{(1i)}}$. The singular factor $\frac{1}{p_1 k}$ from the collinear limit of the squared matrix element is included in this factorization, so

that we have to calculate the integrals of the splitting function over the collinear phase space, with the result

$$\begin{aligned}
C_{q\to qg}^{(i)} &= \mu^{4-D}\int d\Phi_1^{c(i)} P_{q\to qg}(z)\Theta(x_{\text{cut}}-(1-y))\Theta(1-z_{\text{cut}}-z) \\
&= \frac{C_F}{8\pi^2}C_\epsilon\left[\left(\frac{3}{2}+2\ln\left(\frac{x_{\text{cut}}}{1-\mu_i^{(1i)}}\right)\right)\frac{1}{\epsilon}+\frac{3}{2}\ln\left(\frac{2\mu_i^{(1i)2}}{s_{1i}x_{\text{cut}}}\right)\right. \\
&\quad + 2\ln\left(\frac{x_{\text{cut}}}{1-\mu_i^{(1i)}}\right)\ln\left(\frac{2\mu_i^{(1i)2}}{s_{1i}}\right)-4\ln^2(x_{\text{cut}})+2\ln\left(1-\mu_i^{(1i)}\right)\ln(x_{\text{cut}}) \\
&\quad \left.-3\ln\left(1-\mu_i^{(1i)}\right)+2\ln^2\left(1-\mu_i^{(1i)}\right)-\left(\frac{2\pi^2}{3}-\frac{13}{2}\right)\right].
\end{aligned} \tag{5.54}$$

The collinear contributions to the angle integrated differential cross section can be expressed as

$$\begin{aligned}
d\sigma_R^{(ba),c} &= 4\pi\alpha_s\frac{N_c^2}{N_c^2-1}\cdot C_{q\to qg}^{(2)}\cdot d\sigma_1 \\
d\sigma_R^{(ab+ba),c} &= -4\pi\alpha_s\frac{1}{N_c^2-1}\cdot C_{q\to qg}^{(3)}\cdot d\sigma_1.
\end{aligned} \tag{5.55}$$

The total contribution from the collinear part of phase space is therefore given by

$$d\sigma_2^c = d\sigma_1\cdot 4\pi\alpha_s\frac{N_c^2}{N_c^2-1}\left[C_{q\to qg}^{(2)}-\frac{1}{N_c^2}C_{q\to qg}^{(3)}\right]. \tag{5.56}$$

Extracting the IR divergent part from this expression, one obtains

$$\begin{aligned}
d\sigma_2^c\Big|_{\text{IR div}} &= d\sigma_1\frac{\alpha_s N_c}{4\pi}C_\epsilon\frac{1}{\epsilon}\left[\frac{3}{2}\left(1-\frac{1}{N_c^2}\right)+2\ln\left(\frac{x_{\text{cut}}}{1-\mu_2^{(12)}}\right)\right. \\
&\quad \left.-\frac{2}{N_c^2}\ln\left(\frac{x_{\text{cut}}}{1-\mu_3^{(13)}}\right)\right].
\end{aligned} \tag{5.57}$$

The IR divergences of the real corrections are completely given by (5.51) and (5.57). When these two contributions are added, the IR divergent $\ln(x_{\text{cut}})$ terms cancel as necessary.

Finally, comparing with the IR divergences of the virtual corrections (5.25), it can be seen that all IR divergences cancel between real and virtual corrections, as required by the Kinoshita-Lee-Nauenberg theorem. Adding up the virtual corrections, the soft and the collinear contributions therefore yields a finite result, which is numerically integrated over the 3 particle phase space in 4 dimensions using VEGAS.

5.3.5 Contributions from hard phase space

The contributions from hard phase space are completely finite, and are therefore integrated in 4 dimensions using the 4 dimensional squared matrix element. Of course, the 3 contributions in (5.32) have to be treated separately, since we use a different phase space splitting for each one. In principle this integration could be performed using any parameterization of the 4-particle phase space. However, in order to obtain numerically stable results for small values of the slicing parameter x_{cut}, it is necessary to use the variables $x_g^{(ij)}$ and $\cos\theta_{1g}^{(1i)}$, appearing in the definition of the phase space splitting, directly as integration variables. This means that we have to use different parameterizations of phase space for the 3 colour contributions, which we give below.

For the $|S_{ab}|^2$ contribution, we use the parameterization

$$d\Phi_4 = \frac{1}{256 s (2\pi)^8} d\Omega\, d\phi\, ds_{23g}\, d\varphi^{(23)}\, d\cos\theta_{12}^{(23)}\, dx_g^{(23)}\, dx_2^{(23)}\, s_{23g}(s - s_{23g}), \quad (5.58)$$

where Ω and ϕ describe the final state orientation in the overall CMS, while the other variables are defined in the CMS of the $p_2 + p_3 + k$ system. The variables $x_g^{(23)}$ and $x_2^{(23)}$ are the scaled energies of the gluon and gluino defined in (5.41), $\theta_{12}^{(23)}$ is the polar angle between the gluon and the gluino momentum, while $\varphi^{(23)}$ is the azimuthal angle corresponding to a rotation around the $\vec{p}_2$-direction. The integration borders are given by

$$\begin{aligned}
0 \le x_g^{(23)} &\le 1 - \tilde{\mu}_2 - \tilde{\mu}_3 - 2\sqrt{\tilde{\mu}_2 \tilde{\mu}_3} \\
x_2^{(23)} &\leqslant \frac{1}{2(1 - x_g^{(23)})} \Big[(2 - x_g^{(23)})(1 + \tilde{\mu}_2 - \tilde{\mu}_3 - x_g^{(23)}) \\
&\qquad \pm x_g^{(23)} \lambda^{\frac{1}{2}}(1 - x_g^{(23)}, \tilde{\mu}_2, \tilde{\mu}_3) \Big] \\
(m_{\tilde{g}} + m_{\tilde{q}})^2 &\le s_{23g} \le s \\
0 &\le \varphi \le 2\pi \\
-1 &\le \cos\theta_{12}^{(23)} \le +1,
\end{aligned} \quad (5.59)$$

where $\tilde{\mu}_i = \frac{m_i^2}{s_{23g}}$.

The parameterization used for the $|S_{ba}|^2$ contribution is given by

$$\begin{aligned}
d\Phi_4 = \frac{1}{128 s (2\pi)^8} d\Omega\, d\phi\, ds_{12g}\, d\cos\theta_{13}^{(12)}\, d\varphi^{(12)}\, d\cos\theta_{1g}^{(12)}\, dx_g^{(12)} x_g^{(12)} \\
\cdot \lambda^{\frac{1}{2}}(s, s_{12g}, m_3^2) \frac{s_{12g}(1 - x_g^{(12)}) - m_2^2}{[2 - x_g^{(12)}(1 - \cos\theta_{1g}^{(12)})]^2},
\end{aligned} \quad (5.60)$$

where all variables except Ω and ϕ are defined in the $p_1 + p_2 + k$ CMS. The scaled gluon energy $x_g^{(12)}$ is defined in (5.41), $\theta_{1g}^{(12)}/\theta_{13}^{(12)}$ are the polar angles between

the quark and the gluon/squark, and φ is the azimuthal angle associated with rotations around the quark momentum axis. The integration borders for this parameterization are given by

$$\begin{aligned} 0 &\leq x_g^{(12)} \leq 1 - \frac{m_2^2}{s_{12g}} \\ m_2^2 &\leq s_{12g} \leq (\sqrt{s} - m_3)^2 \\ -1 &\leq \cos\theta_{1g}^{(12)} \leq 1 \\ -1 &\leq \cos\theta_{13}^{(12)} \leq 1 \\ 0 &\leq \varphi^{(12)} \leq 2\pi. \end{aligned} \tag{5.61}$$

For the $|S_{ab} + S_{ba}|^2$ contribution the parameterization can be obtained from the one above by exchanging the gluino and the squark, corresponding to the exchange $2 \leftrightarrow 3$ in all indices.

Using these parameterizations, it is possible to choose very small values for x_{cut} without encountering numerical instabilities in the integration, though the relative errors for the complete NLO corrections will grow large due to numerical cancellations between the hard contributions and the soft and collinear contributions. The choice of a suitable value of x_{cut} will be discussed below.

5.4 Checks of the calculation

Since the final results for the NLO corrections are very complicated expressions, it is necessary to perform several checks to ensure the correctness of the calculation.

The cancellation of all UV- and IR-divergences is already such a nontrivial check. Since all mass and wave-function renormalization constants are computed from the self energy corrections, and the coupling constant counterterm is required to render the renormalized $q\bar{q}g$-vertex correction finite, the UV-finiteness of the other renormalized 1PI vertex functions appearing in this process is a first test of the calculation. Furthermore, because all UV divergences are contained within the counterterms and the scalar 1- and 2-point functions A_0 and B_0, generated mostly by the tensorreduction, this is also a test of our implementation of the tensorreduction. The IR-divergences all reside within the scalar 3-point integrals C_0, and the derivative of the scalar 2-point integral B_0'. The IR-finiteness is therefore also a check of the tensorreduction, and at the same time a partial test of the soft and collinear parts of the real corrections.

In the phase space slicing approach used in this calculation the result depends in principle on the slicing parameter x_{cut}, because terms of $\mathcal{O}(x_{\text{cut}})$ are neglected. However, these errors become arbitrarily small for $x_{\text{cut}} \to 0$, and the result must show convergence if this limit is performed numerically. At the same time cancellations between the hard part of the real corrections and the soft and collinear

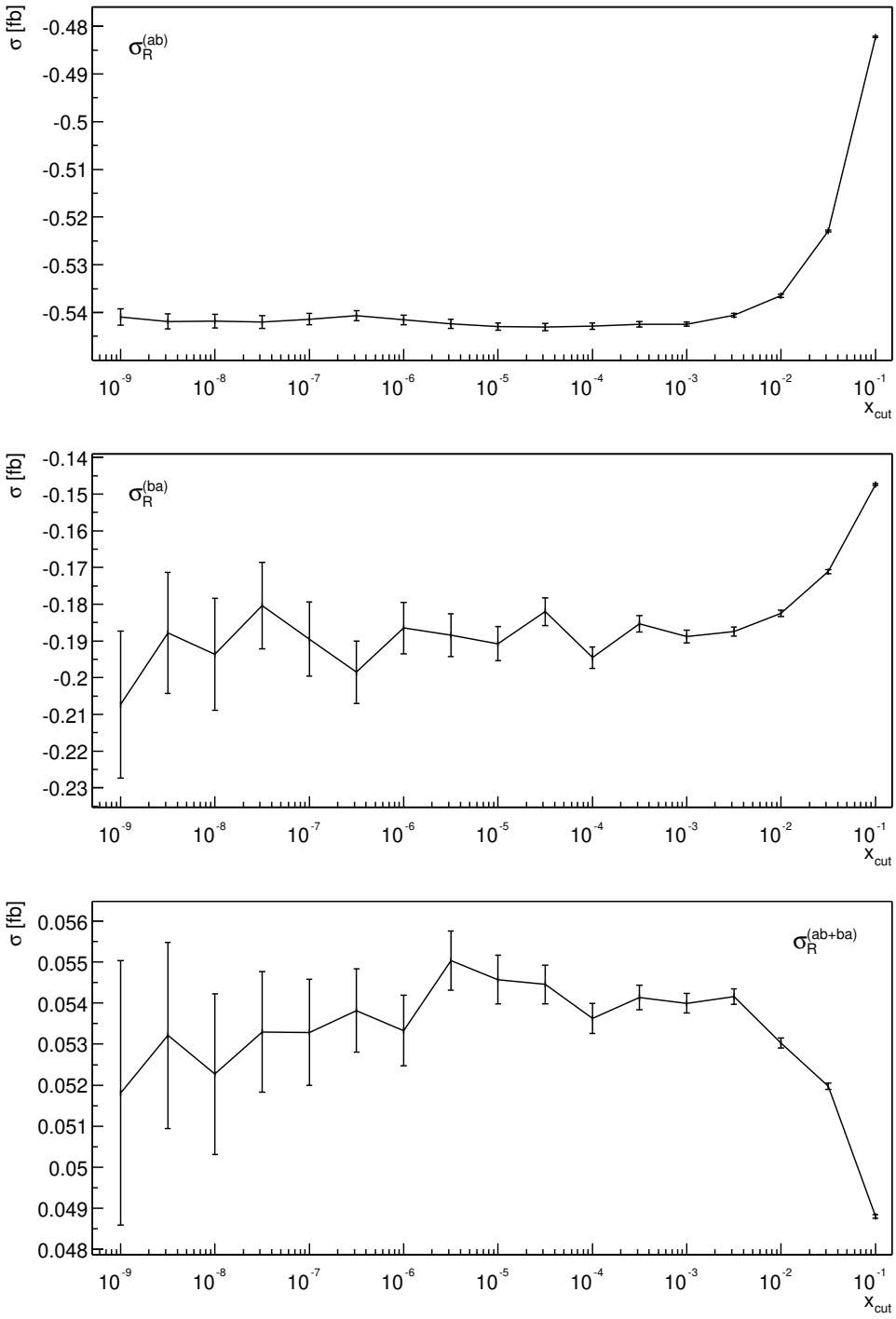

Figure 5.4: Phase space slicing parameter dependence of real corrections. The parameter values $\sqrt{s} = 2000\,\text{GeV}$, $m_{\tilde{g}} = 600\,\text{GeV}$, $m_{\tilde{q}} = 200\,\text{GeV}$, and $\mu = m_{\tilde{q}} + m_{\tilde{g}}$ have been used.

part will grow large, leading to larger numerical errors. Therefore, the value of $x_{\rm cut}$ has to be chosen carefully. In Fig. 5.4 we have shown the $x_{\rm cut}$-dependence of the three colour contributions $d\sigma_R^{(ab)}$, $d\sigma_R^{(ba)}$ and $d\sigma_R^{(ab+ba)}$ of the real corrections at $\sqrt{s} = 2000\,\text{GeV}$, and for the masses $m_{\tilde{g}} = 600\,\text{GeV}$, and $m_{\tilde{q}} = 200\,\text{GeV}$. A value of $\mu = m_{\tilde{q}} + m_{\tilde{g}}$ has been chosen for the renormalization scale. These quantities are of course IR-divergent, and only the finite part is shown. It can be seen that the results are $x_{\rm cut}$-dependent for large values for $x_{\rm cut}$. A plateau is however reached for $x_{\rm cut} \lesssim 10^{-3}$, with numerical errors continually growing as $x_{\rm cut}$ gets smaller. This implies that the implementation of the phase space slicing procedure has been done consistently. We have also investigated other choices of the parameters, which yield similar results. Therefore, we use the value

$$x_{\rm cut} = 10^{-4}, \tag{5.62}$$

which clearly lies in the plateau region, for all subsequent results.

A further check can be made by investigating the renormalization scale dependence of the complete NLO result. The total cross section summed to all orders in perturbation theory is scale independent and can be written as a Taylor series in $\alpha_s(\mu)$ in the usual way

$$\begin{aligned}\sigma &= \sigma_1 + \sigma_2 + \mathcal{O}(\alpha_s^3) \\ &= \alpha_s(\mu) A + \alpha_s^2(\mu) B(\mu) + \mathcal{O}(\alpha_s^3).\end{aligned} \tag{5.63}$$

The NLO coefficient $B(\mu)$ does explicitly depend on μ, while the leading order coefficient A is scale independent. We can now take the derivative of (5.63) with respect to μ on both sides, and rearrange the resulting terms into a series in $\alpha_s(\mu)$. Since the l.h.s is scale independent, each coefficient has to vanish, and from the α_s^2-coefficient we obtain

$$\frac{dB}{d\mu} = -\frac{\beta_0}{\mu} A, \tag{5.64}$$

with β_0 from (5.21). Integrating this, the NLO coefficients at different scales can be related

$$B(\mu) = B(\mu_0) - \beta_0 A \ln\left(\frac{\mu}{\mu_0}\right). \tag{5.65}$$

Note that (5.65) is an exact equation, and does not receive corrections from terms of higher order in $\alpha_s(\mu)$. We have explicitly checked for several parameter sets that the scale dependence of our numerical results is in agreement with (5.65).

5.5 Numerical results

In the results presented below, we have summed up the contributions of the 4 final states (4.10a)-(4.10d) for all 5 light flavours $f = u, d, s, c, b$. The NLO

corrections for the $q\bar{\tilde{q}}_L\tilde{g}$ and $q\bar{\tilde{q}}_R\tilde{g}$ final states are directly obtained by using the corresponding prefactors $C_1^{L/R}$ and $C_2^{L/R}$ in (5.5) and (5.31). As in the tree level case, the final states containing an antiquark are related by (4.12) to the $q\bar{\tilde{q}}\tilde{g}$ final states, yielding a factor 2 for the angle-integrated differential cross sections.

We first consider the case $m_{\tilde{q}} < m_{\tilde{g}}$ (case I in Tab. 4.1). In Fig. 5.5a the $\sqrt{s}$-dependence of the total cross sections in LO and in NLO is shown for the parameters $m_{\tilde{g}} = 600\,\text{GeV}$, $m_{\tilde{q}} = 200\,\text{GeV}$, which lie outside of the current CDF boundaries. The renormalization scale has been chosen as $\mu = m_{\tilde{g}} + m_{\tilde{q}}$. The SUSY QCD corrections are significant and positive, and shift the peak of the cross section downwards by about 500 GeV. The corrections enhance the LO result by +45% in the NLO peak region and fall slowly off towards higher c.m. energies, reaching +15% at $\sqrt{s} = 5000\,\text{GeV}$. For small c.m. energies the NLO corrections become arbitrarily large compared to the LO result, due to the Coulomb singularities directly above the threshold. Fig. 5.5b shows the same quantities for the parameters $m_{\tilde{g}} = 400\,\text{GeV}$, $m_{\tilde{q}} = 300\,\text{GeV}$. The general pattern is similar to the case discussed before. The peak of the cross section is shifted slightly downwards, with the corrections at the peak amounting to +25%. However, the corrections fall off faster, and are getting negative at high energies, with a correction of −10% at $\sqrt{s} = 5000\,\text{GeV}$. The scale dependence for this parameters for a c.m. energy in the peak region is shown in Fig. 5.6. The inclusion of the NLO corrections reduces the scale dependence, thus leading to a more reliable theoretical prediction of the cross section.

For the case $m_{\tilde{q}} > m_{\tilde{g}}$ the process $e^+e^- \to q\bar{\tilde{q}}\tilde{g}$ is relevant only in the region IIb in Tab. 4.1. Fig. 5.7 shows the $\sqrt{s}$-dependence of the LO and NLO cross sections in this region, with the parameters $m_{\tilde{g}} = 200\,\text{GeV}$ and $m_{\tilde{q}} = 500\,\text{GeV}$. In this region the NLO corrections are positive and very large, with values of +75% to +80% in the upper half of the region. Of course this region is rather close to the kinematical threshold, so that large NLO corrections have to be expected here. Furthermore, the scale dependence is increased by the inclusion of the NLO corrections, as is shown in Fig. 5.8. This is not surprising however, given the large value of the corrections. It seems therefore that the perturbative expansion is not very reliable in this region. However, since the absolute value of the cross section is significantly below 1 fb, this region will probably not be relevant for the test of the supersymmetric coupling relation, making it less important to have an accurate theoretical prediction here.

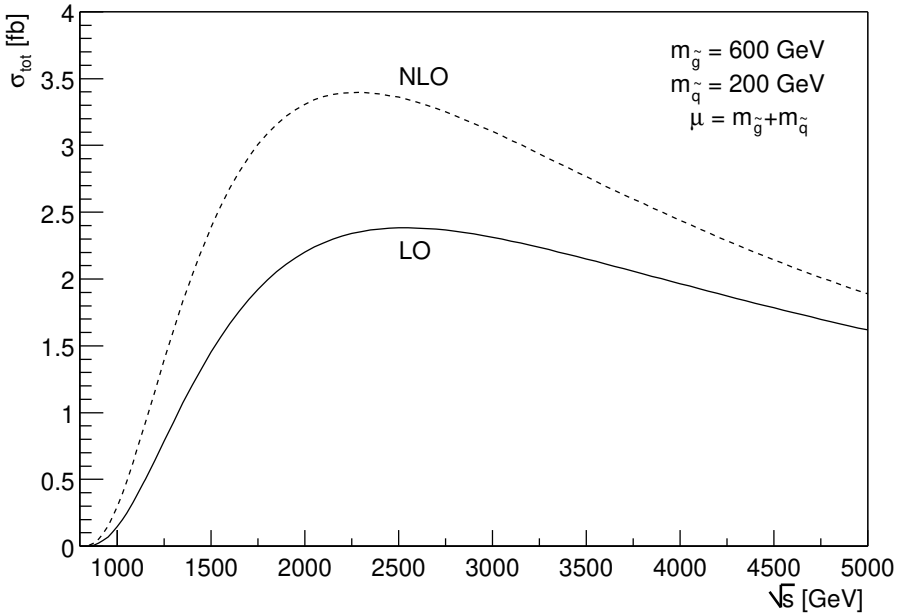

(a)

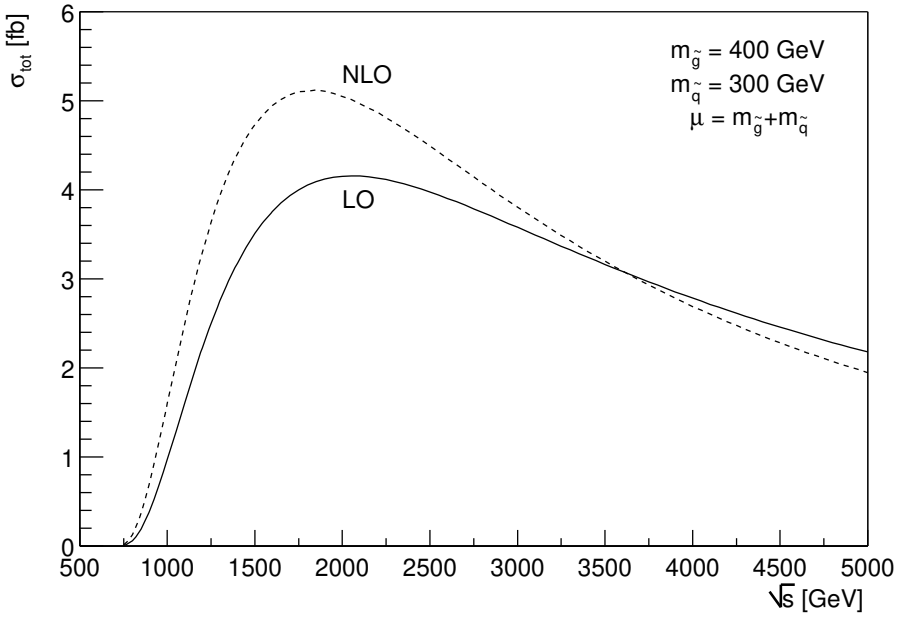

(b)

Figure 5.5: Total cross section for gluino production in LO and NLO. Parameters correspond to case I in Tab. 4.1.

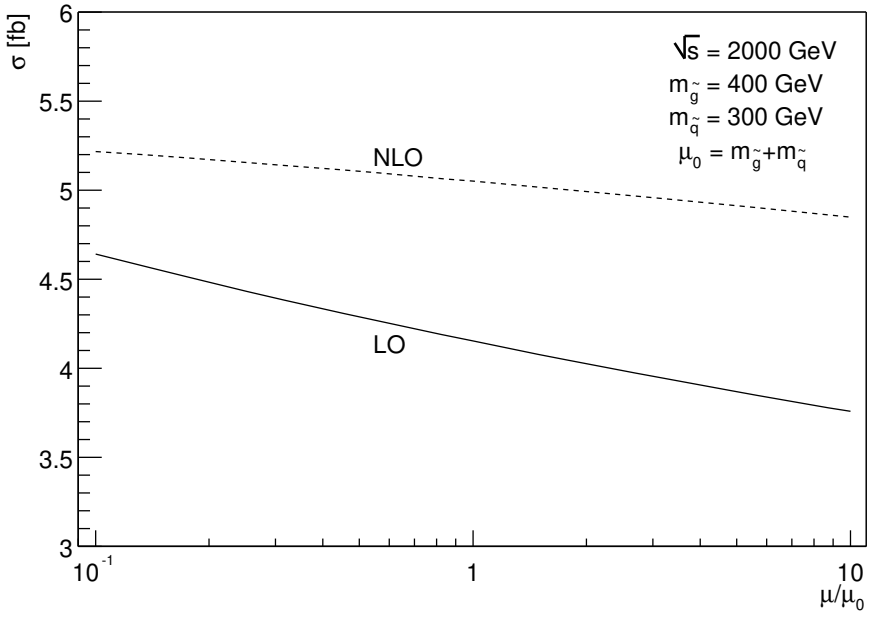

Figure 5.6: Scale dependence in leading and next-to-leading order for $\sqrt{s} = 2000\,\text{GeV}$, $m_{\tilde{g}} = 400\,\text{GeV}$ and $m_{\tilde{q}} = 300\,\text{GeV}$. The reference scale is $\mu_0 = m_{\tilde{g}} + m_{\tilde{q}}$.

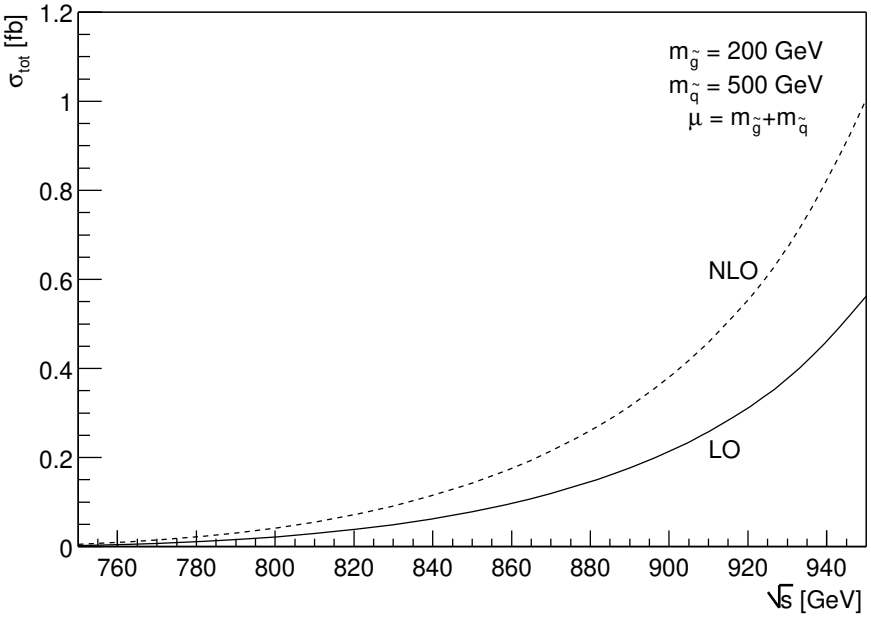

Figure 5.7: Total cross section for gluino production in LO and NLO. Parameters correspond to case II in Tab. 4.1.

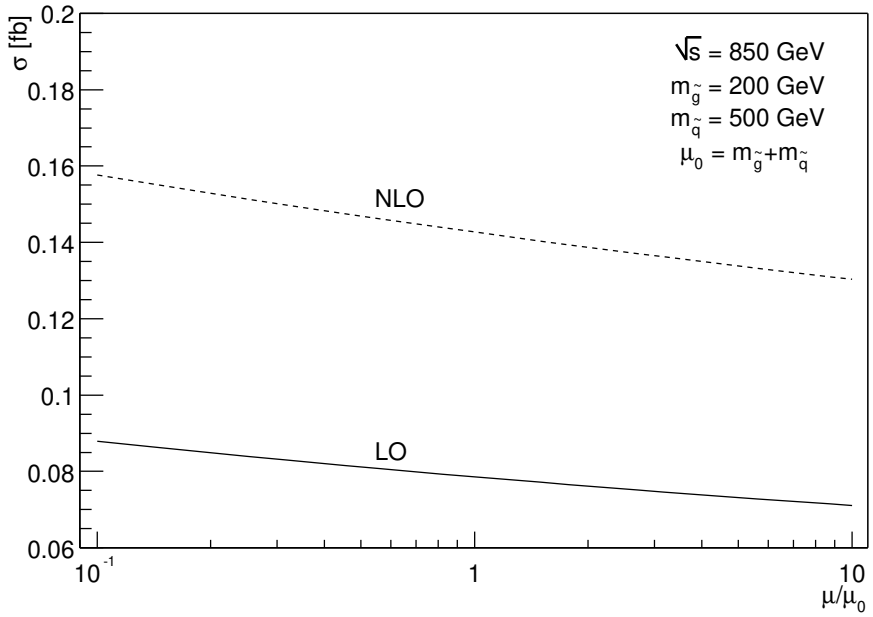

Figure 5.8: Scale dependence in leading and next-to-leading order for $\sqrt{s} = 850\,\text{GeV}$, $m_{\tilde{g}} = 200\,\text{GeV}$ and $m_{\tilde{q}} = 500\,\text{GeV}$. The reference scale is $\mu_0 = m_{\tilde{g}} + m_{\tilde{q}}$.

Chapter 6

Conclusions

The supersymmetric QCD corrections to the process $e^+e^- \to q\bar{\tilde{q}}\tilde{g}$ have been presented. This process can be used to determine the supersymmetric Yukawa coupling $\hat{g}_3$ at future e^+e^- linear colliders. By comparing this coupling to the gauge coupling g_3, measured using the processes $e^+e^- \to q\bar{q}g$ or $e^+e^- \to \tilde{q}\bar{\tilde{q}}g$, it is possible to verify the supersymmetric $SU(3)$ coupling relation, which requires both couplings to be equal and is an important prediction of supersymmetry.

Depending on the squark and gluino masses, and the available c.m. energy, the different processes which are most promising for the verification of this coupling relation have been identified.

For the case $m_{\tilde{q}} < m_{\tilde{g}}$, the supersymmetric Yukawa coupling $\hat{g}_3$ can be measured best in the $q\bar{\tilde{q}}\tilde{g}$-production process. The total cross section reaches several fb for a c.m. energy sufficiently above the kinematical threshold. In this region the radiative corrections are sizeable and enhance the leading order result by up to +45%. At the same time, the large scale dependence of the tree level cross section is significantly reduced. In this important case, the inclusion of the NLO corrections therefore leads to a more accurate and reliable theoretical prediction.

If $m_{\tilde{q}} > m_{\tilde{g}}$, the best possibility for the measurement of the Yukawa coupling lies in the study of squark decays at c.m. energies above the squark pair production threshold. If the c.m. energy is not high enough, the $q\bar{\tilde{q}}\tilde{g}$-production process provides an alternative, though the cross sections are below 1 fb in this region, because the region is close to the kinematical threshold. At the same time, the radiative corrections are large, with enhancements of the leading order result of +75% to +80%, while the scale dependence is not reduced, indicating that the perturbative expansion is not reliable in this region.

This thesis, in conjunction with the parallel calculation of the NLO corrections to the process $e^+e^- \to \tilde{q}\bar{\tilde{q}}g$ [44], therefore provides the theoretical basis for a verification of the supersymmetric $SU(3)$ coupling relation at future e^+e^- linear colliders.

Acknowledgements

I would like to thank my advisor, Prof. Peter M. Zerwas, who suggested this investigation, for the continuous support of this work, and for his enthusiasm and encouragement.

At different stages of this work, I have profited from discussions with Arnd Brandenburg, Michael Spira and Stefan Dittmaier.

Finally, I would like to thank Markos Maniatis, Margarete Mühlleitner, Benedikt Plümper, Ayres Freitas, and all members of the DESY theory group for numerous discussions and an enjoyable working atmosphere.

Appendix A

Feynman rules

In this Appendix we present all Feynman rules used in the calculations. These include the full set of SUSY QCD Feynman rules governing the interactions of gluons (g), gluinos ($\tilde{g}$), quarks (q), squarks ($\tilde{q}$) and Faddeev-Popov ghosts (η) as well as the couplings of quarks and squarks to the neutral electroweak gauge bosons γ and Z^0.

Since gluinos are Majorana fermions one has to cope with fermion number violating interactions. Simple Feynman rules for these can be obtained by introducing a continuous fermion flow for all fermion chains, which is independent of the fermion number flow of Dirac fermions [63]. In this approach no explicit charge conjugation matrices appear and the relative signs of interfering diagrams can be as easily obtained as for Dirac fermions.

The Feynman rules for propagators and external fermions are given in Figs. A.1 and A.3, and the interaction vertices are shown in Figs. A.4, A.5 and A.6. The renormalization constants are included in the expressions for the vertices, thus giving both the normal and the counterterm Feynman rules. The counterterm Feynman rules for the propagators are shown in Fig. A.2. We use the Feynman gauge and therefore have to include ghost particles, denoted by dotted lines. The direction of the continuous fermion flow is indicated by arrows and particle momenta in the vertices are understood to be incoming. $P_{L/R}$ are the chiral projection operators defined as $P_{L/R} = \frac{1}{2}(1 \mp \gamma_5)$. The generators T^a_{ij} of the fundamental representation of $SU(3)$ are normalized according to

$$\mathrm{Tr}[T^a, T^b] = \frac{1}{2}\delta^{ab} \qquad [T^a, T^b] = i f^{abc} T^c. \tag{A.1}$$

In the four-squark-vertices there appear flavour (f, f') and chirality ($h, h' = L/R$) indices and the symbol

$$(-)^{hh'} = \begin{cases} -1 & \text{if } h = h' \\ +1 & \text{if } h \neq h'. \end{cases} \tag{A.2}$$

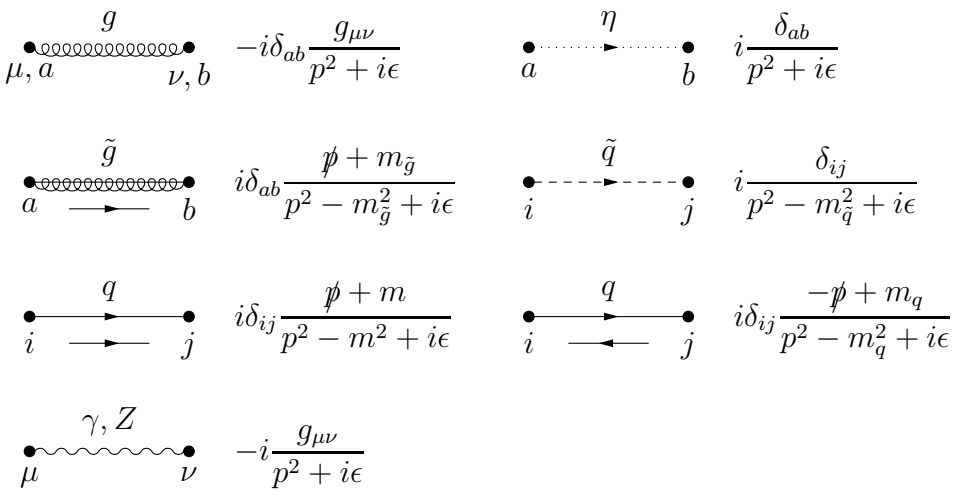

Figure A.1: Feynman rules for propagators. Direction of fermion flow is indicated by arrows. The propagator momentum p flows from left to right.

Feynman rules for the interactions of γ's and Z^0's with quarks and squarks are expressed in terms of the vector- and axialvector-couplings of the left-handed $SU(2)$-doublet fermions of the corresponding flavour, given by

$$\begin{aligned} c_V^\gamma &= Q_q & c_A^\gamma &= 0 \\ c_V^Z &= \frac{T_3^q - 2s_w^2 Q_q}{2s_w c_w} & c_A^Z &= \frac{T_3^q}{2s_w c_w}, \end{aligned} \tag{A.3}$$

with $T_3^q = \pm\frac{1}{2}$, the charge Q_q given in units of e ($Q_{e^-} = -1$), $s_w = \sin(\theta_W)$ and $c_w = \cos(\theta_W)$.

To obtain Feynman amplitudes using these rules the direction of the fermion flow has first to be arbitrarily fixed for every fermion chain in each diagram. Dirac matrices and spinors are then written down in the direction opposite to the fermion flow. Relative signs of different diagrams arise from permutations of external spinors in the conventional way. Each closed fermion or ghost loop contributes a factor of (-1) as usual. Furthermore combinatorial factors arise from gluino loops and diagrams with multiple external gluinos in the same way as for real vector bosons.

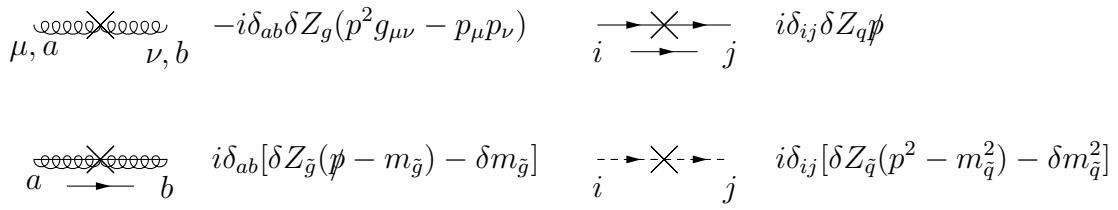

Figure A.2: Counterterm Feynman rules for propagators.

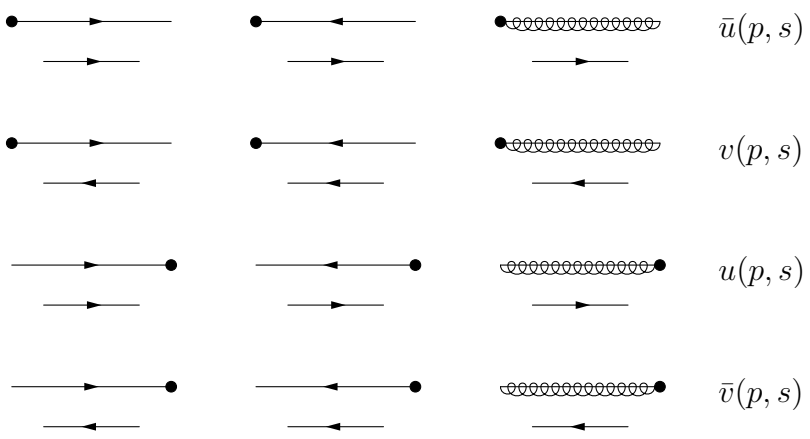

Figure A.3: Feynman rules for external fermions with fermion flow indicated by arrows. The momentum p flows from left to right.

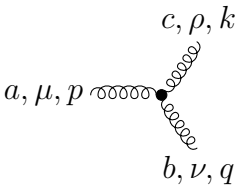

$$g_3(1 + \delta g_3 + \frac{3}{2}\delta Z_g) f_{abc}[(q-p)_\rho g_{\mu\nu} + (p-k)_\nu g_{\mu\rho} + (k-q)_\mu g_{\nu\rho}]$$

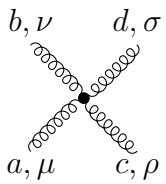

$$-ig_3^2(1 + 2\delta g_3 + 2\delta Z_g)[f_{eab}f_{ecd}(g_{\mu\rho}g_{\nu\sigma} - g_{\mu\sigma}g_{\nu\rho}) + f_{eac}f_{ebd}(g_{\mu\nu}g_{\rho\sigma} - g_{\nu\rho}g_{\mu\sigma}) + f_{ead}f_{ebc}(g_{\mu\nu}g_{\rho\sigma} - g_{\mu\rho}g_{\nu\sigma})]$$

Figure A.4: Feynman rules for interaction vertices.

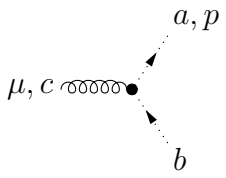

$$g_3 f_{abc} p_\mu$$

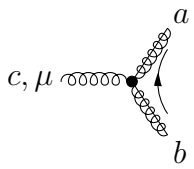

$$-g_3(1+\delta g_3+\tfrac{1}{2}\delta Z_g+\delta Z_{\tilde{g}})f_{abc}\gamma^\mu$$

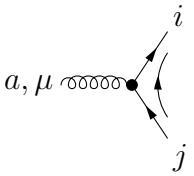

$$-ig_3(1+\delta g_3+\tfrac{1}{2}\delta Z_g+\delta Z_q)T^a_{ij}\gamma^\mu$$

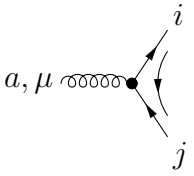

$$+ig_3(1+\delta g_3+\tfrac{1}{2}\delta Z_g+\delta Z_q)T^a_{ij}\gamma^\mu$$

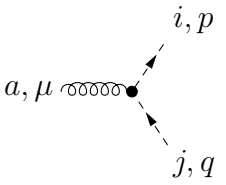

$$ig_3(1+\delta g_3+\tfrac{1}{2}\delta Z_g+\delta Z_{\tilde{q}})T^a_{ij}(p-q)^\mu$$

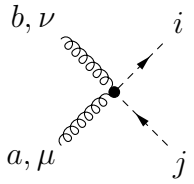

$$ig_3^2(1+2\delta g_3+\delta Z_g+\delta Z_{\tilde{q}})\left\{T^a,T^b\right\}_{ij}g_{\mu\nu}$$

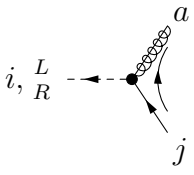

$$\mp i\sqrt{2}g_3(1+\delta g_3+\tfrac{1}{2}\delta Z_q+\tfrac{1}{2}\delta Z_{\tilde{q}}+\tfrac{1}{2}\delta Z_{\tilde{g}})T^a_{ij}P^{\,L}_{\,R}$$

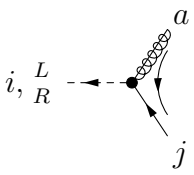

$$\mp i\sqrt{2}g_3(1+\delta g_3+\tfrac{1}{2}\delta Z_q+\tfrac{1}{2}\delta Z_{\tilde{q}}+\tfrac{1}{2}\delta Z_{\tilde{g}})T^a_{ij}P^{\,L}_{\,R}$$

Figure A.5: Feynman rules for interaction vertices (continued).

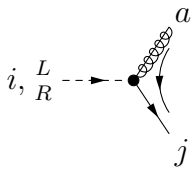

$$\mp i\sqrt{2}g_3(1+\delta g_3+\tfrac{1}{2}\delta Z_q+\tfrac{1}{2}\delta Z_{\tilde{q}}+\tfrac{1}{2}\delta Z_{\tilde{g}})T^a_{ji}P^{R}_{L}$$

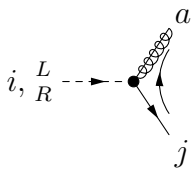

$$\mp i\sqrt{2}g_3(1+\delta g_3+\tfrac{1}{2}\delta Z_q+\tfrac{1}{2}\delta Z_{\tilde{q}}+\tfrac{1}{2}\delta Z_{\tilde{g}})T^a_{ji}P^{R}_{L}$$

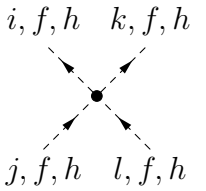

$$-i\tfrac{g_3^2}{3}(1+2\delta g_3+2\delta Z_{\tilde{q}})\left(\delta_{ij}\delta_{kl}+\delta_{il}\delta_{jk}\right)$$

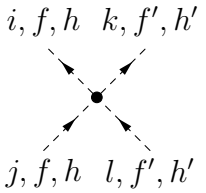

use if $(f,h)\neq(f',h')$

$$i(-)^{hh'}\frac{g_3^2}{2}(1+2\delta g_3+2\delta Z_{\tilde{q}})\left(\delta_{il}\delta_{kj}-\frac{1}{3}\delta_{ij}\delta_{kl}\right)$$

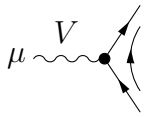

$$-ie(1+\delta Z_q)\left(c_V+c_A\gamma_5\right)\gamma^\mu$$

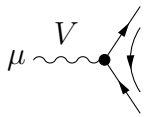

$$+ie(1+\delta Z_q)\left(c_V-c_A\gamma_5\right)\gamma^\mu$$

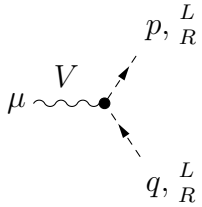

$$ie(1+\delta Z_{\tilde{q}})\left(c_V\pm c_A\right)(p-q)^\mu$$

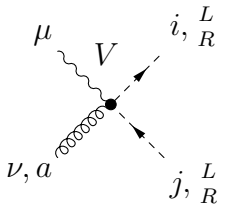

$$2ieg_3(1+\delta g_3+\tfrac{1}{2}\delta Z_g+\delta Z_{\tilde{q}})\left(c_V\pm c_A\right)T^a_{ij}g_{\mu\nu}$$

Figure A.6: Feynman rules for interaction vertices (continued).

Appendix B

Leading order cross section for $e^+e^- \longrightarrow q\bar{\tilde{q}}\tilde{g}$

In this appendix we give the analytical result for the integrated cross section of the process $e^+e^- \to q\bar{\tilde{q}}_{L/R}\tilde{g}$ for the case $m_{\tilde{q}} < m_{\tilde{g}}$. Using

$$\begin{aligned} q &= \frac{m_{\tilde{q}}}{m_{\tilde{g}}} \\ \rho &= \frac{4m_{\tilde{q}}m_{\tilde{g}}}{s} \end{aligned} \tag{B.1}$$

and

$$\begin{aligned} \kappa &= \frac{2 - q\rho - 2\sqrt{1-\rho q}}{\rho} \\ \omega &= \frac{2 - q\rho + 2\sqrt{1-\rho q}}{\rho} \\ \tau_{\min} &= \frac{4q - q^2\rho - \rho - \sqrt{(-4q + q^2\rho + \rho - 2q\rho)(2q\rho - 4q + q^2\rho + \rho)}}{2q\rho}, \end{aligned} \tag{B.2}$$

the result for the total cross section can be expressed in terms of a function $F(\tau)$ as follows

$$\sigma_{\text{tot}}(e^+e^- \to q\bar{\tilde{q}}_h\tilde{g}) = \frac{\alpha^2\alpha_s}{3s} C_1^h \left[F(\tau = 1) - F(\tau = \tau_{\min})\right]. \tag{B.3}$$

The factor C_1^h is defined in (4.2). The function $F(\tau)$ is a little lengthy:

$$
\begin{aligned}
F(\tau) = \frac{\rho}{q}\Bigg\{ \Bigg[& -2\frac{1+\omega^2}{\omega}\ln\left(\frac{\tau\omega-1}{\omega-\tau}\right) - \frac{q^2-1}{q^2\rho}(q\rho-4)\ln(\tau) + \tau - \frac{1}{\tau} \\
& - \frac{1+q^2}{q}\ln\left(\frac{q\tau+1}{q+\tau}\right) + \frac{1+\tau^2}{\tau}\ln\left(\frac{(q+\tau)(\tau\omega-1)(\tau\kappa-1)}{(\omega-\tau)(\kappa-\tau)\tau(q\tau+1)}\right)\Bigg]\frac{q^2\rho-\rho-q}{4} \\
& - \frac{-2q^2\rho+q^4\rho+4q+\rho}{4q}\Bigg[2\,\mathrm{Li}_2\left(\frac{(1-\tau\omega)}{\omega(\omega-\tau)}\right) + 2\,\mathrm{Li}_2\left(\frac{\omega(1-\tau\omega)}{\omega-\tau}\right) \\
& + \mathrm{Li}_2\left(\frac{-\tau}{q}\right) + \mathrm{Li}_2(-q\tau) - \mathrm{Li}_2\left(\frac{\tau(q^2-1)}{q(q\tau+1)}\right) - \mathrm{Li}_2\left(\frac{q(q+\tau)}{q^2-1}\right) \\
& - 2\,\mathrm{Li}_2\left(\frac{(1-\tau\omega)(q+\omega)}{(\omega-\tau)(\omega q+1)}\right) - 2\,\mathrm{Li}_2\left(\frac{(1-\tau\omega)(\omega q+1)}{(\omega-\tau)(q+\omega)}\right) \\
& - 2\ln\left(\frac{(q+\tau)(q\tau+1)\omega}{(q+\omega)(\omega q+1)\tau}\right)\ln\left(\frac{\tau\omega-1}{\omega-\tau}\right) - \ln^2(q) + \ln(q(q+\tau))\ln\left(1-q^2\right) \\
& - \frac{1}{2}\ln^2(q+\tau) + \ln\left(\frac{\tau}{q}\right)\ln(q\tau+1) + \ln(\tau)\ln(q+\tau) - \frac{1}{2}\ln^2(\tau)\Bigg]\Bigg\} \\
& - \frac{\ln(\tau)}{16q^4}\left[7q^6\rho^2 - 4q^5\rho + 2q^4\rho^2 - 16q^4 - 32q^3\rho - 7q^2\rho^2 + 16q^2 + 20q\rho - 16\right] \\
& - \frac{(q^2-1)\rho^2(\kappa-\omega)}{32\omega q^2}\left[q^3\rho + q^2\rho\omega - q\rho - 4\omega q - \omega\rho + 4\right]\ln\left(\frac{\tau\omega-1}{\omega-\tau}\right) \\
& + \left[\frac{3}{16}\frac{\rho^2(1-q^2)^2}{q^2} + \frac{\rho}{q} + \frac{1+2q^2-q^4}{(1-q^2)^2}\right]\ln\left(\frac{q\tau+1}{q+\tau}\right) \\
& - \frac{\rho^2}{32}\left(\tau-\frac{1}{\tau}\right)^2 + \frac{\rho}{16q^2}\left[-7q\rho - 12q^2 + 7q^3\rho + 4 + q^2\rho\tau\right]\left(\tau-\frac{1}{\tau}\right) \\
& - \frac{q^4\rho - 4q^3 - 2q^2\rho + 2q + \rho}{2(q^2-1)(q+\tau)} - \frac{q^2}{2(q+\tau)^2} - \frac{q^4\rho - 2q^3 - 2q^2\rho + \rho}{2q(q^2-1)(q\tau+1)} + \frac{1}{2(q\tau+1)^2} \\
& + (\omega \leftrightarrow \kappa)
\end{aligned}
\tag{B.4}
$$

Appendix C

Scalar and soft integrals

In this Appendix we will list all divergent integrals that appear in our calculation. These include UV divergent and IR divergent scalar loop integrals, as well as the IR divergent integrals arising from the emission of soft gluons. The IR divergent integrals from the collinear region of the real corrections have already been given in Sect. 5.3.4. The integrals have been calculated using dimensional regularization in $D = 4 - 2\epsilon$ space-time dimensions. Within this regularization scheme, the UV divergences and the IR divergences from either the soft or the collinear region appear as simple $\frac{1}{\epsilon}$ poles, while IR divergences from the both soft and collinear region show up as double $\frac{1}{\epsilon^2}$ poles. In all integrals given below, we use

$$C_\epsilon = (4\pi)^\epsilon \Gamma(1+\epsilon) = 1 - \epsilon\gamma + \epsilon \ln(4\pi) \tag{C.1}$$

where $\gamma \approx 0.5772$ is the Euler-Mascheroni constant.

C.1 Scalar integrals

The scalar one-loop integrals with up to four propagators are defined as

$$\begin{aligned}
A_0(m) &= \frac{16\pi^2}{i}\mu^{4-D}\int \frac{d^Dk}{(2\pi)^D}\frac{1}{D_0} \\
B_0(p_1^2, m_1, m_2) &= \frac{16\pi^2}{i}\mu^{4-D}\int \frac{d^Dk}{(2\pi)^D}\frac{1}{D_0 D_1} \\
C_0(p_1^2, (p_2-p_1)^2, p_2^2, m_1, m_2, m_3) &= \frac{16\pi^2}{i}\mu^{4-D}\int \frac{d^Dk}{(2\pi)^D}\frac{1}{D_0 D_1 D_2} \\
D_0(p_1^2, (p_2-p_1)^2, (p_3-p_2)^2, p_3^2, p_2^2, (p_3-p_1)^2, m_1, m_2, m_3, m_4) & \\
&= \frac{16\pi^2}{i}\mu^{4-D}\int \frac{d^Dk}{(2\pi)^D}\frac{1}{D_0 D_1 D_2 D_3} \\
D_0^6(p_1^2, (p_2-p_1)^2, (p_3-p_2)^2, p_3^2, p_2^2, (p_3-p_1)^2, m_1, m_2, m_3, m_4) & \\
&= \frac{1}{i\pi^2}\int d^6k\, \frac{1}{D_0 D_1 D_2 D_3},
\end{aligned} \tag{C.2}$$

where μ is the regularization scale, and the denominator factors D_i are given by

$$\begin{aligned} D_0 &= k^2 - m_1^2 + i\epsilon \\ D_1 &= (k+p_1)^2 - m_2^2 + i\epsilon \\ D_2 &= (k+p_2)^2 - m_3^2 + i\epsilon \\ D_3 &= (k+p_3)^2 - m_4^2 + i\epsilon. \end{aligned} \tag{C.3}$$

Note that within this conventions D_0^6 is not obtained by setting $D = 6$ in the definition for D_0. The integrals can be calculated using Feynman parameterizations. This has been done for the UV-divergent integrals and the finite 3- and 4-point integrals in [65], a more compact expression for the 4-point function is given in [66]. For the numerical calculation of these integrals we use the LoopTools library [67], which is based on the FF package [68]. The same method can also be used for the IR-divergent integrals, and the IR-divergent 3-point integrals shown below have been taken from the literature [57, 69].

For calculating the interference of the virtual with the born matrix element, only the real parts of the integrals are relevant. In the formulas below, we therefore only give the real part. Because we have dropped the $i\epsilon$-prescriptions, except where they are necessary for the determination of the real part, some of the integrals contain spurious imaginary parts, which have to be dropped. The dilogarithm or Spence function appearing in the integrals is defined by

$$\mathrm{Li}_2(x) = -\int_0^1 \frac{\ln(1-tx)}{t} dt. \tag{C.4}$$

Further relations, properties, and tables of integrals leading to dilogarithms are given in [70], while a series expansion suited for numerical evaluation is given in [65].

The scalar one- and two-point functions do only contain UV-divergences and are given by

$$A_0(m) = C_\epsilon m^2 \left[\frac{1}{\epsilon} + 1 - \ln\left(\frac{m^2}{\mu^2}\right)\right] \tag{C.5}$$

and

$$\begin{aligned} B_0(p^2, m_1, m_2) &= C_\epsilon \left[\frac{1}{\epsilon} - \int_0^1 dx\ \ln \frac{p^2x^2 - (p^2 + m_1^2 - m_2^2)x + m_1^2 - i\epsilon}{\mu^2}\right] \\ &= C_\epsilon \left[\frac{1}{\epsilon} + 2 - \ln\left(\frac{m_1 m_2}{\mu^2}\right) + \frac{m_1^2 - m_2^2}{p^2}\ln\left(\frac{m_2}{m_1}\right)\right. \\ &\qquad \left. - \frac{m_1 m_2}{p^2}\left(\frac{1}{r} - r\right)\ln r\right], \end{aligned} \tag{C.6}$$

where r is determined from

$$x^2 + \frac{m_1^2 + m_2^2 - p^2 - i\epsilon}{m_1 m_2} + 1 = (x+r)\left(x + \frac{1}{r}\right). \tag{C.7}$$

Some special cases are

$$\begin{aligned}
B_0(m^2,m,0) &= 1+\frac{A_0(m)}{m^2}\\
B_0(0,m,0) &= \frac{A_0(m)}{m^2}\\
B_0(0,m,m) &= \frac{A_0(m)}{m^2}-1\\
B_0(0,m_1,m_2) &= \frac{1}{m_1^2-m_2^2}\left[A_0(m_1)-A_0(m_2)\right]\\
B_0(p^2,0,0) &= C_\epsilon\left[\frac{1}{\epsilon}+2-\ln\left(\frac{p^2}{\mu^2}\right)\right]\\
B_0(p^2,m,0) &= C_\epsilon\left[\frac{1}{\epsilon}+2-\ln\left(\frac{m^2}{\mu^2}\right)-\frac{p^2-m^2}{p^2}\ln\left(1-\frac{p^2}{m^2-i\epsilon}\right)\right]\\
B_0(p^2,m,m) &= C_\epsilon\left[\frac{1}{\epsilon}+2-\ln\left(\frac{m^2}{\mu^2}\right)+\beta\ln\left(\frac{1-\beta}{1+\beta}\right)\right]\\
\beta &= \sqrt{1-\frac{4m^2}{p^2}}.
\end{aligned} \tag{C.8}$$

The derivative of B_0 defined by

$$B_0'(p^2,m_1,m_2) = \frac{\partial}{\partial q^2}B_0(q^2,m_1,m_2)\Big|_{q^2=p^2} \tag{C.9}$$

appears in the wave function renormalization and is given by

$$\begin{aligned}
B_0'(p^2,m_1,m_2) = &-\frac{m_1^2-m_2^2}{p^4}\ln\left(\frac{m_2}{m_1}\right)+\frac{m_1m_2}{p^4}\left(\frac{1}{r}-r\right)\ln r\\
&-\frac{1}{p^2}\left(1+\frac{r^2+1}{r^2-1}\ln r\right).
\end{aligned} \tag{C.10}$$

It may also contain IR-divergences

$$B_0'(m^2,m,0) = -C_\epsilon\frac{1}{2m^2}\left[\frac{1}{\epsilon}+2-\ln\left(\frac{m^2}{\mu^2}\right)\right]. \tag{C.11}$$

A special case is the integral $B_0(0,0,0)$, which appears in the wave-function counterterms of the massless quarks and gluons. It can be shown that this integral can be consistently set to zero [64], but this cancels UV- against IR-divergences. In order to make separate checks of UV- and IR-finiteness possible, we write

$$B_0(0,0,0) = C_\epsilon\left(\frac{1}{\epsilon_{UV}}-\frac{1}{\epsilon_{IR}}\right), \tag{C.12}$$

where we distinguish between UV and IR poles, though of course $\epsilon_{UV}=\epsilon_{IR}=\epsilon$.

The 3-point integrals can only contain IR- but no UV-divergences. The relevant integrals are

$$C_0(0,s,t;0,0,0) = -C_\epsilon \frac{1}{s-t}\left[\frac{1}{\epsilon}\ln\left(\frac{s}{t}\right) - \frac{1}{2}\ln^2\left(\frac{s}{t}\right) + \ln\left(\frac{s}{t}\right)\ln\left(\frac{\mu^2}{t}\right)\right], \tag{C.13}$$

$$C_0(0,t,m^2;0,0,m) = C_\epsilon \frac{1}{t-m^2}\left[\frac{1}{2\epsilon^2} + \frac{1}{\epsilon}\ln\left(\frac{m\mu}{t-m^2}\right) - \mathrm{Li}_2\left(\frac{m^2}{t}\right) - \frac{1}{2}\ln^2\left(\frac{t}{m^2}\right) + \ln^2\left(\frac{m\mu}{t-m^2}\right) - \frac{2}{3}\pi^2\right], \tag{C.14}$$

$$C_0(0,q_2^2,m_{\tilde{g}}^2;0,0,m_{\tilde{q}}) = -C_\epsilon \frac{1}{q_2^2-m_{\tilde{g}}^2}\left[\frac{1}{\epsilon}\ln(y) + \ln(y)\ln\left(\frac{m_{\tilde{q}}^2\mu^2}{(m_{\tilde{q}}^2-m_{\tilde{g}}^2)^2}\right) - \ln^2(y) + \mathrm{Li}_2\left(\frac{m_{\tilde{g}}^2}{m_{\tilde{q}}^2}\right) - \mathrm{Li}_2\left(\frac{q_2^2}{m_{\tilde{q}}^2}\right)\right], \tag{C.15}$$

with

$$y = \frac{q_2^2 - m_{\tilde{q}}^2}{m_{\tilde{g}}^2 - m_{\tilde{q}}^2}, \tag{C.16}$$

and

$$\begin{aligned} C_0(q_1^2,m_{\tilde{q}}^2,m_{\tilde{g}}^2;m_{\tilde{g}},m_{\tilde{q}},0) = -C_\epsilon \frac{1}{2\lambda^{\frac{1}{2}}(q_1^2,m_{\tilde{g}}^2,m_{\tilde{q}}^2)}\Bigg\{ & \left(\frac{1}{\epsilon} + \ln\left(\frac{\mu^2}{m_{\tilde{q}}^2}\right)\right)\left[\ln\left(1-\frac{1}{x^-}\right) - \ln\left(1-\frac{1}{x^+}\right)\right] \\ & + \frac{1}{2}\ln^2\left(1-\frac{1}{x^+}\right) - \frac{1}{2}\ln^2\left(1-\frac{1}{x^-}\right) \\ & + 2\ln\left(1-\frac{1}{x^+}+i\epsilon\right)\ln\left(1-\frac{x^+}{x^-}-i\epsilon\right) \\ & - \ln\left(1-\frac{1}{x^+}+i\epsilon\right)\ln\left(1-\frac{1}{x^-}-i\epsilon\right) \\ & - 2\ln\left(1-\frac{x^+}{x^-}-i\epsilon\right)\ln\left(1-\frac{x^-}{x^+}+i\epsilon\right) \\ & - 2\,\mathrm{Li}_2\left(\frac{x^-}{x^- - x^+}\right) - 2\,\mathrm{Li}_2\left(\frac{1-x^+}{x^- - x^+}\right) + \frac{\pi^2}{3}\Bigg\}, \end{aligned} \tag{C.17}$$

where

$$x^\pm = \frac{q_1^2 + m_{\tilde{q}}^2 - m_{\tilde{g}}^2 \pm \lambda^{\frac{1}{2}}(q_1^2,m_{\tilde{g}}^2,m_{\tilde{q}}^2)}{2q_1^2}. \tag{C.18}$$

The 4-point integrals also contain only IR-divergences. From the first integral we subtract two 3-point integrals

$$D_0(m_{\tilde{g}}^2, q_1^2, s, q_2^2, m_{\tilde{q}}^2, 0; 0, m_{\tilde{g}}, m_{\tilde{q}}, m_{\tilde{q}}) = \frac{1}{q_2^2 - m_{\tilde{q}}^2} \left[C_0(q_1^2, m_{\tilde{q}}^2, m_{\tilde{g}}^2; m_{\tilde{g}}, m_{\tilde{q}}, 0) \right.$$
$$\left. - C_0(q_2^2, s, m_{\tilde{q}}^2; 0, m_{\tilde{q}}, m_{\tilde{q}}) - 2\widetilde{D} \right], \quad \text{(C.19)}$$

where the remaining finite part $\widetilde{D}$ can be integrated in 4 dimensions with the result

$$\widetilde{D} = \frac{1}{s(v^+ - v^-)} \left[\ln\left(\frac{s}{-q_2^2 + m_{\tilde{q}}^2} + i\epsilon \right) \ln\left(\frac{v^+ - 1}{v^+} + i\epsilon_{v^+} \right) \right.$$
$$\left. - \mathrm{Li}_2\left(\frac{1}{v^+} \right) + I(g^+, v^+) + I(g^-, v^+) + (v^+ \to v^-) \right]$$
$$- \frac{1}{q_1^2(u^+ - u^-)} \left[\ln\left(\frac{s}{-q_2^2 + m_{\tilde{q}}^2} + i\epsilon \right) \ln\left(\frac{u^+ - 1}{u^+} + i\epsilon_{u^+} \right) \right.$$
$$\left. - \mathrm{Li}_2\left(\frac{1}{u^+} \right) + I(g^+, u^+) + I(g^-, u^+) + (u^+ \to u^-) \right], \quad \text{(C.20)}$$

where

$$u^\pm = \frac{q_1^2 + m_{\tilde{q}}^2 - m_{\tilde{g}}^2 \pm \lambda^{\frac{1}{2}}(q_1^2, m_{\tilde{q}}^2, m_{\tilde{g}}^2)}{2q_1^2} \quad \text{(C.21)}$$

$$v^\pm = \frac{s - q_2^2 + m_{\tilde{q}}^2 \pm \lambda^{\frac{1}{2}}(s, q_2^2, m_{\tilde{q}}^2)}{2s} \quad \text{(C.22)}$$

$$g^\pm = \frac{1}{2}\left(1 \pm \sqrt{1 - \frac{4m_{\tilde{q}}^2}{s}} \right). \quad \text{(C.23)}$$

For the integral $I(u, v)$ appearing above, we have to distinguish 3 cases:

- u complex, v real:

$$I(u, v + i\epsilon_v) = \ln\left(\frac{v-1}{v} + i\epsilon_v \right) \ln(v - u) + \mathrm{Li}_2\left(\frac{v}{v-u} \right) - \mathrm{Li}_2\left(\frac{v-1}{v-u} \right) \quad \text{(C.24)}$$

- u,v real, $u > v$:

$$I(u + i\epsilon_u, v + i\epsilon_v) = \mathrm{Li}_2\left(\frac{v}{v-u} \right) + \mathrm{Li}_2\left(\frac{1-v}{u-v} \right) + \ln\left(\frac{1-v}{v-u} \right) \ln\left(\frac{1-u}{v-u} \right)$$
$$+ \ln\left(\frac{1-v}{v} \right) \ln(v - u) - \zeta(2) + \pi^2 \,\mathrm{sign}(\epsilon_u)\,\mathrm{sign}(\epsilon_v) \quad \text{(C.25)}$$

- u,v real, $v > u$:

$$I(u+i\epsilon_u, v+i\epsilon_v) = -\operatorname{Li}_2\left(-\frac{u}{v-u}\right) - \operatorname{Li}_2\left(\frac{v-1}{v-u}\right) + \zeta(2) + \ln\left(\frac{1-v}{v}\right)\ln(v-u) - \ln\left(\frac{v}{v-u}\right)\ln\left(\frac{u}{v-u}\right) \quad \text{(C.26)}$$

The D_0^6 integrals are completely finite.

$$\begin{aligned} D_0^6(m_{\tilde{q}}^2, q_3^2, s, q_1^2, 0, m_{\tilde{g}}^2; 0, m_{\tilde{q}}, 0, 0) = -\frac{\pi}{m_{\tilde{g}}^2}\Bigg\{ & \frac{1}{u^+-u^-}\frac{F_1}{A_1}\Bigg[\frac{F_2+u^+}{A_2+u^+} \\ & \cdot\left(\operatorname{Li}_2\left(\frac{u^+}{F_2+u^+}\right) - \operatorname{Li}_2\left(\frac{u^+-1}{F_2+u^+}\right) - \zeta(2) + \operatorname{Li}_2\left(\frac{u^+-1}{u^+}\right)\right. \\ & \left. - \operatorname{Li}_2\left(\frac{u^+}{D_2+u^+}\right) + \operatorname{Li}_2\left(\frac{u^+-1}{D_2+u^+}\right)\right) + (u^+ \to u^-)\Bigg] \\ & - (u^\pm \to v^\pm, F_i \to G_i)\Bigg\} \\ & - \frac{\pi}{m_{\tilde{g}}^2}\frac{F_1(F_2-A_2)}{A_1(A_2+u^+)(A_2+u^-)}\Bigg[\operatorname{Li}_2\left(\frac{A_2}{A_2-F_2}\right) - \operatorname{Li}_2\left(\frac{A_2-1}{A_2-F_2}\right) \\ & - \operatorname{Li}_2\left(\frac{A_2}{A_2-G_2}\right) + \operatorname{Li}_2\left(\frac{A_2-1}{A_2-G_2}\right)\Bigg] \end{aligned} \quad \text{(C.27)}$$

$$u^\pm = \frac{q_1^2 + m_{\tilde{g}}^2 - m_{\tilde{q}}^2 \pm \lambda^{\frac{1}{2}}(q_1^2, m_{\tilde{g}}^2, m_{\tilde{q}}^2)}{2m_{\tilde{g}}^2} \quad \text{(C.28)}$$

$$v^\pm = \frac{s + m_{\tilde{g}}^2 - q_3^2 \pm \lambda^{\frac{1}{2}}(s, q_3^2, m_{\tilde{g}}^2)}{2m_{\tilde{g}}^2} \quad \text{(C.29)}$$

$$A_1 = -q_2^2 + m_{\tilde{g}}^2 \qquad A_2 = -\frac{s - q_1^2}{q_2^2 - m_{\tilde{g}}^2} \quad \text{(C.30)}$$

$$D_2 = \frac{m_{\tilde{q}}^2}{m_{\tilde{g}}^2} - 1 \quad \text{(C.31)}$$

$$F_1 = q_1^2 \qquad F_2 = -1 \quad \text{(C.32)}$$

$$G_1 = s - q_3^2 + m_{\tilde{q}}^2 \qquad G_2 = -\frac{s}{s - q_3^2 + m_{\tilde{q}}^2} \quad \text{(C.33)}$$

$$
\begin{aligned}
D_0^6(0,q_3^2,s,q_2^2,m_{\tilde{q}}^2,m_{\tilde{g}}^2;0,0,m_{\tilde{q}},m_{\tilde{q}}) = \frac{\pi}{s}\Bigg\{ & \frac{1}{u^+-u^-}\Bigg[\frac{F_2+u^+}{A_2+u^+}\Bigg(\mathrm{Li}_2\left(\frac{u^+}{u^++F_2}\right) \\
& - \mathrm{Li}_2\left(\frac{u^+-1}{u^++F_2}\right) - \mathrm{Li}_2\left(\frac{u^+}{u^+-w^+}\right) + \mathrm{Li}_2\left(\frac{u^+-1}{u^+-w^+}\right) \\
& - \mathrm{Li}_2\left(\frac{u^+}{u^+-w^-}\right) + \mathrm{Li}_2\left(\frac{u^+-1}{u^+-w^-}\right)\Bigg) + (u^+ \to u^-)\Bigg] \\
& - (u^\pm \to v^\pm, F_i \to G_i)\Bigg\} \\
& + \frac{\pi}{s}\frac{F_1A_2}{A_1(A_2+u^+)(A_2+u^-)}\Bigg[\zeta(2) - \mathrm{Li}_2\left(\frac{A_2+1}{A_2}\right) \\
& - \mathrm{Li}_2\left(\frac{A_2}{A_2-G_2}\right) + \mathrm{Li}_2\left(\frac{A_2+1}{A_2-G_2}\right)\Bigg]
\end{aligned}
\tag{C.34}
$$

$$
u^\pm = \frac{s-q_2^2+m_{\tilde{q}}^2 \pm \lambda^{\frac{1}{2}}(s,q_2^2,m_{\tilde{q}}^2)}{2s} \tag{C.35}
$$

$$
v^\pm = \frac{s+q_3^2-m_{\tilde{g}}^2 \pm \lambda^{\frac{1}{2}}(s,q_3^2,m_{\tilde{g}}^2)}{2s} \tag{C.36}
$$

$$
w^\pm = \frac{1}{2}\left(1 \pm \sqrt{1-\frac{4m_{\tilde{q}}^2}{s}}\right) \tag{C.37}
$$

$$
A_1 = -q^2+q_1^2 \qquad A_2 = -\frac{q_3^2-m_{\tilde{q}}^2}{q^2-q_1^2} \tag{C.38}
$$

$$
F_1 = -q_2^2+m_{\tilde{q}}^2 \qquad F_2 = 0 \tag{C.39}
$$

$$
G_1 = q_3^2-m_{\tilde{g}}^2 \qquad G_2 = -\frac{q_3^2-m_{\tilde{q}}^2}{q_3^2-m_{\tilde{g}}^2} \tag{C.40}
$$

C.2 Soft integrals

The soft integrals are defined by

$$
S^{(ij)}(m_i,m_j) = \mu^{4-D} \int\limits_{k^0<\frac{\sqrt{s_{ij}}}{2}x_{\mathrm{cut}}} \frac{d^{D-1}k}{(2\pi)^{D-1}\,2k^0}\left[\frac{2p_ip_j}{(p_ik)(p_jk)} - \frac{m_i^2}{(p_ik)^2} - \frac{m_j^2}{(p_jk)^2}\right]. \tag{C.41}
$$

If both masses are nonzero, the result is given by

$$S^{(ij)}(m_i, m_j) = \frac{1}{8\pi^2} C_\epsilon \left[\left(\frac{t_{ij}}{\lambda^{\frac{1}{2}}(s_{ij}, m_i^2, m_j^2)} \ln(\sigma_i \sigma_j) + 2 \right) \left(\frac{1}{\epsilon} + \ln\left(\frac{\mu^2}{s_{ij} x_{\text{cut}}^2} \right) \right) \right.$$
$$+ \frac{t_{ij}}{\lambda^{\frac{1}{2}}(s_{ij}, m_i^2, m_j^2)} \left[\frac{1}{2} \ln^2(\sigma_i) + \frac{1}{2} \ln^2(\sigma_j) + 2\,\text{Li}_2\left(-\frac{1-\sigma_i}{\sigma_i} \right) \right.$$
$$\left. \left. + 2\,\text{Li}_2\left(-\frac{1-\sigma_j}{\sigma_j} \right) \right] - \frac{1}{\rho_i} \ln \sigma_i - \frac{1}{\rho_j} \ln \sigma_j \right], \tag{C.42}$$

with

$$\rho_i = \frac{\lambda^{\frac{1}{2}}(s_{ij}, m_i^2, m_j^2)}{s_{ij} + m_i^2 - m_j^2} \qquad s_{ij} = (p_i + p_j)^2$$
$$\sigma_i = \frac{1-\rho_i}{1+\rho_i} \qquad t_{ij} = 2 p_i p_j, \tag{C.43}$$

and ρ_j, σ_j can be obtained by exchange of i and j. The result for one zero mass is given by

$$S^{(ij)}(0, m) = \frac{1}{8\pi^2} C_\epsilon \left[\frac{1}{\epsilon^2} + \left(1 + \ln\left(\frac{\mu^2 \sigma}{s_{ij} x_{\text{cut}}^2} \right) \right) \frac{1}{\epsilon} + \frac{1}{2} \ln^2\left(\frac{\mu^2}{s_{ij} x_{\text{cut}}^2} \right) \right.$$
$$+ (1 + \ln\sigma) \ln\left(\frac{\mu^2}{s_{ij} x_{\text{cut}}^2} \right) + \frac{1}{2} \ln^2(\sigma)$$
$$\left. + 2\,\text{Li}_2\left(-\frac{1-\sigma}{\sigma} \right) - \frac{\pi^2}{3} - \frac{1}{\rho} \ln\sigma \right], \tag{C.44}$$

with

$$\rho = \frac{s_{ij} - m^2}{s_{ij} + m^2} \qquad \sigma = \frac{m^2}{s_{ij}}. \tag{C.45}$$

Appendix D

Renormalization constants

In this Appendix we list the explicit results for the renormalization constants in terms of scalar one-loop integrals.

$$
\begin{aligned}
\delta Z_g &= \frac{\alpha_s}{6\pi}\,\mathrm{Re}\Big[\frac{5}{2}N_c B_0(0,0,0) - N_c B_0(0,m_{\tilde g},m_{\tilde g}) - \frac{N_f}{2}B_0(0,m_{\tilde q},m_{\tilde q}) \\
&\quad - (N_f-1)B_0(0,0,0) - B_0(0,m_t,m_t)\Big] \\
\delta m_{\tilde g} &= \frac{\alpha_s}{4\pi}m_{\tilde g}\,\mathrm{Re}\Big[-N_c - 3N_c\frac{A_0(m_{\tilde g})}{m_{\tilde g}^2} + N_f\frac{A_0(m_{\tilde q})}{m_{\tilde g}^2} - \frac{A_0(m_t)}{m_{\tilde g}^2} \\
&\quad + \frac{m_{\tilde g}^2+m_t^2-m_{\tilde q}^2}{m_{\tilde g}^2}B_0(m_{\tilde g}^2,m_{\tilde q},m_t) + (N_f-1)\frac{m_{\tilde g}^2-m_{\tilde q}^2}{m_{\tilde g}^2}B_0(m_{\tilde g}^2,m_{\tilde q},0)\Big] \\
\delta Z_{\tilde g} &= \frac{\alpha_s}{4\pi}\,\mathrm{Re}\Big[-N_c B_0(0,m_{\tilde g},m_{\tilde g}) + 4N_c m_{\tilde g}^2 B_0'(m_{\tilde g}^2,m_{\tilde g},0) + N_f\frac{A_0(m_{\tilde q})}{m_{\tilde g}^2} \\
&\quad - \frac{A_0(m_t)}{m_{\tilde g}^2} + \frac{m_t^2-m_{\tilde g}^2-m_{\tilde q}^2}{m_{\tilde g}^2}B_0(m_{\tilde g}^2,m_{\tilde q},m_t) \\
&\quad - (N_f-1)\frac{m_{\tilde g}^2+m_{\tilde q}^2}{m_{\tilde g}^2}B_0(m_{\tilde g}^2,m_{\tilde q},0) + 2(m_{\tilde q}^2-m_{\tilde g}^2-m_t^2)B_0'(m_{\tilde g}^2,m_{\tilde q},m_t) \\
&\quad + 2(N_f-1)(m_{\tilde q}^2-m_{\tilde g}^2)B_0'(m_{\tilde g}^2,m_{\tilde q},0)\Big] \\
\delta Z_q &= \frac{\alpha_s}{8\pi}C_F\,\mathrm{Re}\Big[-2B_0(0,0,0) - \frac{m_{\tilde g}^2+m_{\tilde q}^2}{m_{\tilde g}^2-m_{\tilde q}^2} \\
&\quad + \frac{2}{m_{\tilde g}^2-m_{\tilde q}^2}[A_0(m_{\tilde q}) - m_{\tilde g}^2 B_0(0,m_{\tilde q},m_{\tilde g})]\Big] \\
\delta m_{\tilde q}^2 &= \frac{\alpha_s}{2\pi}C_F\,\mathrm{Re}\Big[-2m_{\tilde q}^2 - A_0(m_{\tilde g}) - A_0(m_{\tilde q}) + (m_{\tilde q}^2-m_{\tilde g}^2)B_0(m_{\tilde q}^2,m_{\tilde g},0)\Big] \\
\delta Z_{\tilde q} &= \frac{\alpha_s}{2\pi}C_F\,\mathrm{Re}\Big[B_0(m_{\tilde q}^2,m_{\tilde q},0) - B_0(m_{\tilde q}^2,m_{\tilde g},0) + (m_{\tilde g}^2-m_{\tilde q}^2)B_0'(m_{\tilde q}^2,m_{\tilde g},0) \\
&\quad + 2m_{\tilde q}^2 B_0'(m_{\tilde q}^2,m_{\tilde q},0)\Big]
\end{aligned}
\tag{D.1}
$$

Bibliography

[1] S. L. Glashow, *Nucl. Phys.* **22** (1961) 579; S. Weinberg, *Phys. Rev. Lett.* **19** (1967) 1264; A. Salam, in *Elementary Particle Theory*, ed. N. Svartholm, (Almqvist and Wiksell, Stockholm, 1968), p. 367; H. Fritzsch and M. Gell-Mann, *Proc. XVI International Conference on High Energy Physics*, Fermilab.

[2] P. W. Higgs, *Phys. Lett.* **12** (1964) 132; F. Englert and R. Brout, *Phys. Rev. Lett.* **13** (1964) 321; G. S. Guralnik, C. R. Hagen and T. W. Kibble, *Phys. Rev. Lett.* **13** (1964) 585.

[3] R. Brandelik *et al.* (TASSO Collaboration), *Phys. Lett.* **B86** (1979) 243; D. P. Barber *et al.*, *Phys. Rev. Lett.* **43** (1979) 830; C. Berger *et al.* (PLUTO Collaboration), *Phys. Lett.* **B86** (1979) 418.

[4] G. Arnison *et al.* (UA1 Collaboration), *Phys. Lett.* **B122** (1983) 103; G. Arnison *et al.* (UA1 Collaboration), *Phys. Lett.* **B126** (1983) 398; M. Banner *et al.* (UA2 Collaboration), *Phys. Lett.* **B122** (1983) 476; P. Bagnaia *et al.* (UA2 Collaboration), *Phys. Lett.* **B129** (1983) 130.

[5] F. Abe *et al.* (CDF Collaboration), *Phys. Rev. Lett.* **74** (1995) 2626; S. Abachi *et al.* (D0 Collaboration), *Phys. Rev. Lett.* **74** (1995) 2632.

[6] K. Kodama *et al.* (DONUT Collaboration), *Phys. Lett.* **B504** (2001) 218.

[7] Y. Fukuda *et al.* (Super-Kamiokande Collaboration), *Phys. Rev. Lett.* **82** (1999) 2430.

[8] S. Weinberg, *Phys. Rev.* **D13** (1976) 974; *Phys. Rev.* **D19** (1979) 1277; L. Susskind, *Phys. Rev.* **D20** (1979) 2619; G. t'Hooft, in *Recent Developments in Gauge Theories*, Proceedings of the NATO Advanced Summer Institute, Cargese 1979, ed. by G. t'Hooft *et al.*, Plenum, New York, 1980

[9] V. P. Akulov and D. V. Volkov, *Phys. Lett.* **B46** (1972) 109; J. Wess and B. Zumino, *Nucl. Phys.* **B70** (1974) 39.

[10] P. Fayet, *Phys. Lett.* **B69** (1977) 489; P. Fayet and S. Ferrara, *Phys. Rep.* **32** (1977) 249.

[11] H. P. Nilles, *Phys. Rep.* **110** (1984) 1.

[12] H. E. Haber and G. L. Kane, *Phys. Rep.* **117** (1985) 75.

[13] E. Gildener, *Phys. Rev.* **D14** (1976) 1667; S. Weinberg, *Phys. Lett.* **B82** (1979) 387; L. Susskind, *Phys. Rep.* **104** (1984) 181.

[14] H. Georgi and S. L. Glashow, PRL32 (1974) 438; H. Georgi, H. R. Quinn and S. Weinberg, *Phys. Rev. Lett.* **33** (1974) 451; G. Ross, *Grand Unified Theories*, Benjamin/Cummings, Menlo Park, California, 1984.

[15] S. A. Martin, *A Supersymmetry Primer*, in [16].

[16] *Perspectives on Supersymmetry*, ed. G.L. Kane, World Scientific, Singapore 1998.

[17] J. Bagger, S. Dimopoulos and E. Masso, *Phys. Lett.* **B156** (1985) 357; J. Bagger, S. Dimopoulos and E. Masso, *Phys. Rev. Lett.* **55** (1985) 920; M. B. Einhorn and D. R. Jones, *Nucl. Phys.* **B196** (1982) 475.

[18] S. Dimopoulos, S. Raby and F. Wilczek, *Phys. Rev.* **D24** (1981) 1681; U. Amaldi *et al.*, *Phys. Rev.* **D36** (1987) 1385; P. Langacker and M. Luo, *Phys. Rev.* **D44** (1991) 514; J. Ellis, S. Kelley and D. Nanopoulos, *Phys. Lett.* **B260** (1991) 131; U. Amaldi, W. deBoer and H. Furstenau, *Phys. Lett.* **B260** (1991) 447; N. Sakai, *Z. Phys.* **C11** (1982) 153.

[19] S. Coleman and J. Mandula, *Phys. Rev.* **159** (1967) 1251.

[20] R. Haag, J. Lopuszanski and M. Sohnius, *Nucl. Phys.* **B88** (1975) 257.

[21] S. Mandelstam, *Nucl. Phys.* **B213** (1983) 149; R. Flume and D. Wyler, *Phys. Lett.* **B108** (1982) 317; M. F. Sohnius and P. C. West, *Phys. Lett.* **B100** (1981) 245.

[22] E. Cremmer, B. Julia, J. Scherk, S. Ferrara, L. Girardello and P. van Nieuwenhuizen, *Nucl. Phys.* **B147** (1979) 105; see also Section 3.1. in Ref. [11].

[23] D. Z. Freedman, P. van Nieuwenhuizen and S. Ferrara, *Phys. Rev.* **D13** (1976) 3214; S. Deser and B. Zumino, *Phys. Lett.* **B62** (1976) 335.

[24] J. Wess and J. Bagger, *Supersymmetry and Supergravity*, 2nd ed., Princeton University Press, Princeton, 1992.

[25] P. P. Srivastava, *Supersymmetry, Superfields and Supergravity: An Introduction*, Adam Hilger, Bristol and Boston, 1986.

[26] G. Altarelli *et al.*, hep-ph/9703276; H. Dreiner, *An Introduction to explicit R-parity violation*, in [16].

[27] G. R. Farrar and P. Fayet, *Phys. Lett.* **B76** (1978) 575; S. Dimopoulos and H. Georgi, *Nucl. Phys.* **B193** (1981) 150; S. Weinberg, *Phys. Rev.* **D26** (1982) 287; N. Sakai and T. Yanagida, *Phys. Rev.* **D197** (1982) 533; S. Dimopoulos, S. Raby and F. Wilczek, *Phys. Lett.* **B112** (1982) 133.

[28] H. Goldberg, *Phys. Rev. Lett.* **50** (1983) 1419; J. Ellis, J. Hagelin, D. V. Nanopoulos, K. Olive and M. Srednicki, *Nucl. Phys.* **B238** (1984) 453.

[29] For recent reviews of gauge-mediated supersymmetry breaking, see C. Kolda, hep-ph/9707450, or G. F. Guidice and R. Rattazi, hep-ph/9801271.

[30] L. Giradello, and M. Grisaru, *Nucl. Phys.* **B194** (1982) 65.

[31] J. L. Feng, M. E. Peskin, H. Murayama and X. Tata, *Phys. Rev.* **D52** (1995) 1418.

[32] M. M. Nojiri, K. Fujii and T. Tsukamoto, *Phys. Rev.* **D54** (1996) 6756.

[33] H. C. Cheng, *Int. J. Mod. Phys.* **A13** (1998) 2329.

[34] M. Klasen, talk given at 1st Workshop of the Extended ECFA/DESY Study, Cracow, 2001, available at http://fatcat.ifj.edu.pl/ecfadesy-krakow/confmatsql.php

[35] D. E. Groom *et al.*, *Eur. Phys. J.* **C15** (2000) 1, and 2001 off-year partial update for the 2002 edition available on the PDG WWW pages (URL: http://pdg.lbl.gov/).

[36] B. Abbott *et al.* (D0 Collaboration), *Phys. Rev. Lett.* **83** (1999) 4937.

[37] F. Abe *et al.* (CDF Collaboration), *Phys. Rev. Lett.* **76** (1996) 2006.

[38] M. Spiropulu, talk given at FNAL, November 2000, available at http://www-cdf.fnal.gov/physics/exotic/conference/conference.html.

[39] D. Abbaneo *et al.* (ALEPH Collaboration, DELPHI Collaboration, L3 Collaboration, OPAL Collaboration, SLD Heavy Flavor Group and Electroweak Group, LEP Electroweak Working Group and SLD Heavy Flavor and Electroweak Group), SLAC-REPRINT-2000-098, CERN-EP-2000-016, Jan 2000.

[40] A. Arhrib, M. Capdequi-Peyranere and A. Djouadi, *Phys. Rev.* **D52** (1995) 1404; H. Eberl, A. Bartl and W. Majerotto, *Nucl. Phys.* **B472** (1996) 481.

[41] M. J. Herrero, C. Lopez and F. J. Yndurain, *Phys. Lett.* **B127** (1983) 463; G. Altarelli, B. Mele and R. Petronzio, *Phys. Lett.* **B129** (1983) 456; H. D. Dahmen, D. H. Schiller and D. Wahner, *Nucl. Phys.* **B227** (1983) 291; D.H. Schiller and D. Wähner, *Nucl. Phys.* **B259** (1985) 597.

[42] B. A. Campbell, J. R. Ellis and S. Rudaz, *Nucl. Phys.* **B198** (1982) 1.

[43] W. Beenakker, R. Höpker and P. M. Zerwas, *Phys. Lett.* **B378** (1996) 159.

[44] M. Maniatis, Ph. D. thesis, Hamburg, 2001.

[45] TESLA Technical Design Report, DESY-2001-11.

[46] G. 't Hooft and M. Veltman, *Nucl. Phys.* **B44** (1972) 189.

[47] F. Bloch and A. Nordsieck, *Phys. Rev.* **52** 1937 54.

[48] T. Kinoshita, *J. Math. Phys.* **3** (1962) 650; T. D. Lee and M. Nauenberg, *Phys. Rev.* **133** (1964) B1549.

[49] W. T. Giele and E. W. N. Glover, *Phys. Rev.* **D46** (1992) 1980.

[50] G. P. Lepage, *J. Comput. Phys.* **27** (1978) 192.

[51] G. Passarino and M. Veltman, *Nucl. Phys.* **B160** (1979) 151.

[52] J. A. M. Vermaseren, *Symbolic manipulation with FORM*, Amsterdam, 1991.

[53] Z. Bern, L. Dixon and D. A. Kosower, *Phys. Lett.* **B302** (1993) 299, Erratum-ibid. **B318** (1993) 649.

[54] W. Siegel, *Phys. Lett.* **B84** (1979) 193; D. M. Capper, D. R. T. Jones and P. van Nieuwenhuizen, *Nucl. Phys.* **B167** (1980) 479.

[55] W. Siegel, *Phys. Lett.* **B94** (1980) 37.

[56] I. Jack and D. R. Jones, *Regularisation of supersymmetric theories*, in [16].

[57] W. Beenakker, H. Kuijf, W. L. van Neerven and J. Smith, *Phys. Rev.* **D40** (1989) 54.

[58] S. P. Martin and M. T. Vaughn, *Phys. Lett.* **B318** (1993) 331.

[59] W. Hollik and D. Stöckinger, *Eur. Phys. J.* **C20** (2001) 105.

[60] D. A. Ross and J. C. Taylor, *Nucl. Phys.* **B51** (1973) 125, Erratum-ibid. **B 58** (1973) 643.

[61] A. Sirlin, *Phys. Rev.* **D22** (1980) 971; W. J. Marciano and A. Sirlin, *Phys. Rev.* **D22** (1980) 2695, Erratum-ibid. **D31** (1980) 213; A. Sirlin and W. J. Marciano, *Nucl. Phys.* **B189** (1981) 442.

[62] W. A. Bardeen, A. J. Buras, D. W. Duke and T. Muta, *Phys. Rev.* **D18** (1978) 3998.

[63] A. Denner, H. Eck, O. Hahn and J. Küblbeck, *Nucl. Phys.* **B387** (1992) 467.

[64] G. Leibbrandt, *Rev. Mod. Phys.* **47** (1975) 849.

[65] G. 't Hooft and M. Veltman, *Nucl. Phys.* **B153** (1979) 365.

[66] A. Denner, U. Nierste and R. Scharf, *Nucl. Phys.* **B367** (1991) 637.

[67] T. Hahn and M. Perez-Victoria, *Comput. Phys. Commun.* **118** (1999) 153.

[68] G. J. van Oldenborgh, *Comput. Phys. Commun.* **66** (1991) 1.

[69] W. Beenakker, R. Höpker, M. Spira and P. M. Zerwas, *Nucl. Phys.* **B492** (1997) 51; R. Höpker, *Hadroproduktion und Zerfall von Squarks und Gluinos*, Ph. D. thesis, DESY-T-96-02, Hamburg, 1996.

[70] R. Lewin, *Polylogarithms and associated functions*, North Holland, Amsterdam, 1983.